VUF-1026
FINAL REPORT

VELA UNIFORM PROGRAM

PROJECT DRIBBLE

SALMON EVENT

TATUM SALT DOME, MISSISSIPPI

22 OCTOBER 1964

part of an experiment in seismic decoupling at the nuclear level

SPONSORED BY THE ADVANCED RESEARCH PROJECTS AGENCY OF THE DEPARTMENT OF DEFENSE AND THE U. S. ATOMIC ENERGY COMMISSION

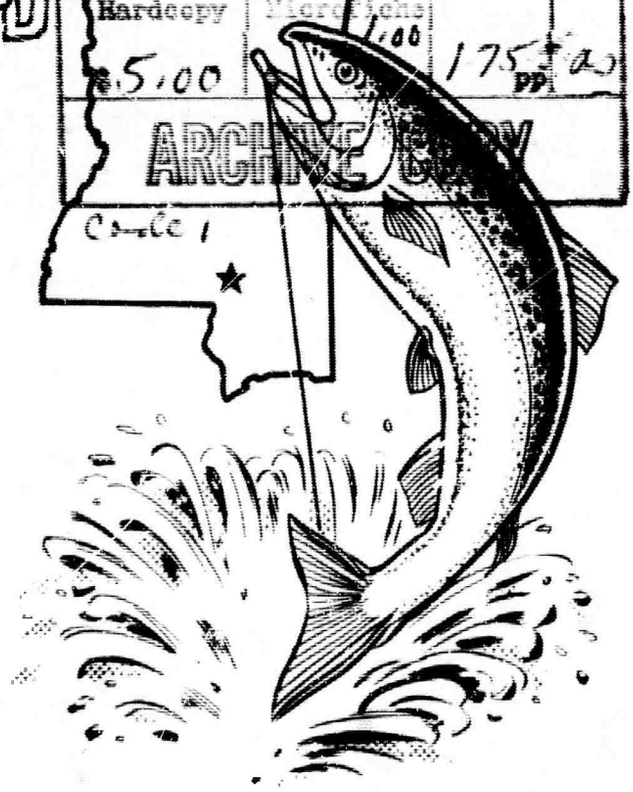

Analysis of Ground Motion and Containment

ROLAND F. BEERS, INC.

Issuance Date: November 30, 1965

DISCLAIMER NOTICE

THIS DOCUMENT IS THE BEST QUALITY AVAILABLE.

COPY FURNISHED CONTAINED A SIGNIFICANT NUMBER OF PAGES WHICH DO NOT REPRODUCE LEGIBLY.

LEGAL NOTICE

This report has been reproduced directly from the best available copy.

Printed in USA. Price $5.00. Available from the Clearinghouse for Federal Scientific and Technical Information, National Bureau of Standards, U. S. Department of Commerce, Springfield, Va.

VUF-1026
NUCLEAR EXPLOSIONS – PEACEFUL
APPLICATIONS (TID-4500, 45th. Ed.)

ANALYSIS
OF
GROUND MOTION AND CONTAINMENT

SALMON EVENT, PROJECT DRIBBLE
Final Report

August 26, 1965

ROLAND F. BEERS, INC.
Alexandria, Virginia

Prepared under
Contract AT(29-2)-1163
for the
Nevada Operations Office
U. S. Atomic Energy Commission

TABLE OF CONTENTS

TABLE OF CONTENTS (Cont.)

INDEX OF TABLES

INDEX OF FIGURES

INDEX OF FIGURES (Cont.)

INDEX OF FIGURES (Cont.)

INDEX OF FIGURES (Cont.)

BLANK PAGE

ABSTRACT

Predictions and evaluations of ground motion, stemming, containment and physical effects of ground motion on subsurface facilities and aquifers were made for the Salmon event. These predictions have been compared with observed data where available.

Analysis of seismic records included corrections for instrument response and the derivation of non-recorded motions by differentiation and integration. The observed ground motions along the instrumented lines to the east and south compared favorably with predictions but records from other stations indicate that large azimuthal variations in ground motions occurred. Additionally, uncertainty exists concerning amplitude of motions owing to lack of complete low frequency measurements

The prediction of containment and the evaluation of the adequacy of the stemming plan were substantiated by the test results. Available post-shot data permits the following quantitative comparisons: Cavity radius 19 meters predicted, 16.8 meters observed; cracking radius 58 meters predicted, 45-60 meters observed; radioactive crack radius 46 meters predicted, 37 meters observed; depth of spall 10 meters predicted, 12 meters observed; vertical displacement of spall 0.14 meters predicted, 0.1 meters observed.

CHAPTER 1

INTRODUCTION

1.1 BACKGROUND

Roland F. Beers, Inc., under Contract AT(29-2)-1163 with the Nevada Operations Office (NVOO), U. S. Atomic Energy Commission (AEC) is responsible to the Operational Safety Division of that office for the following:

a) Evaluation of containment of underground nuclear explosions

b) Prediction of ground motions

c) Evaluation of the physical effects of ground motions on aquifers and subsurface facilities.

The 5±kt Salmon event was the second contained underground nuclear test conducted in a salt medium and the first in a salt dome. This event presented special prediction problems due to the absence of directly applicable experience and its location off the Nevada Test Site in the vicinity of populated areas in southwestern Mississippi.

The possibility of a containment failure is a problem for essentially every event. This hazard becomes particularly important when an off-site event is considered.

In analyzing Salmon from this viewpoint, Gnome provided the only previous experience in a salt medium upon which to base predictions. The prediction of phenomenology, therefore, was based primarily on the available Gnome data. Where conditions were dissimilar, theoretical analyses and extrapolation of experience from other media were employed.

Ground motion resulting from underground testing of nuclear devices is a substantial as well as a continuing operational safety problem. Current methods of predicting ground motion employ empirical relationships derived from observed data. Proper use of these relationships for prediction purposes requires that the test conditions for which predictions are to be made be comparable with those which provided the data used in deriving the relationships.

Scaling of ground motion for yield and distance are fundamental steps in making predictions. To perform such scaling, the variation in amplitude with yield and distance must be defined. Appreciable departure in yield, source geometry, method of emplacement and physical properties of the transmission path from previous experiments substantially affect the manner of scaling and the agreement

between predicted and observed ground motions.

The results of the earlier 3.1 kt Gnome event in salt near Calsbad, N. M. were used to the greatest extent possible. As Gnome was the only test conducted in salt prior to Salmon, the observed ground motions at Gnome were applied to Salmon by using cube-root scaling modified by calculations to account for the differences in geologic environment. The scope of the transmission problem is defined in Section 1.4.

1.2 OBJECTIVES

The purpose of containment studies was to provide the Operational Safety Division with an independent evaluation of the probability of containment and the adequacy of the stemming concept and plan. In performing this function, dependence was placed on theoretical considerations and on empirical data collected in large measure by others. This supply of data was generally arranged by NVOO, but also was obtained by direct contact with the Technical Director where appropriate.

The objectives of Roland F. Beers, Inc. participation in seismic aspects of the Salmon event were to provide Operational Safety Division with predictions of anticipated ground motion, to provide a plan of instrumentation which would include monitoring of selected locations as well as providing benefit to the long range seismic studies, and to provide processing and analysis of the recorded seismic data.

The purpose of studies of the effects of ground motion on aquifers was to evaluate the possibility of physical damage. This information could then be used in analyses of the possibility of ground water contamination.

The purpose of studies of the effects of ground motion on the Sand shaft, oil and gas facilities, and other underground installations was to evaluate the possibility of damage.

1.3 INSTRUMENTATION

The measurement program designed to meet the needs of Operational Safety consisted of instruments on two radial lines from surface zero, at selected cities and points of interest, and a safety net encircling Tatum Dome at radii of approximately 56 to 64 kilometers.

Each of the radial lines, one to the east and the other to the south, were approximately 6.4 km long and consisted of 6 stations measuring three components of particle acceleration and particle displacement with the USC&GS strong motion accelerograph. The locations of these stations are shown in Figure 1.1.

Additionally, accelerographs measuring the same quantities as above were placed at Purvis, Lumberton and the Baxterville Oil Field. Vibration meters were used to record three components of displacement at Hattiesburg and Columbia. The safety net consisted of Wood-Anderson seismographs measuring two horizontal components (N-S and E-W) at six surrounding communities: Tylertown, Prentiss, Ellisville, Beaumont, Perkinston and Bogalusa.

Additional instrumentation supplementing the Safety Program was provided by USC&GS; Wiss, Janney, Elstner and Assoc.; and AFTAC. The additional USC&GS stations were located 16 km south (10S), 32 km south (20S), at Ville Platte, Louisiana (160 SW), Silsbee, Texas (272 SW) and Hockley, Texas (380 SW). Each of these stations consisted of an array of NC-21 velocity meters. Vertical,

radial and transverse components plus three additional vertical components at 300 meter intervals were employed.

Wiss, Janney, Elstner and Assoc. instrumented three stations to the north of surface zero at distances of 8.8, 16.6 and 20.2 kilometers. Three components of displacement were measured at all three stations th Sprengnether Portable Blast and Vibration Seismographs. In addition, three components of velocity were measured at the closest station using a system consisting of M-B vibration pick-ups (type 124) and a four-channel Edin oscillograph and associated amplifiers. At the middle station three components of acceleration were measured using Shure Bros. Model 61B acceleration pick-ups and an Esterline Angus Instrument Co. three-channel oscillograph and associated amplifiers. These stations were designated 1N, 2N and 3N in order of increasing distance.

The AFTAC stations were located at Eutaw, Alabama; Jena, Louisiana; Cumberland Plateau Observatory, Tennessee; Grapevine, Texas; and Wichita Mountain Observatory, Oklahoma. Long-period Sprengnether (2.5 sec. period) and Benioff seismographs were employed at these stations.

All station locations are shown on Figures 1.1-1.3. Table 1.1 lists all stations, the type of instrument used

and the type of motion and number of components measured.

1.4 THEORY

1.4.1 Seismic Effects

The Tatum Dome, site of Project Dribble, has a configuration and geologic environment typical of most salt domes in the gulf coast section of the United States. The dome is shaped roughly like a vertical cylinder, about 1.6 kilometers in diameter, which has pushed up through relatively soft sedimentary deposits. The top of the salt is approximately 457 meters below the surface. Directly overlying the salt is a caprock of anhydrite roughly 152 meters thick. This is overlain by 30-61 meters of limestone caprock. The areal extent of the anhydrite and limestone is approximately equivalent to that of the salt. Overlying the limestone are about 229-244 meters of sediments (clays, shale, sandstone, etc.). The physical properties of each of these layers overlying the salt affect the ground motion amplitude and were considered when predictions were computed.

Since the Salmon event was in salt, the ground motion measurements recorded for the Gnome event (3.1 kt in salt) provided a basis for making Dribble predictions.

Because of the many differences in geologic environment, Gnome surface measurements were not considered reliable indicators of motions to be expected for Salmon. However, the subsurface measurements in salt at Gnome were considered applicable to surface predictions of the Salmon event as long as the local geology was taken into account.

Prior to the Dribble chemical explosive (HE) tests, it was believed that the structural configuration of the dome might cause a variable rate of amplitude decay with distance; therefore, possible shadow zones as well as azimuthal variations were anticipated. However, the Dribble HE tests and a review of data observed from HE shots in a dome in Louisiana (Project Cowboy) indicated that while some azimuthal variation could be expected, the decay of surface amplitudes with distance would follow a relatively uniform exponential rate.

The presence of a fairly thick section of soft, poorly consolidated sediments near the surface suggested the possibility of the generation of large amplitude surface waves. The empirical data furnished by the Dribble HE tests indicated that it was possible to generate surface waves in this area by detonating shots in the near-surface

sediments. However, for the three 1000-pound (454 kg) shots in salt no evidence of surface waves was observed. While these data seemed to indicate that surface waves would not be a hazard for shots in salt, it was emphasized that considerable uncertainty accompanied the scaling effects of 1000 pounds (454 kg) to 5 kt (yield ratio of 10,000 to 1).

1.4.2 Phenomenology and Containment

The evaluation of containment of the Salmon event was based on procedures developed as part of a long-range program directed to the continuing improvement of confidence in predictions.

Currently, greater dependence is placed on empirical relationships, and it is probable that experience will always be a major factor in evaluation. However, a large part of the improvement will come from greater knowledge of the pressure-time history and temperature-time history of underground explosions. This is being actively pursued, and some of the results were employed in the development of predictions and the evaluation for Salmon.

1.4.3 Effects of Ground Motion on Aquifers and Subsurface Facilities

The evaluation of the physical effects of ground

motion on aquifers was based on the predicted transient motions and permanent displacements in relation to geologic factors.

The evaluation of the effects of ground motion on subsurface facilities was based primarily on earthquake experience and nuclear test effects on similar facilities. Correlation of predicted motions with those which damaged or failed to damage similar facilities in earthquakes or nuclear tests provided criteria.

TABLE 1.1

U.S.C. & G.S.

STATION	INSTRUMENT	ACCCELERATION	DISPLACEMENT	VELOCITY
S-1	Strong Motion	ZRT	ZRT	
S-1	Accelerograph	ZRT	ZRT	
S-2	"	ZRT	ZRT	
S-3	"	ZRT	ZRT	
S-4	"	ZRT	ZRT	
S-5	"	ZRT	ZRT	
S-6	"	ZRT	ZRT	
E-1	"	ZRT	ZRT	
E-1	"	ZRT	ZRT	
E-2	"	ZRT	ZRT	
E-3	"	ZRT	ZRT	
E-4	"	ZRT	ZRT	
E-5	"	ZRT	ZRT	
E-6	"	ZRT	ZRT	
Bexterville	"	ZRT	ZRT	
Oil Field	"			
Purvis	"	ZRT	ZRT	
Lumberton	"	ZRT	ZRT	
Gulf Refinery	Vibration Meter		ZRT	
Hattiesburg	" "		RT	
Columbia	" "		RT	
10S	NC-21 Velocity Meter			ZZZZRT
20S	" " "			ZZZZRT
160SW	" " "			ZZZZRT
272SW	" " "			ZZZZRT
380SW	" " "			ZZZZRT
Tylertown	Wood-Anderson		N-S, E-W	
Prentiss	" "		" "	
Ellisville	" "		" "	
Beaumont	" "		" "	
Perkinston	" "		" "	
Bogalusa	" "		" "	

WISS, JANNEY, ELSTNER & ASSOCIATES

1N	Sprengnether		ZRT	
	M-B 61 Vibration			ZRT
2N	Sprengnether		ZRT	ZRT
	Shure Bros.	ZRT		
3N			ZRT	

AFTAC-LONG RANGE SEISMIC MEASUREMENTS

Eutaw	L.P. Sprengnether	ZRT
	Benioff	ZRT
Jena	L.P. Sprengnether	ZRT
	Benioff	ZRT

TABLE 1.1 CONTINUED

AFTAC-LONG RANGE SEISMIC MEASUREMENTS

Cumberland	L.P. Sprengnether	ZN
Plateau	Benioff	NE
Grapevine	L.P. Sprengnether	Z
	Benioff	Not Analyzed
Wichita Mt.	L.P. Sprengnether	Z E

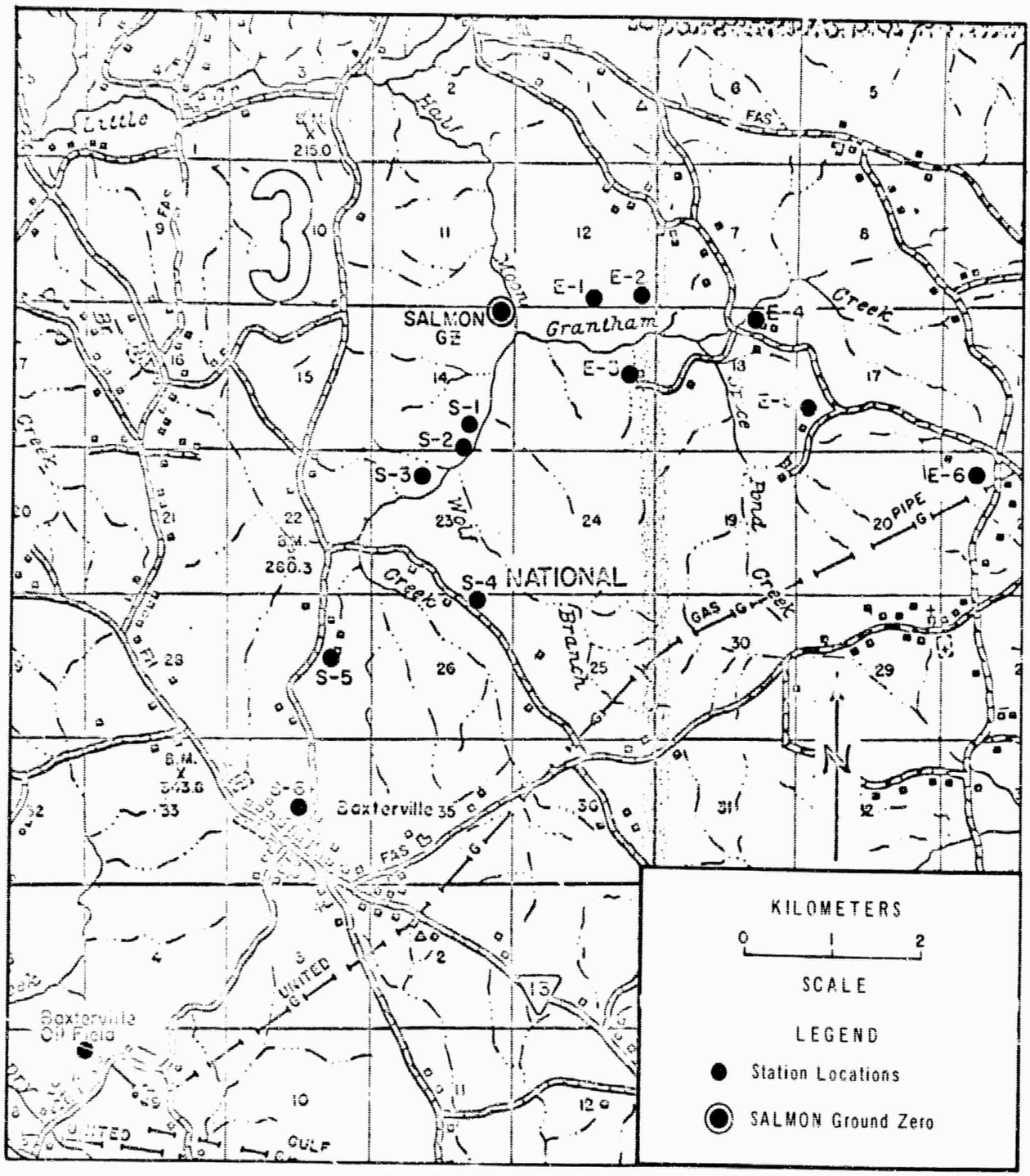

Figure 1.1 Area Map Showing Locations of USC&GS Instrument Stations Within 10 Kilometers of Ground Zero.

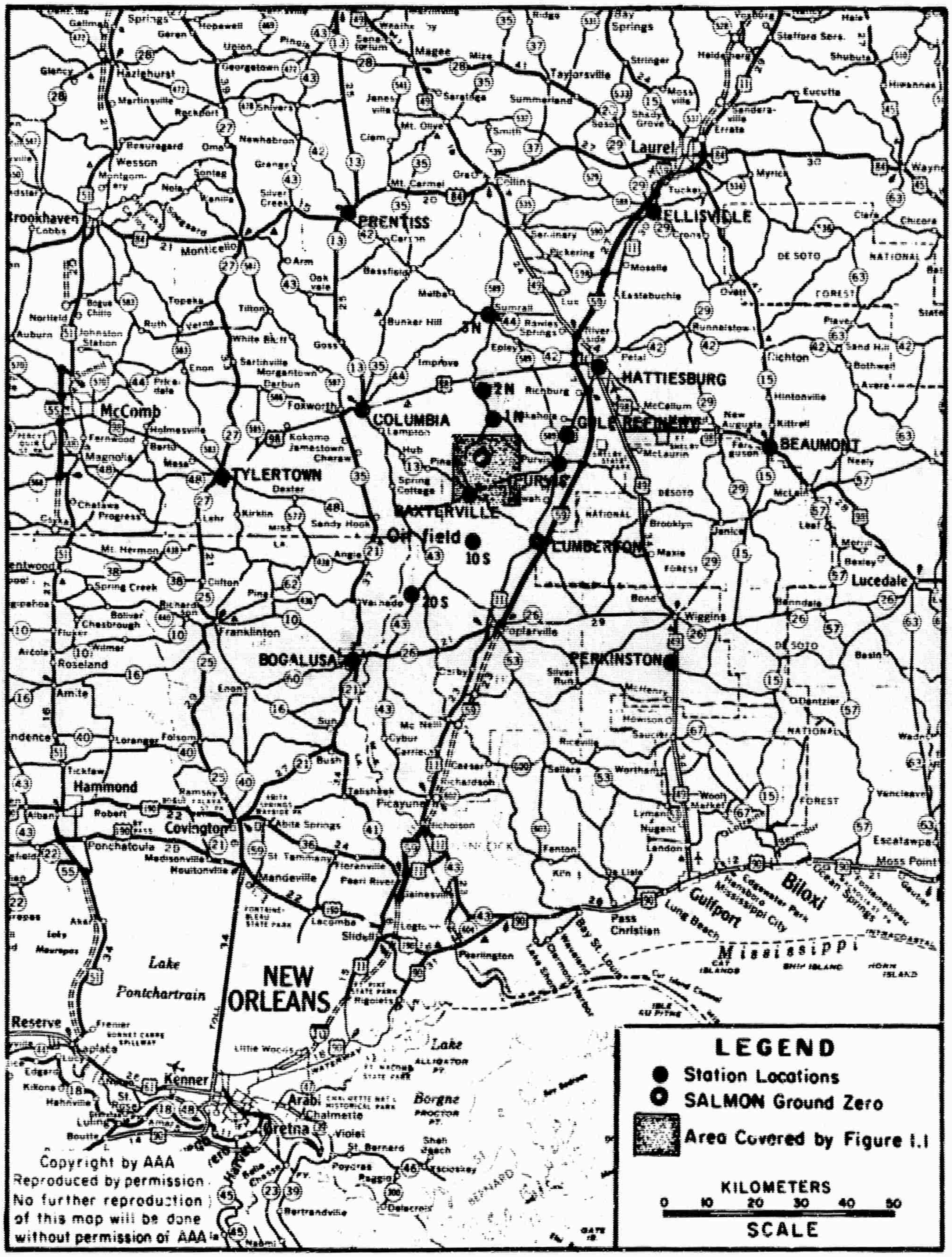

Figure 1.2 Area Map Showing Instrument Stations Located at Intermediate Distances.

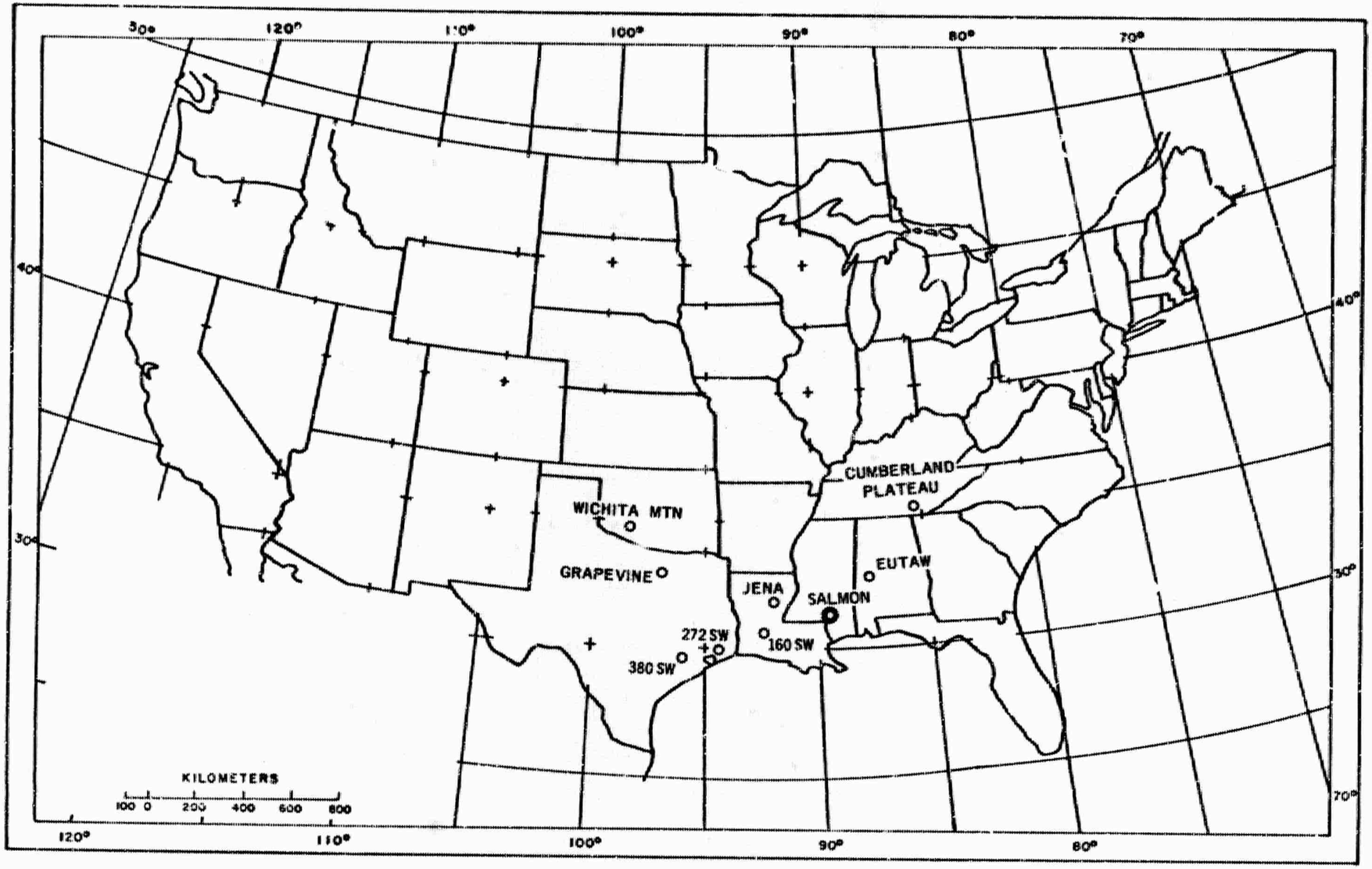

Figure 1.3 Long Range Instrumentation

CHAPTER 2

PREDICTIONS

2.1 ENVIRONMENT

2.1.1 Location and Topography

The Tatum Dome area is about 75 to 100 meters above sea level, and is moderately dissected with narrow, flat-topped ridges rising about 30 meters above intervening valleys. The hills are well drained, but usually the bottomlands are wet during most of the year. The principal streams in the area are Half Moon and Grantham Creeks which flow into Lower Little Creek about one to two kilometers north of the dome (Reference 2.1). The area immediately over the dome is a topographic low.

2.1.2 Geologic Setting

All formations outcropping in the State of Mississippi are of upper Cretaceous and Tertiary age. The older formations, exposed along the northern edge of the State, are overlain to the south-southwest by progressively younger beds, which outcrop in roughly parallel bands. In general, the formations thicken to the south-southwest. Younger beds dip about 1.9 meters per kilometer to the south whereas dips on the base of the older, deeper Eocene beds are about 6.6 meters per kilometer southward (Reference 2.1).

Tatum Dome is a large buried salt stock that has pierced sedimentary deposits of early Cretaceous to Oligocene (middle Tertiary) age. Sediments of Miocene age surround and overlie the dome but are thinner over the dome than in the surrounding area. Rocks of Eocene age are absent on the crest of the dome (Reference 2.2). Regional strikes and dips are locally disturbed around the dome.

2.1.3 Local Stratigraphy and Lithology

Stratigraphic relations over and around the dome are shown in the attached cross section (Figure 2.1) extending southwest through the dome. Figure 2.2 shows the location of this section and all drill holes presently in the dome area.

Figure 2.3 is a generalized stratigraphic section through Station 1, the former location of the Salmon Event. A section through Station 3, the location of the Sand Event, is shown in Figure 2.4. Lithologic descriptions of the various rock types in the dome area are given on this figure. The sediments over the dome are mainly sands, clays and silts in varying mixtures. The true caprock which underlies the Catahoula Sandstone is composed of two dominant lithologic units. The upper unit is gray to brown, fine- to medium-grained, crystalline limestone. The limestone contains

zones of high permeability, in which varying quantities of drilling fluid were reported lost while drilling. It also contains some lenses of gray to brown, medium-grained, calcareous, loose sand. This sand may be either contained as lenses within the limestone or as interfingering lenses of the Catahoula Sandstone with the caprock limestone (Reference 2.3). In some places, the limestone has been leached, forming channels and vugs. The lower 6 meters of the limestone (in WP-4) consists of vuggy brecciated black calcitic limestone. The limestone at its base grades into several meters of gypsum which in turn grades down into the anhydrite which composes the lower dominant lithologic unit of the caprock. The anhydrite is medium gray, hard, and finely crystalline. In WP-4, the upper part of the anhydrite has been highly fractured, and gypsum veins line the slickensided surfaces. Its basal contact with the salt is sharp. The salt varies from gray to very light gray, anhydrite-bearing halite to transparent, very coarse crystalline, almost pure halite. The salt is banded with nearly vertical alternating thin bands of anhydrite-bearing halite and almost pure halite (Reference 2.4).

Tabulations of drill hole information and lithologic logs are shown in Tables 2.1 and 2.2. Lithologic logs are

available for the following holes on or near Tatum Salt Dome:

WP-1	DR-15
WP-4	DR-19
E-1	DR-8
E-2	DR-16
E-3	DR-17
E-4	DR-12
E-5	DR-13
E-6	DR-14
E-7	DR-16
E-9	DR-17
HT-1	DR-6, DR-32, DR-40
HT-2	DR-7, DR-32, DR-40
HT-3	DR-31

2.1.4 Physical Properties

Physical properties for the salt and surrounding sediments are compiled in Tables 2.3 and 2.4.

2.1.5 Structure

Physical properties applied to calculation of the compound transmission coefficient in a vertical section at HT-3 are shown on Table 2.5. The enclosed cross section (Figure 2.1) extending southwest through HT-1 and HT-2 best shows the structural relations across the dome. Figure 2.5 shows the location of all other available cross sections through Tatum Dome.

Faulting of the caprock is indicated in the vicinity of E-7, 610 meters southeast of Sand shot point (See Figure 2.1). There a 41 meter section of brecciated sandstone, calcite conglomerate and black chert gravel was found where the anhydrite would normally be. Numerous fractures are present in the anhydrite -- as mentioned previously.

Although little mention of jointing is made specifically in the literature, it seems reasonable to expect its moderate development in the more brittle lithologic types including sandstones, limestones, anhydrites and gypsum. The salt within the dome, is essentially free from jointing and fracturing.

2.1.6 Hydrology

A complete and up-to-date review of the hydrology of the dome area is contained in USGS Technical Letter: DRIBBLE-34. There are five aquifers of importance in the Tatum Dome area (shown on Figure 2.1); all of which are under artesian pressure except the "Local Aquifer" which holds perched water. Aquifer 5 in the Cook Mountain limestone is the shallowest of the saline aquifers in the area and is about 790 meters deep near the dome. It is separated from the deepest fresh water aquifer (#4) by several hundred meters of impervious clays. Both of these aquifers are discontinuous

over the dome. Aquifer 4 has a very small yield and is not presently a water supply source.

Aquifers 1, 2, and 3 are Miocene sandstone units which are continuous over the dome. Locally they are the principal sources of fresh water. Aquifer 2a in the Pascagoula and Hattiesburg Formations has the highest permeability.

The calcitic portion of the caprock is another major water-bearing unit. The following is quoted from Reference 2.2:

> "The calcite caprock contains numerous open fractures filled with water that probably have been enlarged by solution. In nearly all test holes drilled through the calcite caprock, lost circulation has been a major problem in drilling. When drilling fluid is lost from a hole being drilled through the caprock, the loss is reflected almost immediately as a rise in water levels in an observation well along the east margin of the calcite caprock. These conditions suggest that the calcite caprock has a high permeability.
>
> The aquifer in the caprock may be in hydraulic continuity .... with aquifer 4 along the flank of the dome."

Possible aquifer contamination is summarized in the same reference:

> "On the remote chance that radioactivity might escape from the salt stock in which the nuclear devices are proposed to be detonated, the activity would most likely enter the caprock, the overlying sands of aquifer 3, or aquifers 4 and 5 on the flank. Computed values of the rate of

movement of water in aquifers 3, 4, and 5 indicate the movement will be less than 3 meters per year. This slow rate of movement coupled with the high [ion] exchange capacity of the material comprising the aquifers lead to the conclusions that the off site contamination potential is small to nil. The highest rate of movement, about 49 meters per year, was computed for aquifer 2a. It is unlikely that radioactivity would be released into this aquifer, several hundred feet above the caprock."

2.2 PHENOMENOLOGY AND CONTAINMENT

2.2.1 Radius of Cavity

The prediction of cavity radius for the Salmon Event was based upon the cavity realized from the Gnome Event, a 3.1 kt detonation in a similar medium (revised from 3.5 kt on the basis of information in Reference 2.5). The Gnome cavity was not spherical but resembled an oblate spheroid with the vertical dimension from the W.P. to the bottom of the cavity being about 16 meters and the average horizontal radius being on the order of 25 meters. The Salmon cavity was anticipated to more nearly approach a spherical shape since the bedding plane effects existent at Gnome would not be present, and prediction of the cavity radius was accomplished by applying cube root scaling to the Gnome radii. The predictions were stated in terms of a "most

probable" radius and a "maximum probable" radius to account for possible variations due to stratigraphy.

$$\left(\frac{5.0}{3.1}\right)^{\frac{1}{3}} \times 16 \approx 19 \text{ meters - Most probable radius}$$

$$\left(\frac{5.0}{3.1}\right)^{\frac{1}{3}} \times 25 \approx 30 \text{ meters - Maximum probable radius}$$

For comparative purposes, both of these figures were utilized where applicable to subsequent calculations.

2.2.2 Cracking Radius

The fracturing of the medium surrounding the post-shot cavity were divided into several zones for the purposes of analysis. In the region immediately surrounding the cavity, displacement associated with cavity expansion was expected to occur by plastic deformation such that the condition of post-shot rock would closely resemble that of the original in situ condition. Farther out, larger block-type shear failures were expected which would mask any fractures developed from tension. The outer limit of fracturing was expected to have a radial orientation and to be tensional. This outer limit is of particular interest since these fractures present possible channels for radioactive transfer.

The creation of these fractures can be attributed to the passage of the shock wave and the subsequent expansion of the cavity wall, causing radial displacements and strains throughout the medium. An investigation was made of these possible mechanisms in relation to the fracturing which occurred at Gnome. Here, the outer limit of cracking, other than bed separation, was estimated to be 76 meters, with the major lateral shock-induced effects being confined to a radius of 43 meters.

Figure 2.6 shows the predicted and observed horizontal radial displacements for the Gnome Event. Predictions were obtained by use of the method outlined in Appendix A. The permanent displacement at the outer limit of cracking was found to be one meter. The creation of fractures is more logically associated with strains rather than gross displacements, and therefore, the radial strain was computed and found to be .021 meters per meter or 2.1%. The allowable compressive strain for salt was obtained from the Waterways Experiment Station test of the Dribble cores (Reference 2.6) by uniaxial compression. The strain at ultimate strength for 12 tests averaged 2.07% which compares remarkably well with that computed above on the basis of displacements. Predictions of the anticipated permanent displacements and

strains for the Salmon Event were made, based on the most probable cavity radius of 19 meters and the maximum probable cavity radius of 30 meters. These are shown in Figure 2.7. Utilizing a radial strain of 2.1%, the outer limits of cracking associated with these radii for the Salmon Event were predicted to be 58 and 91 meters, respectively.

2.2.3 Radius of Radiation Injection into Cracks by Particulates and Condensates

At the Gnome Event, injection of intrusive breccia into post-shot fissures occurred to a distance of at least 34 meters, and fracturing to 76 meters (Reference 2.7). Other estimates have placed the limit of radioactivity at distances as large as 61 meters. Accepting the greater distance and assuming that the ratio of the radius of radioactivity to the radius of cracking would be similar for Gnome and Salmon events, the outer limit for Salmon was predicted to be:

$$\frac{61}{76} \times 58 \approx 46 \text{ meters - Most probable}$$

$$\frac{61}{76} \times 91 \approx 73 \text{ meters - Maximum probable.}$$

The cracking limits of 58 and 91 meters were derived in Section 2.2.2.

A similar computation was performed using data from Rainier where fracturing extended 85 meters (Reference 2.8) and radioactivity 58 meters (Reference 2.9). For Salmon, the radioactive radius would then be:

$$\frac{58}{85} \times 58 \approx 39 \text{ meters - Most probable}$$

$$\frac{58}{85} \times 91 \approx 62 \text{ meters - Maximum probable.}$$

These agree fairly well with the values obtained above; therefore, 46 and 73 meters were predicted as being, respectively, the most probable and maximum probable limits of radiation injection into fractures.

2.2.4 Height of Chimney

For other events, an estimate of chimney height has been made on the basis of

$$H = \frac{2R/3\ (1 + n)}{n - 1} \qquad (2.1)$$

where (H) is the height above the working point, (R) is the radius of both the cavity and chimney, and (n) equals the swell factor, or ratio of volume of chimney rubble to the volume occupied *in situ* (see Appendix A).

An appropriate salt swell factor has not been determined on the basis of past experience. Gnome did not lend itself

to this purpose since the formation of a chimney was incomplete. Thus, in order to predict a possible maximum chimney height for the Salmon Event, the swell factor was assumed to be 1.35. This was the value determined for the massive granodiorite at Hardhat. An assessment of the range of swell factors associated with the excavation of hard materials indicated that this factor was reasonable for the intended purpose. Thus, with most probable and maximum probable cavity radii values of 19 and 30 meters, respectively, and a swell factor of 1.35, a most probable chimney height was calculated as 85 meters while a maximum probable height was calculated as 133 meters. Based upon Salmon stratigraphy and Gnome experience wherein a chimney did not form in the halite (though cavity collapse did occur to a height of about 28 meters above the Zero Point), it was considered unlikely that a similar chimney would develop for the Salmon Event. Therefore, it was emphasized that the values of chimney height represented those based upon the assumption that a chimney would develop as at Hardhat. By reason of the experience at Gnome, it was considered unlikely that the chimney height would attain a value as large as these figures.

2.2.5 Depth of Spalling

The possibility of spalling at ground zero owing to the detonation of a 5 kt device at a depth of 823 meters was

investigated by means of a graphical analysis. The geologic setting, densities and velocities of the various beds and transmission coefficients used are shown in Tables 2.6 and 2.7.

The analysis presented in Figure 2.8 was constructed from the physical and computed data by a procedure similar to that outlined in Appendix A. The use of this method required a prediction of the anticipated pressure versus distance. The prediction procedure for obtaining pressure was re-examined, and was found to be of sufficient accuracy to permit an estimate of the order of magnitude of spalling effects. In this analysis, the conservative single spall method was employed. An assumption of multiple spalls would have permitted energy to be trapped in the initial spalls, thereby decreasing the depth of spalling predicted. A tensile strength of zero was assumed for the medium.

Results predicted on this basis indicated that spalling should occur to a maximum depth of about 40 meters. The driving force, or difference between net tension and overburden pressure, to produce spalling in this region was, however, very low -- less than 1 bar (10^6 dynes/sq. cm.). This means that if the atmospheric pressure of approximately 1 bar is added to the overburden, spalling would be predicted

to only about 10 meters. Any tensile strength of the medium would also add restraint. The conclusion, therefore, was that the probability of major spalling at surface ground zero was rather low, but that some projection of unconsolidated surface material might take place.

Predicted displacement at the surface of any possible spall was computed using the predicted free-field particle velocity obtained from machine calculations and multiplying this by the compound transmission coefficient as follows:

$$d = \frac{V^2}{2g} = \frac{(47 \times 3.52)^2}{2\ (981)} = 14 \text{ cm} \qquad (2.2)$$

The vertical displacement of any dislodged material would thus be of small magnitude.

2.2.6 Radius of Spalling

The demarcation line between the region where spalling occurs and that where surface motion is solely due to seismic waves is essentially non-existent. Rather, a transition occurs from the maximum vertical displacement, which occurs at surface zero due to spalling, to a region where displacements by this mechanism are infinitesimal. Since the probability of a major spall at surface zero was low and the magnitude of the anticipated displacement was only 14 cm,

the lateral extent of spalling was not expected to be very great. From an examination of surface displacement versus horizontal distance (Figure 2.9) for several events, it was seen that displacements due to spalling decreased rapidly with increasing range. The anticipated Salmon displacement was seen to be much less than those of the previous events shown. The lateral extent of spalling would also be small, something less than 300 meters.

2.2.7 Elastic Radius

From an analysis of the Gnome data on measured particle velocity (Reference 2.10) a distinct change in the attenuation rate was seen at 100 meters. This corresponded to a particle velocity of about 1.2×10^5 cm/sec. In terms of pressure, a value of 1.1 K bars was taken as the limit on the elastic precursor for salt (Reference 2.11).

Scaling the 100 meter distance to the Salmon yield gave:

$$\left(\frac{5}{3.1}\right)^{\frac{1}{3}} \times 100 \approx 118 \text{ meters.}$$

2.2.8 Stemming Predictions

The evaluation was accomplished by correlating stemming data from previous events at NTS and Project Gnome with the stemming plan for the Salmon event.

Emplacement Holes - Stations 1 and 1A - The satisfactory containment of drill hole events in alluvium or granite by complete stemming with sand, and more recently with pea-sized gravel, has been generally demonstrated at the Nevada Test Site. For the Salmon Event, the emplacement hole was originally designated as Station 1; however, considerable difficulties were encountered in the drilling, casing, and grouting of this hole. These resulted in the decision to abandon this location (N537,328.14, E269,540.96) and to drill a new hole about 9.21 meters north to be designated as Station 1A (N537,358.14, E269,540.96). The Station 1 hole was bottomed at 464.5 meters, and it was understood that this was to be used both as a pre- and post-shot hole. The difficulties referred to are enumerated in the Fenix and Scisson, Inc. report dated January, 1964 (Reference 2.12). This report and the Fenix and Scisson, Inc. revised specifications for Station 1A (Reference 2.13) were reviewed to ascertain those factors pertinent to an evaluation of operational safety.

In regard to Station 1, Fenix and Scisson, Inc. data (Reference 2.12) showed this hole to be grouted to the surface with 50-50 pozmix, salt-saturated cement, 6% gel.

However, it was understood (Reference 2.14) that the grout terminated some 76 meters below the surface, and that the material left in the hole from surface to 76 meters was apparently mud-contaminated cement. Further, it was indicated that Lawrence Radiation Laboratory had requested that the following actions be taken to enable this hole to be used for pre- and post-shot activities:

1. Place a 9 to 12 meter plug of salt-saturated cement in the bottom of the subject hole;

2. Backfill hole to surface with a graded river run sand;

3. Bolt a steel flange on top of either the 66 centimeter (26") conductor pipe or the 51 centimeter (20") casing after completion of the blow-out preventer collar.

It was concluded that either of the above situations constituted adequate stemming of the Station 1 hole from the viewpoint of containment inasmuch as this hole penetrated only to a depth of 464.51 meters.

In regard to Station 1A, Reference 2.15 shows that cement grout would be placed both inside of the hole and the 14 centimeter (5½") diameter casing to a level approximately 183 meters above the center of the device. This would place

the top of the grout some 30 meters into the bottom of the 51 centimeter (20") diameter casing. Above this level, pea-sized gravel was to be placed in both casings throughout the remaining hole to the surface. Chimney development appeared particularly critical in respect to the integrity of the stemming. It was previously stated in Section 2.2.4 that the calculated possible maximum chimney height was 133 meters. If the full height developed, there would still remain some 50 meters of grout plug which would be effective as stemming and in preventing the loss of gravel by flow into the cavity. However, based upon experience at Gnome and a comparison of media, it was considered likely that little, if any, chimney would develop for the Salmon Event.

On the basis of the foregoing, it was concluded that the stemming proposed for Station 1A was adequate for preventing immediate release of radioactive products through the emplacement hole.

Instrument Holes -

E-15 (N537,415.13, E269,491.64) and
E-16 (N537,414.35, E269,591.63):

These holes were located about 23 meters laterally from Station 1A; however, E-16 was planned for a depth of only 297.2 meters while E-15 was to penetrate to a depth of

823 meters. Accordingly, the lower portion of E-15 would be within the predicted cavity radius of 30 meters while the bottom of E-16 would be well beyond the predicted cracking radius of 91 meters. Reference 2.16 indicates that both these holes were to be grouted to the surface, and this manner of stemming was considered adequate.

E-4 (N537,915.26, E270,425.47), E-6 (N538,050.45, E268,734.48), and WP-4 (N536,303.98, E269,172.86):

Reference 2.17 states that the shortest conceivable venting path was through the brine-filled holes above the grout in E-4 and WP-4. It was also stated that these two holes would be grouted to a radial distance of at least 350.52 meters from the device. The same treatment would apply to E-6 which would also be brine-filled to the surface. This distance of 350.52 meters provided a factor of safety against any unknown geologic effects. Thus, the stemming for these three holes was considered adequate.

E-14 Complex: E-14 (N537,199.25, E269,006.28) E-14T (N537,199.25, E268,986.28), and E-14B (N537,121.75, E269,026.12):

Initially, only hole E-14 was planned, and this was to have been grouted to the surface; however, grouting of full depth was not achieved due to failure of grout hoses. Reference 2.18 provides a historical summary of the events

connected with the drilling, casing, and grouting of this hole and the subsequent attempts to achieve a satisfactory installation of instrumentation by means of grouting through two additional holes, E-14T and E-14B. These were drilled and whipstocked to connect with E-14 at approximate depths of 580 and 1220 meters, respectively. Attempts were then made to circulate grout from E-14B into E-14 and out of E-14T. Circulation was achieved; however, grouting was only partially successful in that only the canister at a depth of 610 meters was grouted. After study, it was concluded that grout was cutting across the holes somewhere around a depth of 610 meters.

Laterally, these holes were 171 to 177 meters from Station 1A. This placed them some 79 meters beyond the predicted cracking radius of 91 meters. Vertically, the device and presumed channel were separated by a little over 200 meters, thus placing the channel at about 125 meters beyond the predicted cracking radius. Thus, it was considered unlikely that communication would be established either laterally or vertically.

The conclusions summarized below were based upon study of Reference 2.18 and upon knowledge gained from March 13, 1964, Dribble Review Panel meeting at NVOO. The data from these sources constituted the latest official information available to Beers, Inc. regarding E-14 complex. Conclusions, and reasons therefor, regarding operational safety predictions and securing E-14 complex were as follows:

1. In regard to all 3 holes of E-14 complex, Beers, Inc. assumed casing to be satisfactorily grouted to medium as there was no information to the contrary;

2. E-14T was considered to be adequately stemmed and no additional treatment was required. This hole became fully plugged with grout in process of attempting to grout E-14. For the lack of information to the contrary, the grout within this hole was assumed to be satisfactory;

3. It was learned at the NVOO meeting of March 13 that E-14B would be utilized as an instrument hole. It was assumed by Beers, Inc. that the installation would normally include grouting to the surface in this hole. On this and the further assumption that this grouting would be accomplished without difficulty, this hole would be considered to be adequately stemmed, and no further treatment would be required;

4. E-14 had a grout plug which was presumed to be a little over 600 meters in length. Although this plug was not consistent as fluid bled from hole for several weeks following cessation of grouting operations, it was still considered to be adequate stemming for this hole. This statement was based on the opinion that the possibility of communication being established between E-14 and Station 1A was remote. There was less assurance of safety with the condition of inconsistent grout than with a hole which is tightly grouted; however, it was emphasized that the possibility of communication was considered remote. From the March 13 meeting at NVOO, it was understood that LRL was either designing, or could design, a pressure seal device for E-14 hole which would provide for cable installation, as it was desired to maintain instrumentation capability in this hole. Beers, Inc. concurred with the principle of use of such device from standpoint of increasing degree of safety in regard to uncertainty of grout condition; however, Beers, Inc. did not lay on a requirement for the use because the possibility of communication was considered remote. It was interpreted from Reference 2.21 that the plug in E-14 hole extended from approximately 610 meters to surface.

This was based on a statement by Fenix and Scisson, Inc. that grout was observed coming out of hole after pumping in 34.4 cubic meters. It was calculated that this volume of grout was sufficient to fill 28 centimeters (11") ID casing to a depth of approximately 578 meters, considering approximate volume of cables and hoses. The plug, therefore, was considered essentially continuous from the surface to a depth of about 610 meters.

2.2.9 Possibility of Secondary Explosions

The halite at a depth of 823 meters had no significant water content (Reference 2.6, Table 6). The planned procedure for emplacement of the device required grouting around the device and inside the casing to an elevation 183 meters above the working point. Therefore, there was a high degree of assurance that there would be no substantial quantities of water present in the vicinity of the shot point. Also, the volume of air would be extremely small. Accordingly, following the explosion, when the condensation of all gaseous halite, grout and metal had occurred and the temperature had dropped to the melting point of halite, about 788°C (1450°F), the cavity would be expected to have a very low absolute pressure. Theoretically, if there were

no steam and no air present, the absolute pressure would approach zero.

If water flowed into the cavity following the explosion, the steam pressure could build up in the cavity. However, assuming that there would be no very large opening through which the water could flow, the pressure buildup would be self-limiting. The head, assuming the water table at the surface, would be 823 meters, and the corresponding pressure would be 81 bars. Accordingly, a buildup of pressure to 81 bars would prevent further inflow of water and further increase in pressure. The lithostatic pressure would be on the order of 193 bars, over twice the maximum probable pressure that would develop from leakage of water into the cavity and its conversion to steam.

In view of the above considerations, no hazard from secondary explosions was predicted.

2.2.10 Estimate of Prompt Venting

It was estimated that the likelihood of prompt venting to the surface through existing and shot induced fractures was remote. The possibility of venting by means involving man-made openings is discussed in Section 2.2.8.

Examination of the geologic settings for the Salmon Event did not indicate any potential fissures or faults which would permit the prompt transfer of radioactive products. The shot induced fractures were anticipated to extend to only 91 meters and collapse of the chimney, if any, was predicted to be less than 133 meters. Considering these distances in relation to the maximum spalling depth of 40 meters, it was seen that

$$823 - (133 + 40) = 650 \text{ meters}$$

of relatively undisturbed material would remain as a barrier to prompt release. This thickness was considered sufficient to prohibit any prompt venting by this means.

2.2.11 Damage to Grout Seals and Aquifer Contamination

Concern had been expressed that, as a result of the explosion, there could be relative movement of the casing and surrounding media, particularly at the depth of aquifers 1, 2 and 3. Such relative motion might cause damage to the seal established by grouting the space between the casing and the hole, particularly where grouting might not be sound.

An important consideration was that the casing (51 centimeter (20") OD, 197.9 kilograms per meter, J-55,

ST&C, 8rd), extended into the top of the halite to a total depth of approximately 670 meters. This placed the bottom at about 152 meters above the W.P. This was a distinctly different situation from that in other events where the explosion occurred at the bottom of the casing, causing it to be pushed upward. While precise calculations were not feasible, an approximate evaluation indicated that the relative motion of the casing and surrounding media would be unlikely to damage the seal if properly placed.

Should there be damage, two possibilities exist: (a) Flow of water between aquifers, and (b) Escape of radioactive gases if communication should develop between the cavity and bottom of casing. In either case it was difficult to find any reason for alarm. All aquifers penetrated by the Station 1A hole contained fresh water, and the head on each was such that flow through any channel along the casing would be small. Radioactive contamination outside the casing at this distance from the explosion was not believed to be a consideration. However, this was a question beyond the scope of Beers, Inc. contract.

The second possibility was felt to be very remote as communication was not likely on the basis of the circumstances predicted. These are described elsewhere in this report. An evaluation of the degree of damage to the grout seal was not possible since the effectiveness of grouting was indeterminate. However, on the basis of previous remarks, the escape of hazardous quantities of radioactive gases could not be visualized, even if communication was established between the cavity and the bottom of the casing.

2.2.12 Securing of Station 3 Holes

Reference 2.19 transmitted the Fenix and Scisson, Inc. proposal for providing a new Station 3A Access Shaft. This information was transmitted for the purpose of providing basic data on which to base predictions of damage to these shafts at Station 3 as a result of the Salmon Event. This Section pertains solely to means for securing Station 3 holes because the status of Station 3 holes was uncertain at the time predictions were made.

The vent and access holes were located approximately 610 meters from Station 1A Emplacement Hole. Insofar as containment was concerned, the possibility of any

communication between Station 3 holes and Station 1A was considered to be extremely remote.

Vent Hole - According to Reference 2.18 and the preliminary asbuilt drawing, this hole was drilled to a total depth of 636 meters, and the 76 centimeter (30") casing was bottomed at 50 meters. Difficulty was encountered in grouting, and a leak developed. Subsequent attempts to seal were unsuccessful, and shortly after drill rig demobilization, the water level was found to be 94.5 meters below the surface. Due to the aforementioned opinion regarding possibility of venting at this range, it was deemed satisfactory to stem this hole by filling approximately to the surface with water and, as an added safeguard, seal the top of the casing either with a grout plug or a welded cap.

Access Shaft - According to Reference 2.18, numerous difficulties were encountered in setting and grouting the 178 centimeter (70") casing which was ultimately bottomed at design depth of approximately 290 meters. After bailing to a depth of 119 meters several breaks in casing occurred, water was found to be entering the casing and grout invaded

the casing. Corrective measures were attempted, and efforts to continue drilling were made. However, obstructions were encountered and it was not possible to penetrate beyond 205 meters with a 162 centimeter (64") bit.

At one time, water was known to be at a depth of 114 meters; however, it was not known if this was the condition at the time of evaluation. Due to the aforementioned opinion regarding possibility of venting at this range, it was deemed satisfactory to also stem this hole by filling approximately to surface with water and, as an added safeguard, to seal the top of the casing either with grout plug or welded cap.

2.2.13 Containment Predictions

On the basis of the results of the foregoing evaluations and the assumption that construction and emplacement would be accomplished in accordance with the proposed construction and emplacement plans, it was predicted that the Salmon detonation at a yield of 5 kt would be essentially contained.

2.3 SEISMIC EFFECTS

2.3.1 Prediction Methods

Predictions of particle motions, for the Salmon model described in Chapter 1, were made using the procedures

discussed below. A tabulation of predicted motion at various distances is provided in Table 2.8.

2.3.1.1 Acceleration

Predictions of peak surface particle acceleration were based on the observed radial accelerations measured in salt at Gnome (References 2.10 and 2.20) and illustrated in Figure 2.10 in scaled form, i.e., scaled acceleration versus scaled distance. Surface accelerations for Salmon were determined from this graph in the following manner. Given the yield and distance, the scaled distance was computed by dividing distance by the cube root of the yield, and the corresponding scaled acceleration was read from the graph. The scaled acceleration was converted to real acceleration by dividing by the cube root of the yield. At or near surface zero the value of acceleration was then multiplied by a factor of 3.52, called the compound transmission coefficient, which compensates for alterations of amplitude due to the free surface and the various stratigraphic units which would be traversed by the seismic waves which reach the surface. The compound transmission coefficient is the product of transmission coefficients computed at each interface encountered. Each transmission coefficient, T,

at an individual interface was computed using

$$T = \frac{2\rho_1 c_1}{\rho_2 c_2 + \rho_1 c_1} \qquad (2.3)$$

where ρ is density, c is sonic velocity and subscripts 1 and 2 refer to the incident and transmitting media respectively. This equation is valid only at normal incidence. Computation of the coefficient at other angles of incidence was quite complex and required accurate ray tracing which in the case of the Tatum Dome was not feasible. Therefore, the values computed from the above equation were used near surface zero only. At all other locations, a factor of 2.0 was used. A graphical display of predicted acceleration versus distance is given in Figure 2.11.

2.3.1.2 Velocity

At Gnome, subsurface measurements of radial particle velocity in salt were made by Sandia Corporation (Reference 2.10) and Stanford Research Institute (Reference 2.20). A least squares regression line through these data yielded the following relationships between velocity and distance:

$$u = 3.04 \times 10^6 \, R^{-1.64} \qquad (2.4)$$

where particle velocity, u, is in cm/sec and distance, R, is in meters. Utilizing point source cube root scaling

theory where

$$u = K\left(\frac{R}{W^{\frac{1}{3}}}\right)^{n} \tag{2.5}$$

equation 2.4 was written

$$u = 1.63 \times 10^{6}\ W^{.55}\ R^{-1.64} \tag{2.6}$$

where the yield, W, for Gnome was assumed to be 3.1 kt. Multiplying equation 2.6 by the compound transmission coefficient (3.52) gave

$$u = 5.74 \times 10^{6}\ W^{.55}\ R^{-1.64} \tag{2.7}$$

which was the equation used to obtain Salmon surface predictions of peak particle velocity at surface zero. For other locations equation 2.6 was multiplied by 2.0 yielding

$$u = 3.26 \times 10^{6}\ W^{.55}\ R^{-1.64} \tag{2.8}$$

The resulting predictions of particle velocity versus distance are shown in Figure 2.12.

2.3.1.3 Energy Ratio

The energy ratio, ER, is defined as

$$ER = \frac{a^2}{f^2} \tag{2.9}$$

where a is acceleration in cm/sec/sec and f is frequency in cycles/sec. Using the simple harmonic motion relationship

$$a = 2\pi f\ u \tag{2.10}$$

where u is particle velocity in cm/sec (since a is in cm/sec/sec), the energy ratio may be expressed

$$ER = 4\pi^2 \quad u^2 \tag{2.11}$$

for particle velocity, u, in cm/sec, thus

$$ER = \frac{4\pi^2 \quad u^2}{(30.48)^2} \tag{2.12}$$

Energy ratio predictions versus distance are given in Figure 2.13.

2.3.1.4 Displacement

Recorded displacement data at Gnome was not considered to be of equal reliability to the acceleration and velocity data. Consequently, simple harmonic motion was assumed; and displacements computed using the relationship

$$d = \frac{u^2}{980a} \tag{2.13}$$

where d = displacement in centimeters

u = particle velocity in cm/sec at the same distance at which displacement is required

a = particle acceleration in units of gravity (g) at the same distance at which displacement is required.

Displacement predictions are shown graphically versus distance in Figure 2.14.

2.3.2 Hazards to Existing Facilities

Based on the prediction procedures just discussed, it was predicted that 0.1g, and therefore possible damage, would extend to a distance of 7.24 km from surface zero. It was also predicted that ground motion would be perceptible at a distance of 48.27 km from surface zero, assuming 0.001g to be the limiting value of perceptibility. The relationship of these predicted distances to the surrounding population centers is shown on Figure 2.15.

The evaluation of possible damage also included consideration of all oil and gas wells and pipelines in the vicinity. The characteristics of these structures were described in detail in Reference 2.21. Briefly, the nearest pipeline (United Gas) was a 40 cm (16") line, passing at a distance of 4.5 kilometers from surface zero, and operating at a pressure of 68.97 bars. It was buried in about one meter of clay and soil.

For gas wells, the State of Mississippi requires the producing stringer to be cemented into the casing from the surface to a depth of 152.4 meters and from the bottom of the casing to a height of 518.6 meters. If the distance is less than 671 meters the complete well is cemented.

The casing is 27 cm (10 3/4") in diameter. The casing requirements for oil wells vary. All of the wells considered had casing at least to a depth of 259.08 meters and were generally tested for 144.83 bars.

Predicted peak motions at pertinent facilities are listed in Table 2.9. During the 1952 California earthquake, buried steel pipes at the Paloma Cycling Plant received damage only where they were placed in very poor soil (Reference 2.22).

Also, in nuclear tests, pipe lines exposed to ground shock have shown a high resistance to damage. In general, based on results of bombing in Japan, damage occurred only to subsurface pipes where they passed from a relatively rigid soil into fill. Considering the above general factors and the high pressure carried which would require rugged construction, it was believed that the pipe line would not be damaged by the indicated ground motions (Table 2.9).

The oil and gas wells were considered safe and support was given for this conclusion by data shown in Table 2.10.

An evaluation of possible damage to the Sand Shaft then under construction by the Salmon event was made in

March 1963. It was concluded that there was very small possibility of damage to the cased sections of the access and vent shafts and to grout seals around the casing which might allow water to flow into access and vent holes. The possibility of tunnel damage was judged greater than that to unlined sections of the shafts because of the rectangular shape of the tunnel. It was stated that a final evaluation of damage possibilities to unlined sections of the shafts and the tunnel would have to consider the static tangential stresses at the time of the Salmon event, which would depend partly on the status of construction.

In September 1964 Roland F. Beers, Inc. was asked by Olin Mathieson Chemical Corporation (with approval of NVOO) to evaluate the effect of anticipated ground motions at their facilities at McIntosh, Alabama. The conclusion of this study was that no damage would occur at the Olin facilities.

TABLE 2.1 DRILL HOLES OF TATUM SALT DOME AREA, MARCH 1964 (All measurements in meters.)

Hole	Coordinates (New)		Elevation (Datum) GL-Ground Level C - Collar	Total Depth (Measured from Datum)	Limestone Caprock		Anhydrite		Salt	Reference
					Depth of Top Below Sea Level	Thickness	Depth of Top Below Sea Level	Thickness	Depth of Top Below Sea Level	
E-1	N635,240.99	E267,506.33	81.4 GL	1372.5	203.9	36.6	240.5	134.1	374.6	DR-8
E-2	N535,590.86	E268,672.29	78.9 GL	511.8[c]	196.6	>24.4	no samples		373.7	DR-16
E-3	N536,395.03	E270,833.63	76.2 GL	467.9[c]	212.1	39.3	251.5	123.1	374.6	DR-17
E-4	N537,915.26	E270,425.47	75.0 GL	1375.3	211.5	40.5	252.1	122.8	374.9	DR-12
E-5	N537,880.71	E267,162.10	76.8 GL	1070.8	213.7	29.0	242.6	133.5	376.1	DR-13
E-6	N538,050.45	E268,734.48	73.2 GL	911.7	192.0	46.3	238.4	137.2	375.5	DR-14
E-7	N535,597.66	E268,698.34	78.9 GL	1079.6	193.5	105.2[a]	298.7[a]	74.7[a]	373.4	DR-16
E-9	N536,390.38	E270,916.59	75.6 GL	1070.2	221.9	30.2	252.1	123.4	375.5	DR-17
E-11	N536,856.87	E267,585.96	84.4 C	1079.0	205.1				377.0	
E-12	N537,330.87	E267,623.85	86.0 C	878.4	200.6				374.3	
E-13	N537,047.73	E268,098.43	82.6 C	875.1	200.9				374.9	
E-14	N537,199.25	E269,006.28	73.8 C	1220.7	199.3				375.8	
E-15	N537,414.13	E269,491.64	73.5 C	777.2	194.5	41.8	236.2	138.1	374.3	Densilog
E-16[b]	N537,414.35	E269,591.63	proposed							
E-8	N538,530	E271,160	proposed							
E-14T	N537,199.25	E268,986.28	73.8 C	509.0	196.3				374.6	
E-14B	N537,121.75	E269,026.12	73.8 C	1024.1	201.8				376.4	
HT-1	N5[illegible].390	E272,660	96.0 GL	795.5	off dome					DR-6
HT-1A[d]	N539 [illegible]40	E272,400	86.3 C	334.0	off dome					
HT-1B[d]	N539 [illegible]0	E271,880	82.9 C	271.0	off dome					
HT-2	N532,750	E265,455	89.9 GL	797.1	off dome					DR-7
HT-2A[e]	N532,610	E265,830	89.6 C	329.2	off dome					
HT-2B[e]	N532,380	E266,380	89.0 C	306.3	off dome					DR-37
HT-3	N535,800	E268,730	81.4 GL	320.6	205.7±					DR-31,37,
HT-4	N535,800	E268,770	81.1 C	144.8	does not reach caprock					Sonic Log
HT-5	N535,780	E268,730	80.5 C	207.3	does not reach caprock					
HT-6	N535,800	E268,780	81.1 C	247.5	does not reach caprock					DR-37
HT-7	N535,790	E268,680	80.8 C	268.8	does not reach caprock					

Notes:
a. 243.8-298.7 meters, fault zone
b. E-16 conductor pipe was cemented in and abandoned; elevation top of pad - 73.50 meters
c. Abandoned
d. HT-1A and -1B are observation wells 1 and 2 respectively.
e. HT-2A and 2B are observation wells 3 and 4 respectively.

TABLE 2.2 DRILL HOLES OF TATUM SALT DOME AREA, MARCH 1964 (All measurements in meters.)

Hole	Coordinates (New)		Elevation (Datum) GL - Ground Level C - Collar RT - Rotary Table	Total Depth (Measured from Datum)	Limestock Caprock		Anhydrite		Salt	Reference
					Depth of Top Below Sea Level	Thickness	Depth of Top Below Sea Level	Thickness	Depth of Top Below Sea Level	
FS #1	N534,820	E268,545	87.8 GL	483.7	333.5	20.4	353.9	29.6	383.4	f,h,l
FS #2	N534,540	E266,940	84.4 GL	618.4	456.9	2.4[g]	459.3	18.3	off dome	f,h,l
FS #3	N537,010	E268,110	87.8 GL	469.4	204.5	31.7	237.1	140.5	377.0	f,h,l
FS #4	N537,550	E269,740	75.3 GL	317.3	188.1	44.5	232.6	> 9.4		f,h,l
FS #5	N538,325	E268,190	75.9 GL	333.8	197.5	37.8	235.3	>22.6		f,h,l
FS #6	N535,820	E266,940	86.9 GL	471.2	271.6	65.8	337.4	34.1	371.6	f,h,l
FS #7	N535,090	E270,830	76.8 GL	636.1	off dome					f,h,l
FS #8	N536,020	E270,120	75.6 GL	370.3	214.9	20.7	235.6	>59.1		f,h,l
FS #9	N539,150	E268,210	79.2 GL	476.1	272.2	38.7	310.9	65.5	376.4	f,h,l
FS #10	N537,400	E266,910	82.6 GL	393.5	220.4	38.1	258.5	>52.4		f,h,l
Shell Hibernia #1	N536,740	E265,400	103.0 RT	2915.4	441.0	48.8[g]				DR-1,h,i
Humble Hibernia #1	N533,760	E272,840	101.5 GL	1828.2	off dome					h,l
Willmut #1	N535,680	E268,450	83.8 GL	597.1	220.4	30.5	250.9	126.8	377.6	DR-1,h,l
Willmut #2	N533,310	E273,020	112.8 RT	2462.8	off dome					h,l
Willmut #3	N534,220	E266,670	87.2 RT	2120.2	off dome				2011.7	DR-29,h,l
Willmut #4	N533,850	E269,890	80.8 GL	1440.5	off dome					h,l
WP-1	N537,263.56	E267,949.31	82.6 GL	1067.1	198.1	36.3	234.4	140.5	374.9	DR-15
WP-4	N536,303.98	E269,172.86	74.4 GL	1065.8	207.0	26.2	233.2	142.3	375.5	DR-19
STA. 1[j]	N537,328.14	E269.540.96	73.5 C	502.9±						
STA. 1A	N537,358.14	E269,540.96	73.5 C	incomplete						
STA. 2	N537,011.77	E268,228.55	proposed	609.6[k]						
STA. 3[i]	N537,198.21	E267,553.84		609.6[k]						
Vent	N537,180.52	E267,544.51	86.6 C	816.9						
Access[j]	N537,273.38	E267,593.51	86.3 C	289.6±	does not reach caprock					

Notes:
f. H & N Drawing E-055-C4, 4/10/61
g. Caprock overhang
h. Letter: OSA:RLK 923, Enclosure: "Tabulation Pre-Dribble Holes"
i. Subsurface W.P.
j. Abandoned
k. Proposed depth, LRL drawing L6-15364, 10/31/62
l. H & N drawing, E-055-C3, 4/19/61

TABLE 2.3

PHYSICAL PROPERTIES: Tatum Salt Dome
Section Over Dome

	Rock Unit	Compressional Velocities (meters/sec)			Natural Bulk Density (g/cc)		
		min.	max.	mean	min.	max.	mean
Sediments	Costal Terrace Deposits	--	--	365.8[d]	1.9[j]	2.05[j]	1.98
	Pascagoula & Hattiesburg	1752.6[a]	1874.5[a]	1809.0	1.60[e]	2.21[e]	1.93[e]
	Catahoula Sandstone	1905.0[a]	2383.5[a]	2142.7	1.88[e]	2.56[e]	2.05[e]
Caprock	Limestone	2377.4[a]	4724.4[a]	3301.0	2.24[f]	2.71[f]	2.47[f]
	Gypsum	2539.0[b]	2651.8[b]	2595.4	2.2[j]	2.4[j]	2.3
	Anhydrite	5547.4[a]	5861.3[a]	5699.8	2.85[f]	2.92[f]	2.90[f]
	Salt	4358.6[a]	4550.7[a]	4480.6[a,g]	2.13[d]	2.215[d]	2.181[j]

Porosity and Elastic Properties of Salt

	min.	max.	mean
Porosity %	1.53[h]	8.59[h]	3.61[h]
Poisson's Ratio	0.215[g]	0.267[g]	0.239[g]
Shear Modulus (kilobars)	133.[g]	149.[g]	142.[g]
Young's Modulus (kilobars)	325.[g]	371.[g]	348.[g]
Bulk Modulus (kilobars)	224.[g]	244.[g]	230.[g]
Tensile Strength (kilobars)	5860.	10140.	8280.
Compressive Strength (kilobars)			
Standard	3050.[h]	3700.[h]	3330.
L/D* = 1/1	4140.[h]	4450.[h]	4250.
L/D = 3/1	3240.[h]	3450.[h]	339[illegible].

*L/D = Length/Diameter Ratio

References Listed on Table 2.4

TABLE 2.4

PHYSICAL PROPERTIES: Tatum Salt Dome
Section Beside Dome

Rock Unit	Compressional Velocity (meters/sec) min.	max.	mean	Natural State Bulk Density (g/cc)
Coastal Terrace deposits	--	--	365.8[d]	1.98[j]
Pascagoula & Hattiesburg fms.	1920.2[c]	1953.8[c]	1941.6	1.93[e]
Catahoula Sandstone	2286.0[c]	2499.4[c]	2392.7	2.05[e]
Paynes Hammock & Chickasaway	2103.1[c]	2164.1[c]	2133.6	2.5[k]
Upper Vicksburg	2057.4[c]	2316.5[c]	2138.2	2.2[j]
Lower Vicksburg	3109.0[c]	3596.7[c]	3252.8	2.5[k]
Red Bluff Clay	2651.8[c]	2895.6[c]	2773.7	2.2[j]
Yazoo Clay	2103.1[c]	2255.5[c]	2145.8	2.2[j]
Moody's Branch fm.	2651.8[c]	3261.4[c]	3026.7	2.5[k]
Cockfield fm.	1981.2[c]	2240.3[c]	2133.6	2.2[j]
Cook Mountain fm.	2956.6[c]	3276.6[c]	3144.0	2.1[j]

References:
a. In hole Velocity logs on dome (see Tables 1 and 2)
b. In hole Velocity log WP-1, tabulated, in DR-19
c. In hole Velocity logs off dome (HT-1, HT-2, Humble Hibernia #1)
d. Seismic Profile of the Southeast Flank of the Tatum Salt Dome, UED Inc., Dec. '62
e. Gamma gamma density log, HT-3
f. Gamma gamma density log, E-15
g. Memo: D.M. Christensen, LRL-N May 14, 1963
Statistical Summary of Calculations from in hole Velocity logs: E-14, E-15, WP-1
h. RFB 4085, Petrographic Examination and Physical Tests of Cores, Tatum Salt Dome, Mississippi, Table 6, WES, Jan. 1963
j. Birch, Francis, 1942 Handbook of Physical Constants, GSA sp. paper 36
k. Heiland, C. A., 1946, Geophysical Exploration, Prentice-Hall

Unmarked means are by compiler.

TABLE 2.5

Physical Properties Applied to Calculation of the Compound Transmission Coefficient at HT-3, Tatum Salt Dome

	Rock Unit	Depth meters	Thickness meters	Description	Velocity meters/sec	Density gm/cc
Pascagoula & Hattiesburg fms., undifferentiated	15	0.0-32.0	32.0	Clay	1485.9(1)	1.94(2)
	14	32.0-54.9	22.9	Sand & Clay	1566.7(1)	1.90(2)
	13	54.9-114.3	59.4	Sand & Clay	1722.1(1)	1.96(2)
	12	114.3-144.8	30.5	Sand, Aquifer 1	1789.2(1)	1.70(2)
	11	144.8-179.2	34.5	Clay	1938.5(1)	2.00(2)
	10	179.2-204.8	25.6	Sand, Aquifer 2A	1889.8(1)	1.96(2)
	9	204.8-228.6	23.8	Clay	1966.0(1)	2.02(2)
	8	228.6-240.8	12.2	Sand, Aquifer 2B	1965.0(1)	1.96(2)
Catahoula Sandstone	7	240.8-253.0	12.2	Clay	1956.8(1)	2.00(2)
	6	253.0-265.2	12.2	Sand, Aquifer 3A	2005.6(1)	1.94(2)
	5	265.2-274.3	9.1	Clay	2179.3(1)	2.12(2)
	4	274.3-286.5(?)	12.2(?)	False caprock, sandstone	2133.6(3)	2.18(2)
Caprock	3	286.5(?)-323.1(?)	36.6(?)	Limestone caprock	3810.0(3)	2.47(4)
	2	323.1(?)-455.7	132.6(?)	Anhydrite	5791.2(3)	2.90(4)
	1	455.7-		Salt	4541.5(3)	2.17(4)

(1) From Sonic Log HT-3

(2) From Gamma-Gamma Density Log HT-3

(3) Generalized from sonic logs in various holes in dome

(4) From Gamma-Gamma Density Log E-15

TABLE 2.6

Approximate Physical Properties of the Stratigraphic Section

Tatum Salt Dome

Rock Unit	Depth Meter	Thickness Meter	Description	Velocity, V m/sec	Density, P gr/cm^3
11	0- 10.67	10.67	Soil, silt	1219.20(1)	1.70(1)
10	10.67- 62.79	52.12	Clay, silt, sand	1524.00(1)	1.85(1)
9	62.79-103.63	40.84	Clayey silt	1905.00(2)	1.95(1)
8	103.63-134.11	30.48	Sand	1600.20(2)	1.92(1)
7	134.11-152.40	18.29	Silt, caly	1828.80(2)	1.97(1)
6	152.40-182.88	30.48	Sand w/silt, clay	1706.88(2)	1.94(1)
5	182.88-204.22	21.34	Sand	1645.92(2)	1.93(1)
4	204.22-283.46	79.25	Clay, sand, silt	1981.20(2)	1.97(1)
3	283.46-320.04	36.58	Vuggy limestone	2651.76(2)	2.63(3)
2	320.04-460.25	140.21	Anhydrite	5861.30(2)	3.06(3)
1	460.25-822.96	362.71	Salt, massive	4480.56(2)	2.254(3)

(1) Estimated
(2) TL-DRIBBLE-15, Table V
(3) "Project DRIBBLE, Petrographic Examination and Physical Tests of Cores, Tatum Salt Dome, Mississippi", Technical Report 6-614, U. S. Army Waterways Experiment Station, Corps of Engineers, Vicksburg, Mississippi.

TABLE 2.7

Development of Compound Transmission Coefficients

Project DRIBBLE

Rock Unit	Vxp	2Vp	$V_{p1}+V_{p2}$	Transmission Coefficient, UP $\frac{2V_{p1}}{V_{p1}+V_{p2}}$	Compound Transmission Coefficient, UP	Transmission Coefficient, DOWN	Compound Transmission Coefficient, DOWN
Air	-	-			3.625		
			2,072.64	2		2	
11	2,072.64	4,145.28			1.762		1.762
			4,892.04	1.153		.847	
10	2,819.40	5,638.80			1.529		1.493
			6,534.15	1.137		.863	
9	3,714.75	3,42950			1.345		1.289
			6,787.13	.905		1.095	
8	3,072.38	6,144.76			1.485		1.411
			6,675.12	1.080		.921	
7	3,602.74	7,205.48			1.376		1.299
			6,914.09	.958		1.042	
6	3,311.35	6,622.70			1.437		1.353
			6,487.98	.979		1.021	
5	3,176.63	6,353.26			1.467		1.381
			7,079.59	1.103		.897	
4	3,902 96	7,805.92			1.330		1.240
			10,877.09	1.282		.718	
3	6,974.13	13,948.26			1.038		.890
			24,909.71	1.440		.560	
2	17,935.58	35,871.16			.720		.498
			28,034.76	.720		1.280	
1	10,099.18	20,198.36			1.000		.637

TABLE 2.8

Surface Peak Particle Motions

Horizontal Range From Surface Zero (km)	Acceleration (g)	Velocity (cm/sec)	Energy Ratio	Displacement (cm)
0	10.4	232	2340	5.3
.10	10.2	228	2260	-
1.53	1.8	38	69	-
2.09	1.2	25.0	25	-
2.74	.80	17	12	-
3.54	.50	12	6.0	.26
3.70	.45	11	5.0	-
4.34	.34	8.4	3.0	-
5.63	.19	5.4	1.3	-
6.11	.16	3.8	1.0	.14
7.24	.10	3.6	.60	-
8.04	.079	3.1	.42	-
9.17	.056	2.5	.27	-
9.81	.047	2.3	.21	.10
48.27	.001	-	-	-

TABLE 2.9

Maximum Predicted Surface Motions
On Oil and Gas Structures

Structure	Horizontal Range (km)	Maximum Predicted Acceleration (g's)	Maximum Predicted Velocity (cm/sec)	Energy Ratio
United Gas Pipe Line	4.31	.31	7.9	2.6
Nearest Oil Well	7.72	.09	3.3	.48
Nearest Gas Well	7.72	.09	3.3	.48
Baxterville Dehydration Plant	9.65	.05	2.3	.23

TABLE 2.10

Surface Motions On Oil Wells
Near GNOME Event Which Were Undamaged

Well	Horizontal Range (km)	Peak Particle Acceleration (g)	Peak Particle Velocity (cm/sec)
Texaco #1 Remrida Basin Unit	7.08[a]	about .1[b]	(?)
Shell James Ranch #1	9.81	.094[c]	2.17[c] 2.93

(a) PNE-127F.
(b) PNE-150F, Figure 3.
(c) Beers, Inc. Memo to O. H. Roehlk, December 20, 1962.

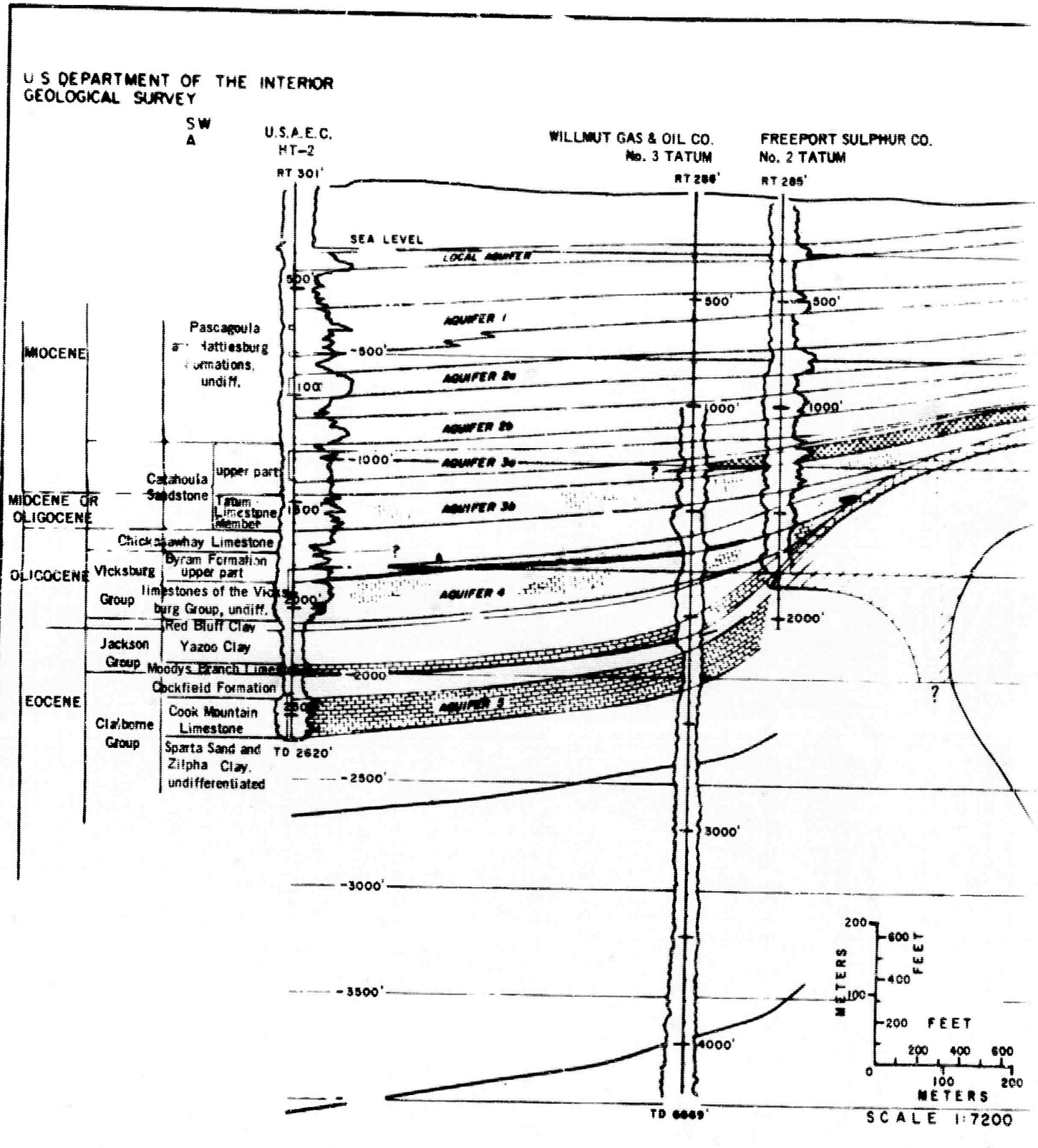

Drafted by B. O Davis
U.S.G.S. Austin, Texas
February 26, 1963

A

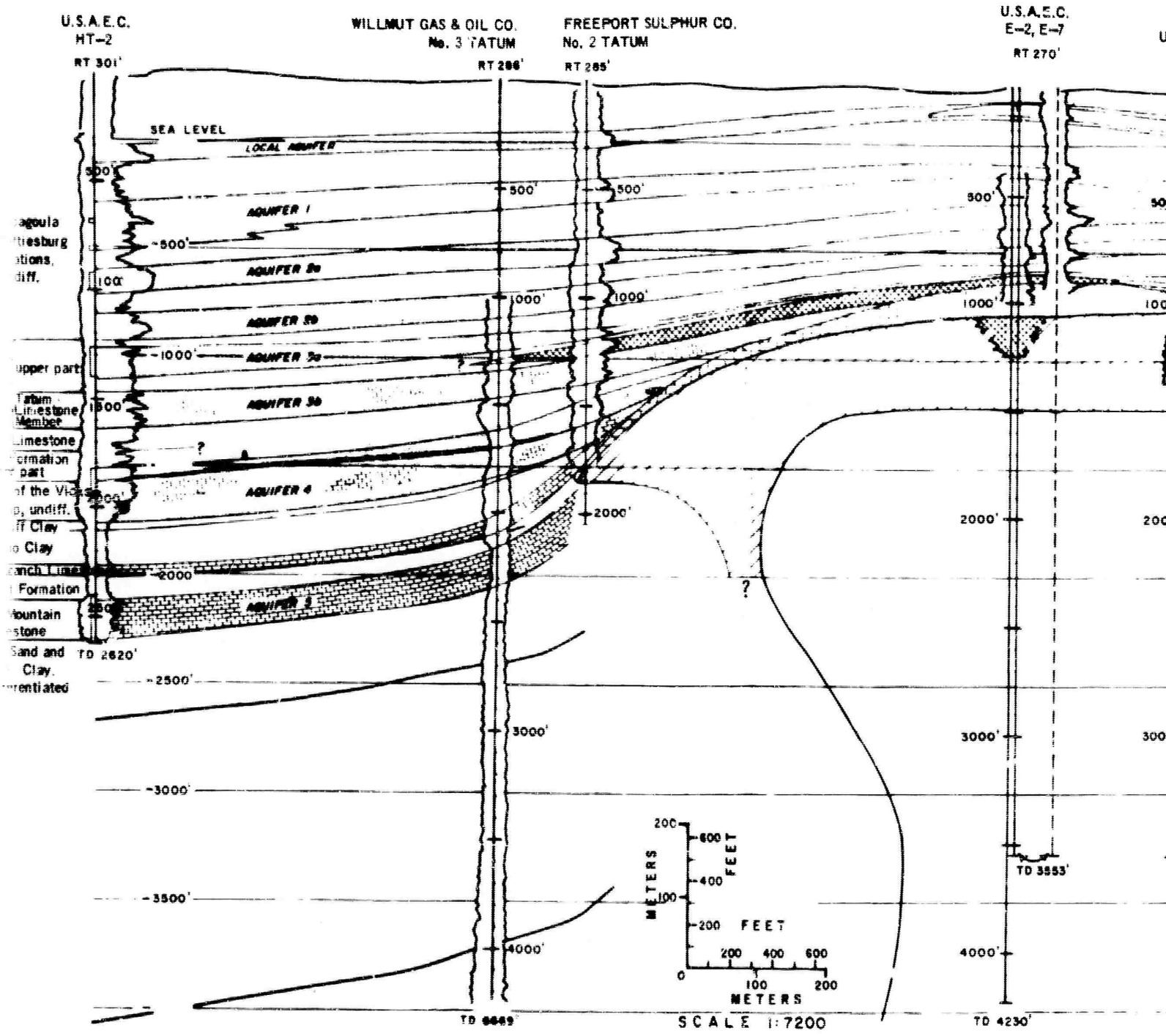

FIGURE 2.1 – SOUTHWEST

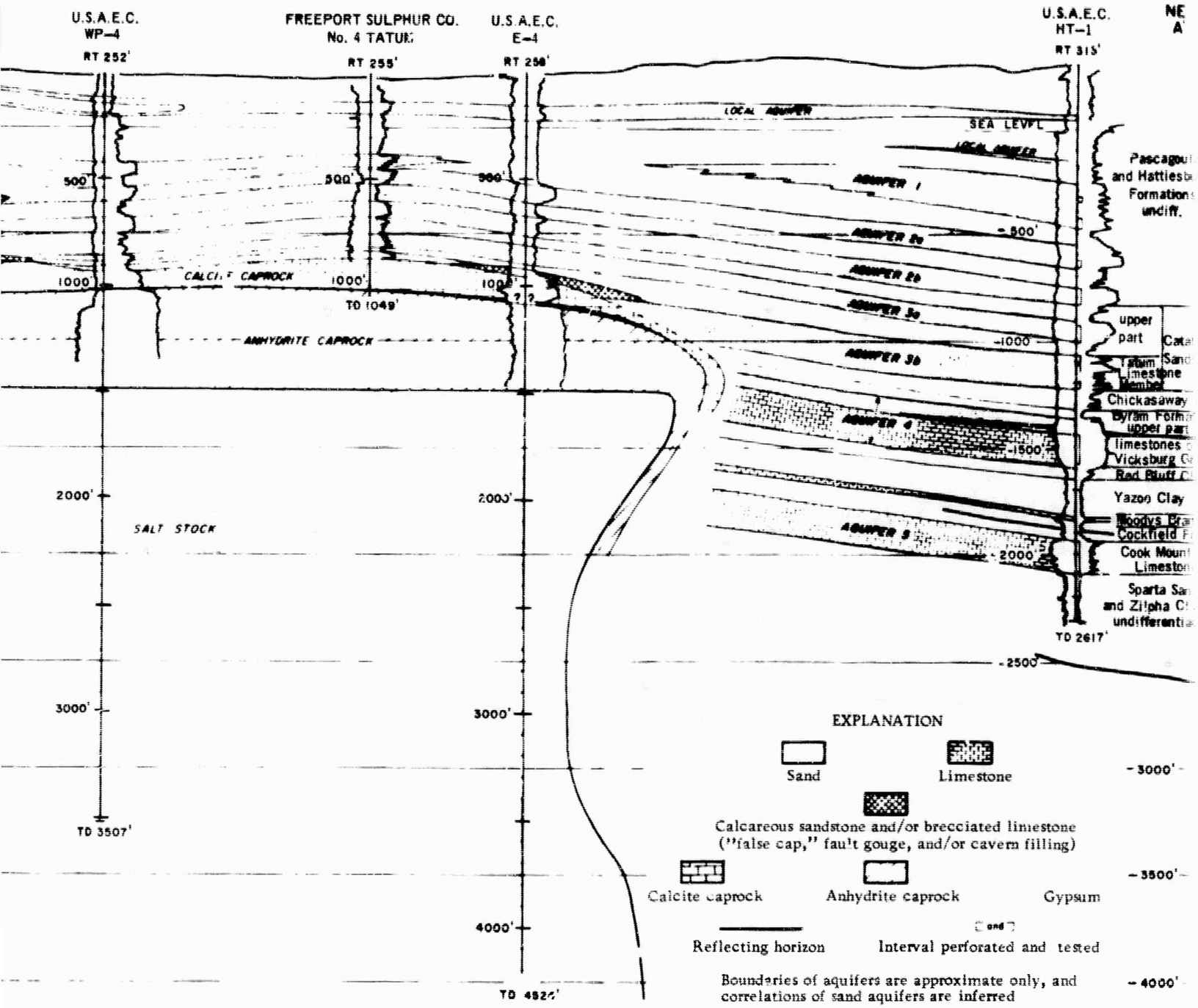

HWEST–NORTHEAST SECTION THROUGH TATUM DOME

Modified after Figure 2,
USGS Tech. Letter,
DRIBBLE-29, April 3,

TECHNICAL LETTER
DRIBBLE-29

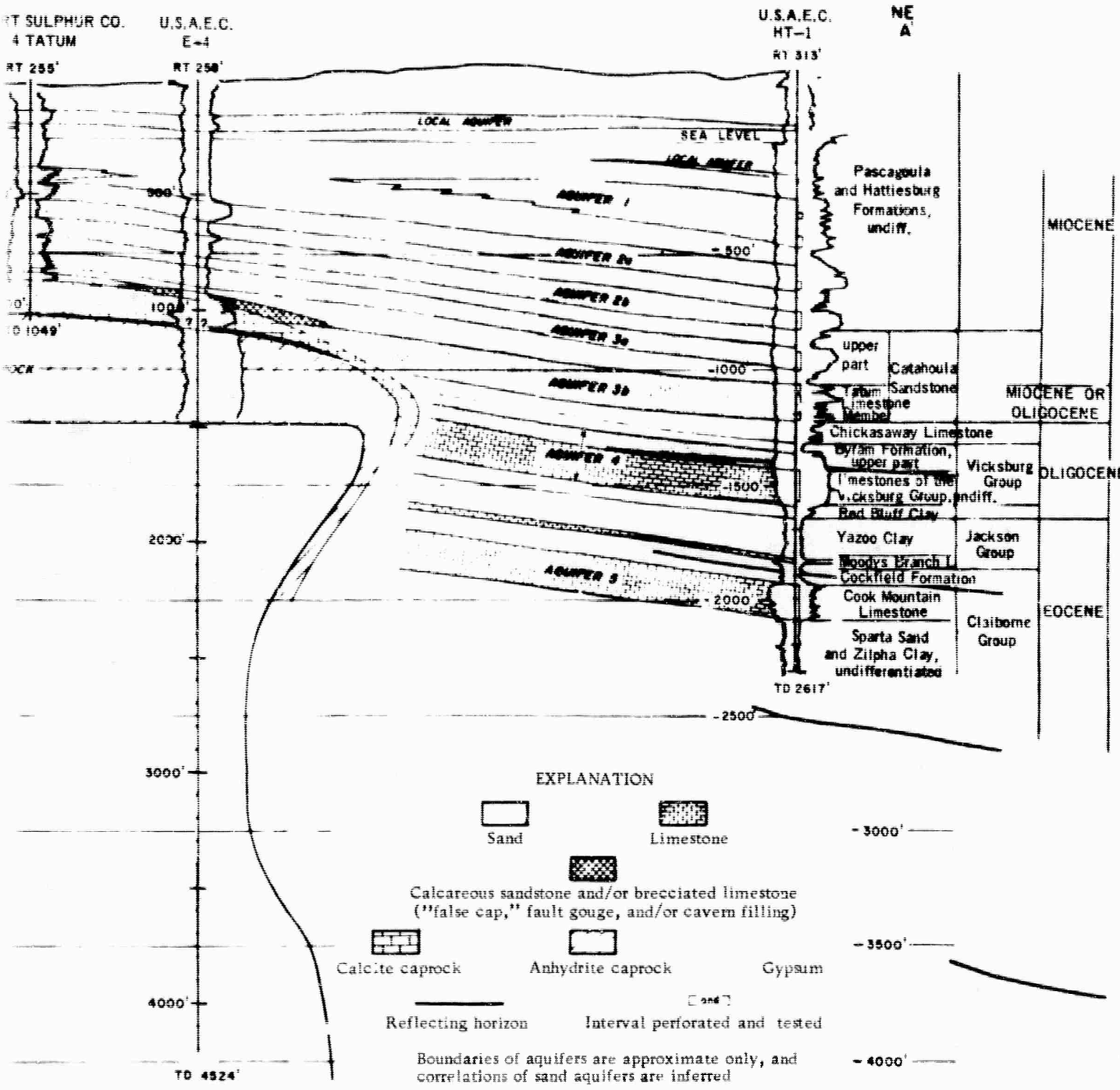

THROUGH TATUM DOME

Modified after Figure 2,
USGS Tech. Letter,
DRIBBLE-29, April 3, 1963

D

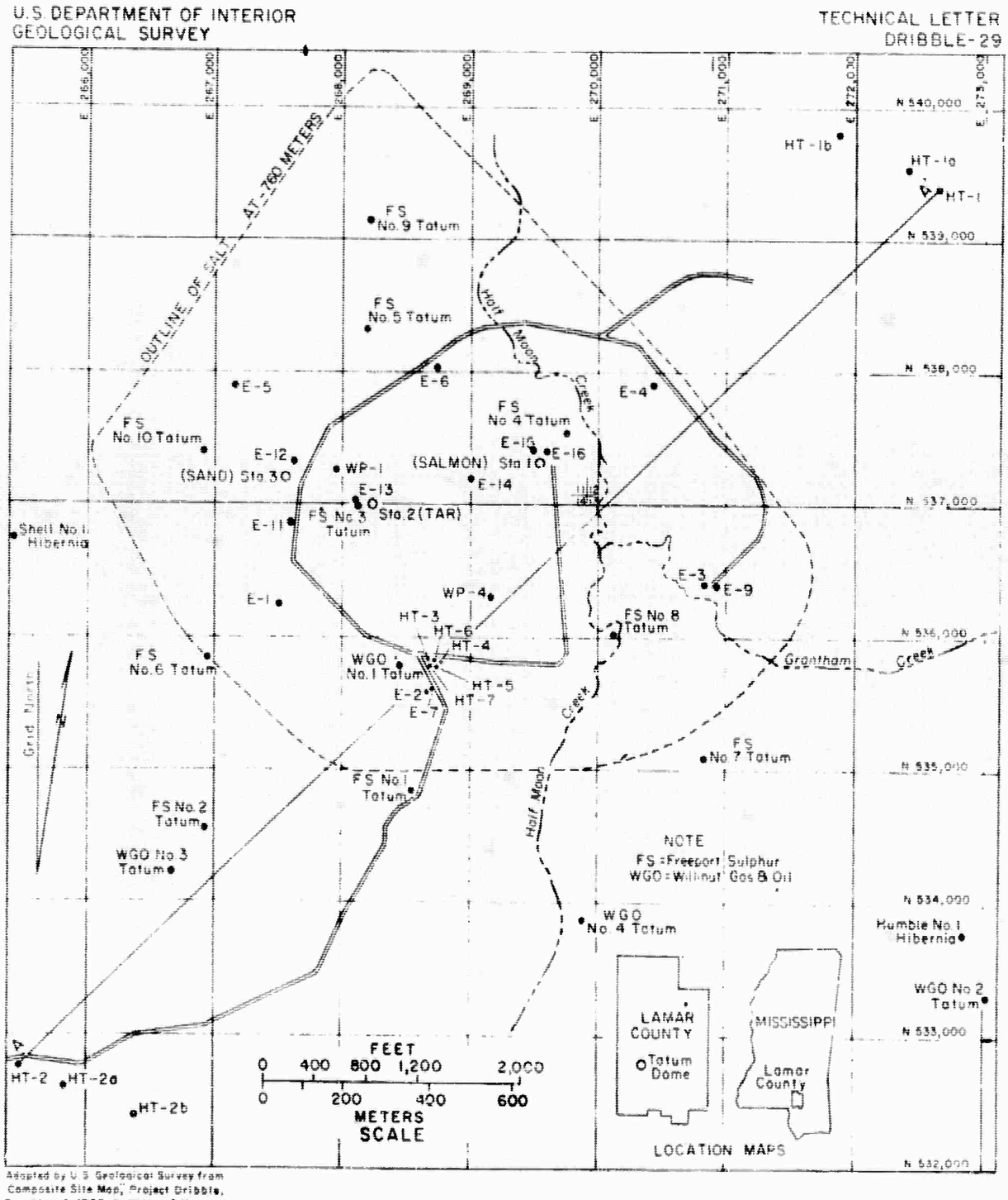

Adapted by U.S. Geological Survey from Composite Site Map, Project Dribble, December 4, 1962, by Holmes & Narver, Inc.

Figure 2.2 Map of Tatum Dome Area Showing All Holes Drilled on Dome
(Note: A-A' is location of cross section, figure 2.1)

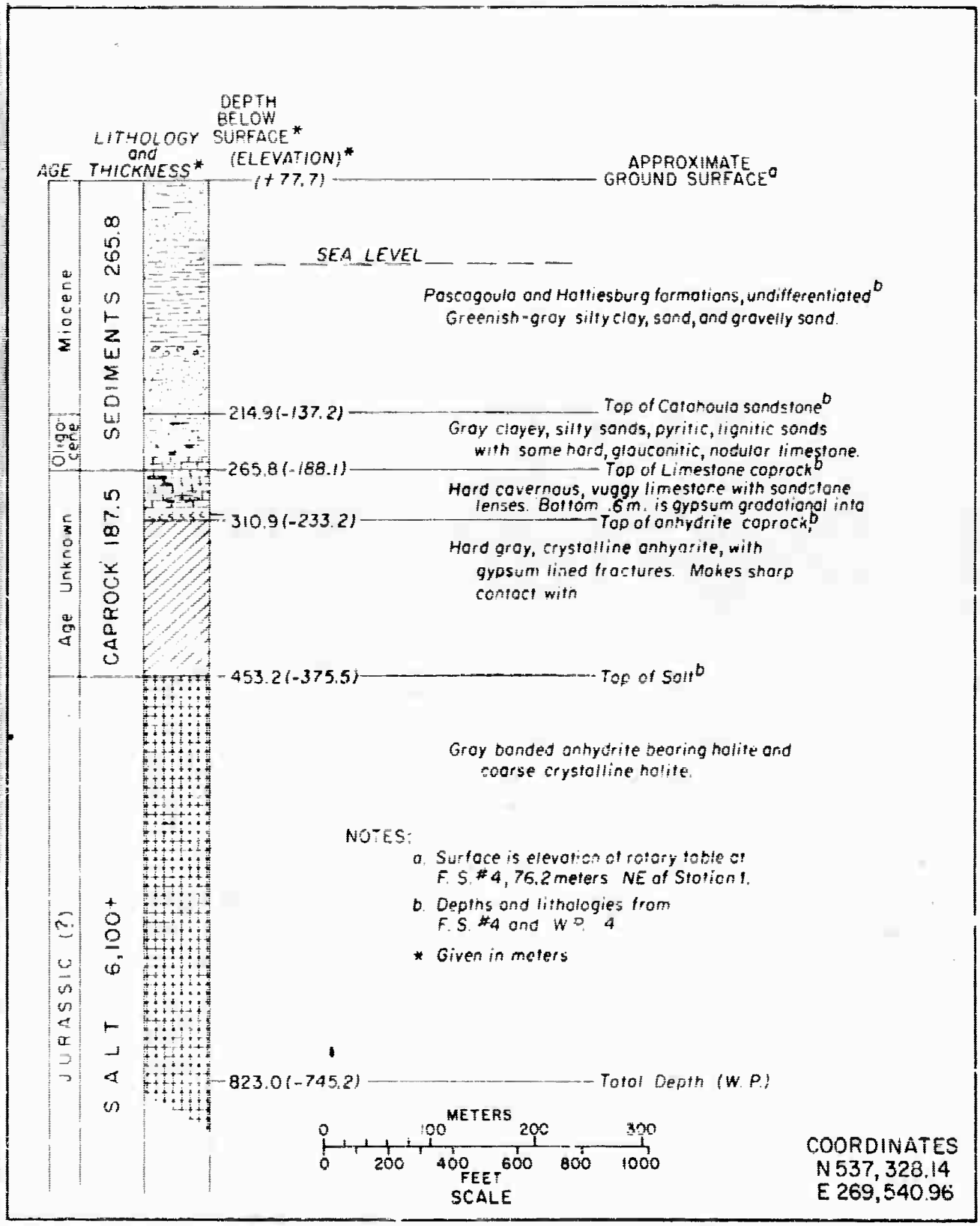

Figure 2.3 Generalized Stratigraphic Section Salmon (Station 1)

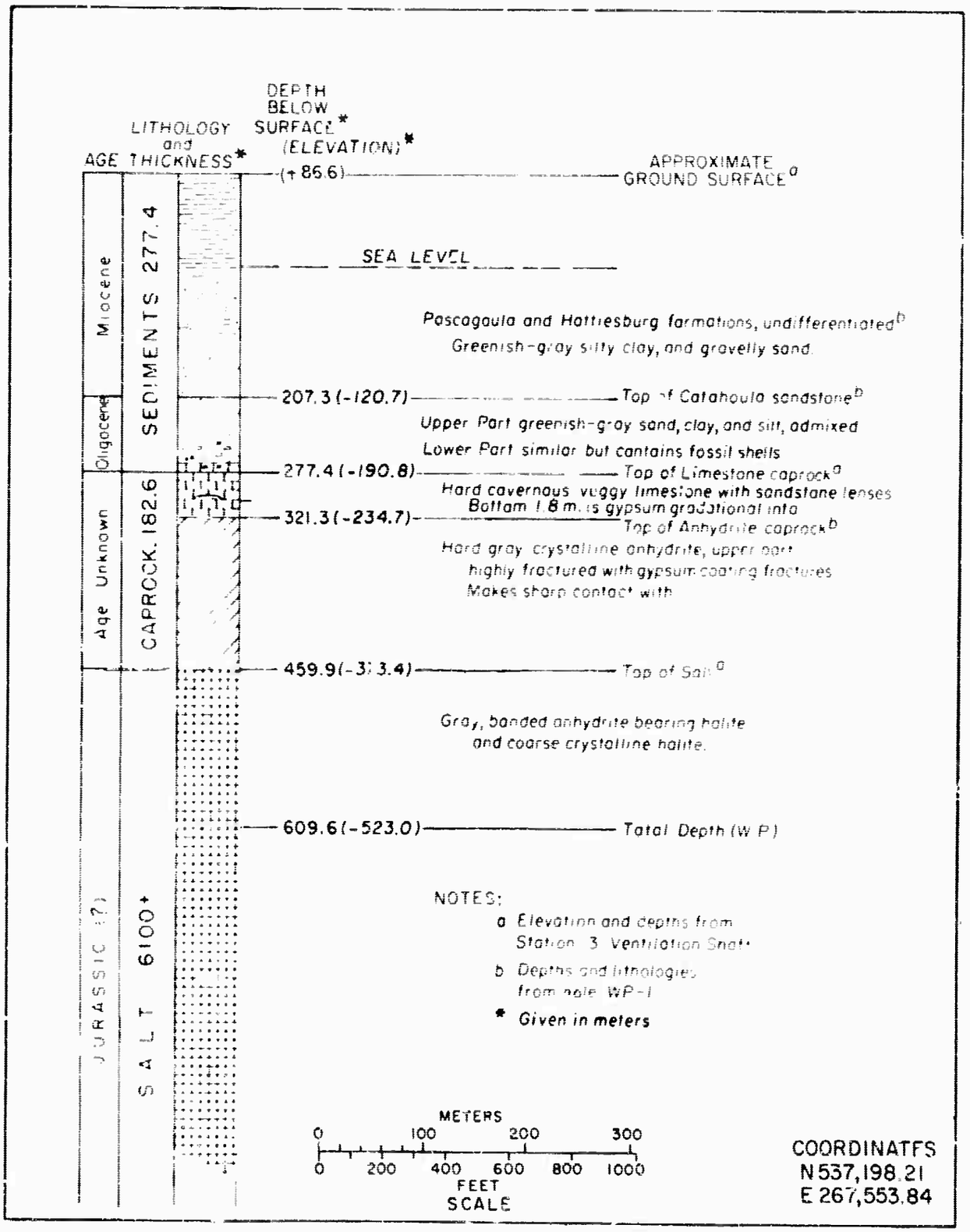

Figure 2.4 Generalized Stratigraphic Section Sand (Station 3)

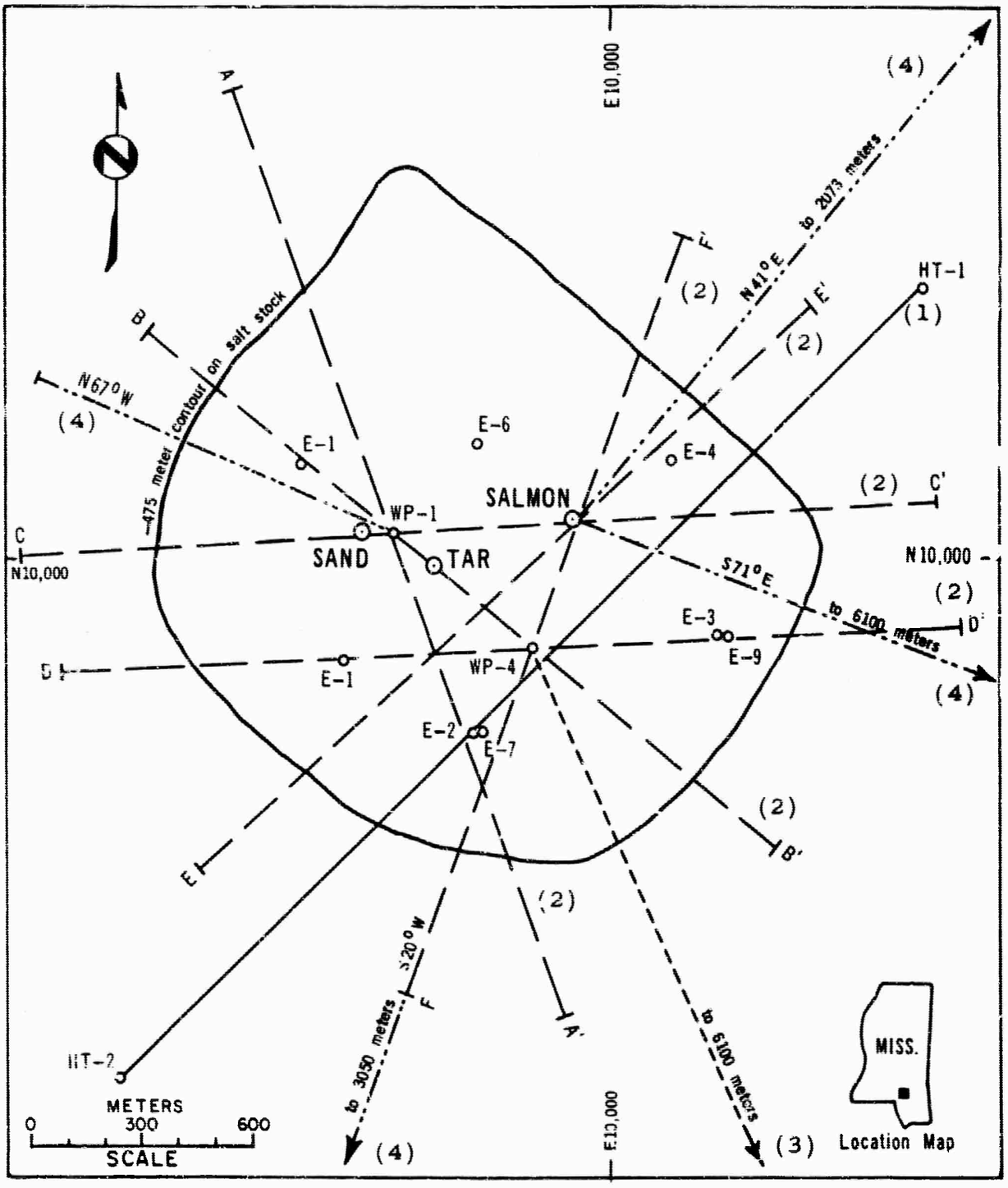

Figure 2.5 Map Showing Location of Cross-Sections.

References:

(1) DRIBBLE-29.
(2) DRIBBLE-1, includes sections A-A' through F-F'.
(3) RFB 4094 - (Project DRIBBLE, Seismic Profiling of the Southeast Flank of the Tatum Salt Dome. UED, Inc., Dec. 1962).
(4) Beers, Inc. files, compiled from DRIBBLE-1 and DRIBBLE-1C.

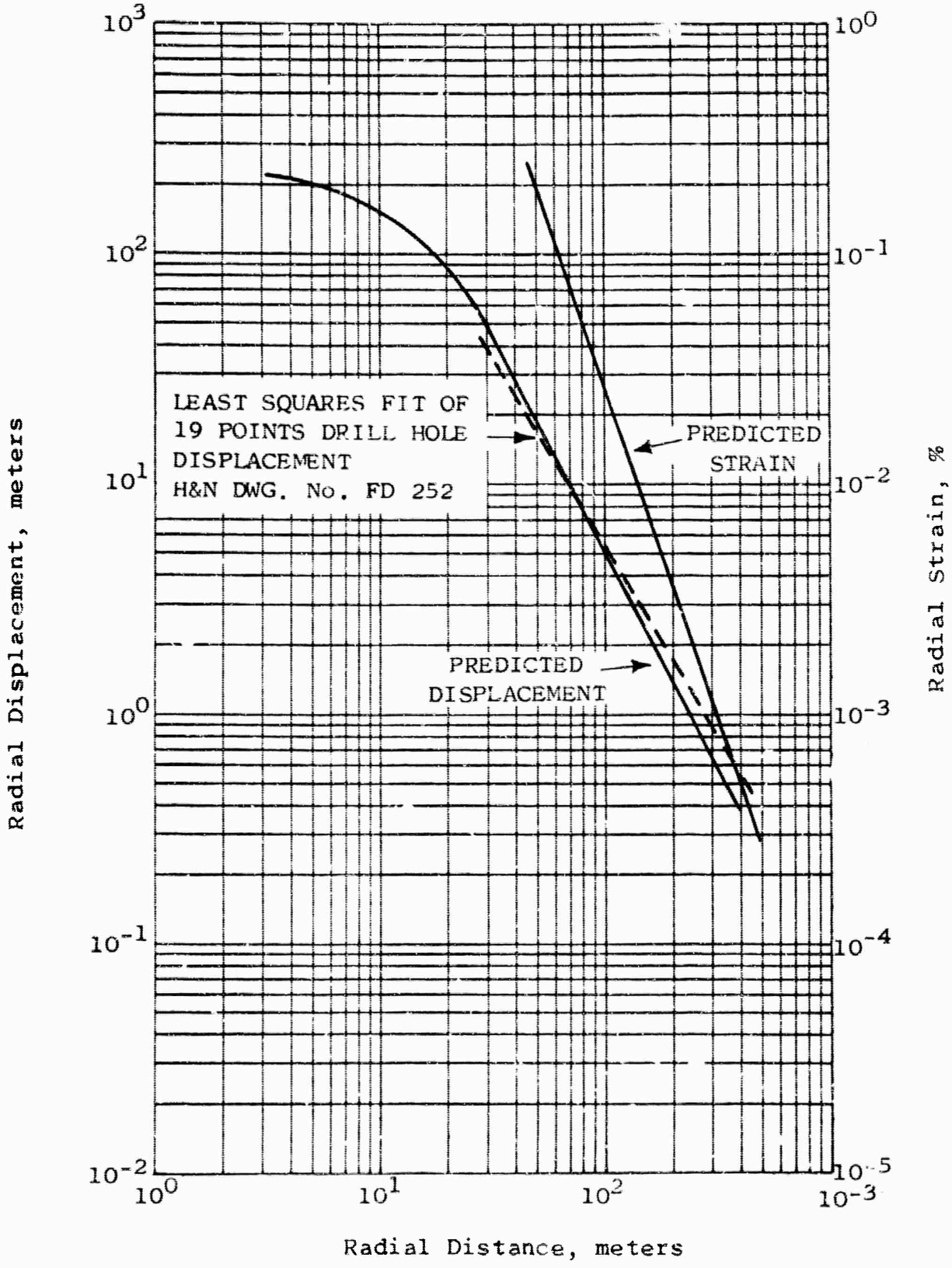

Figure 2.6 Predicted and Observed Radial Displacement and Strain versus Radial Distance, Gnome.

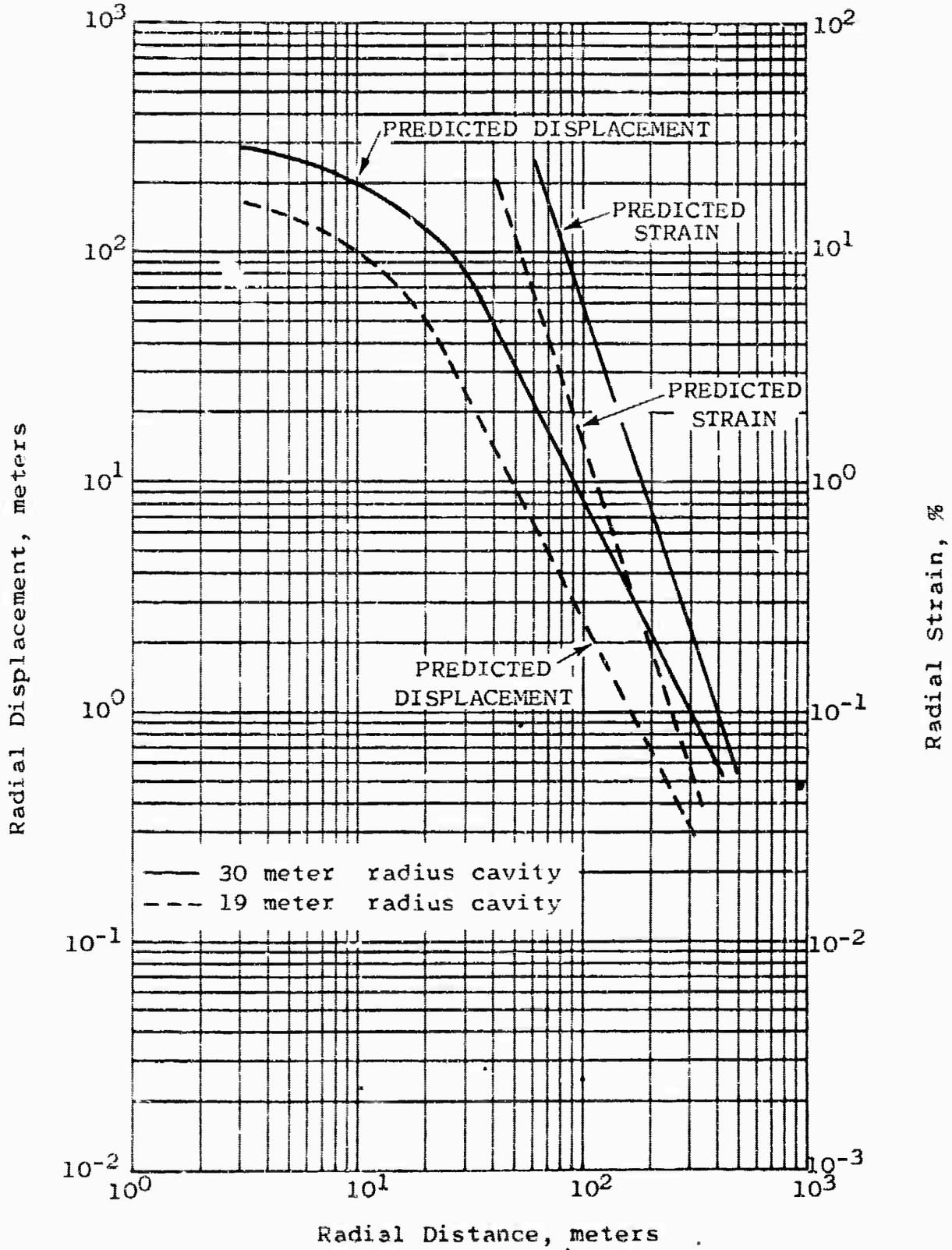

Figure 2.7 Predicted Radial Displacement and Strain versus Radial Distance, Salmon Event

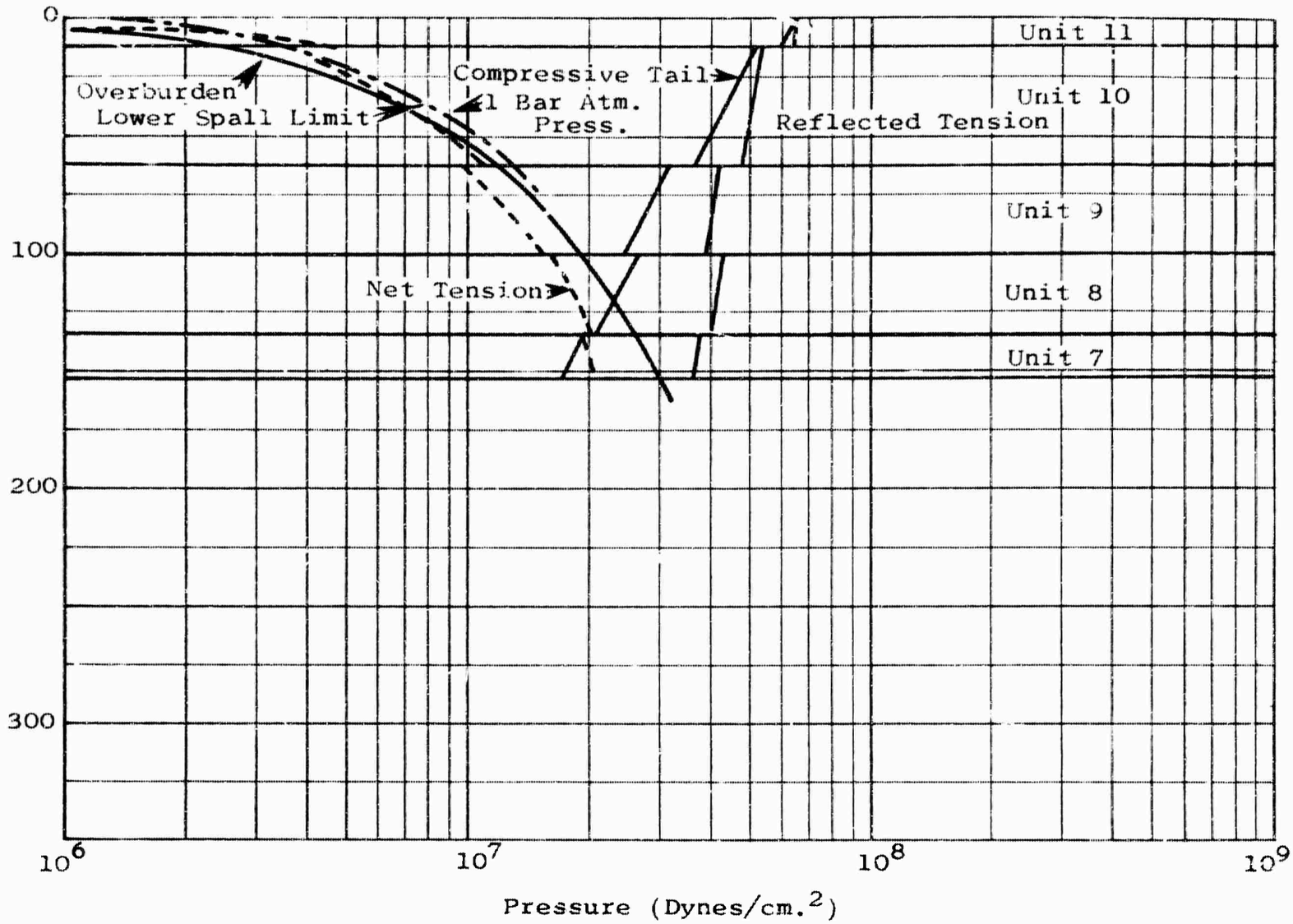

Figure 2.8 Predicted Pressure versus Depth, Salmon Event.

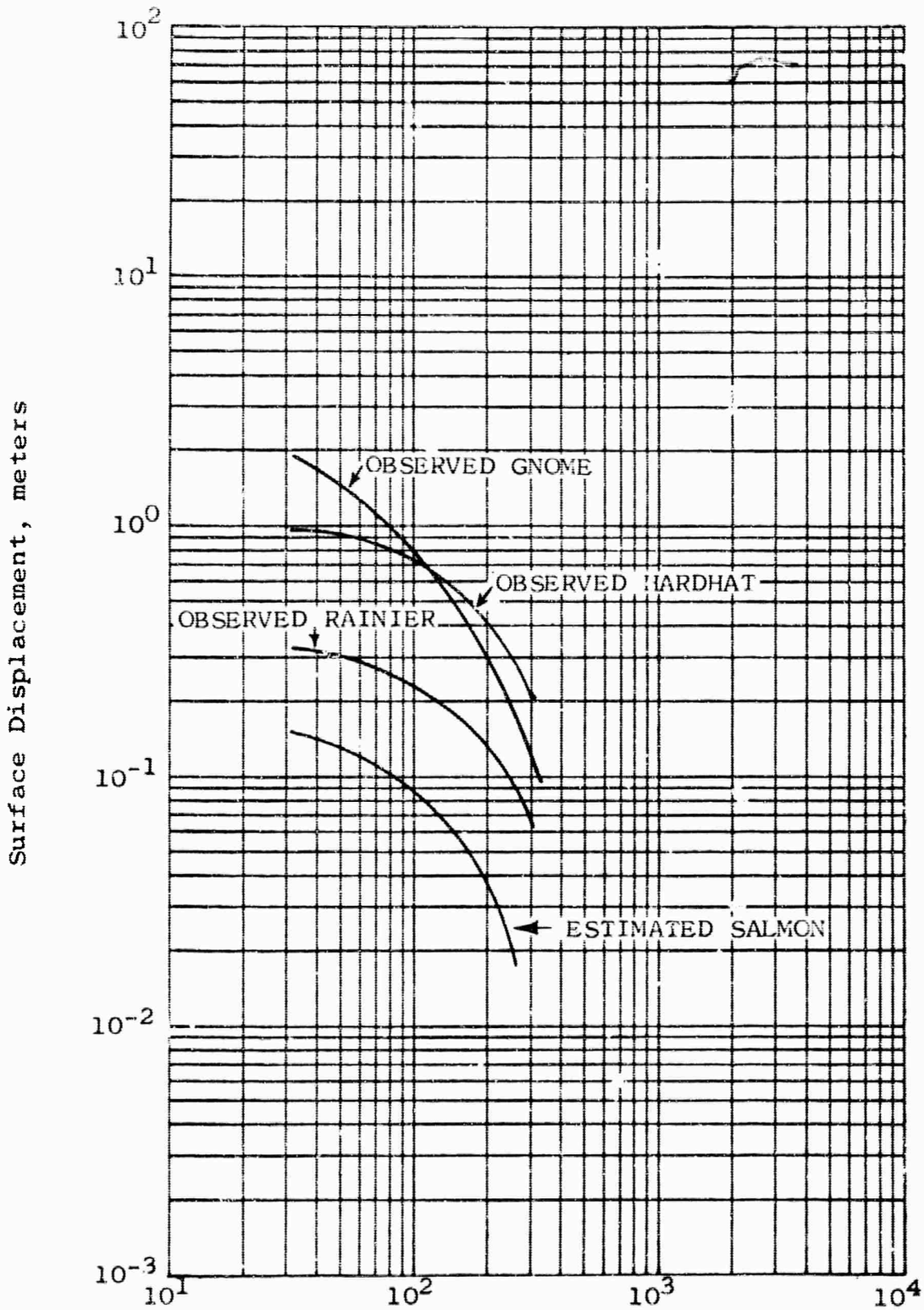

Figure 2.9 Surface Displacement versus Horizontal Distance.

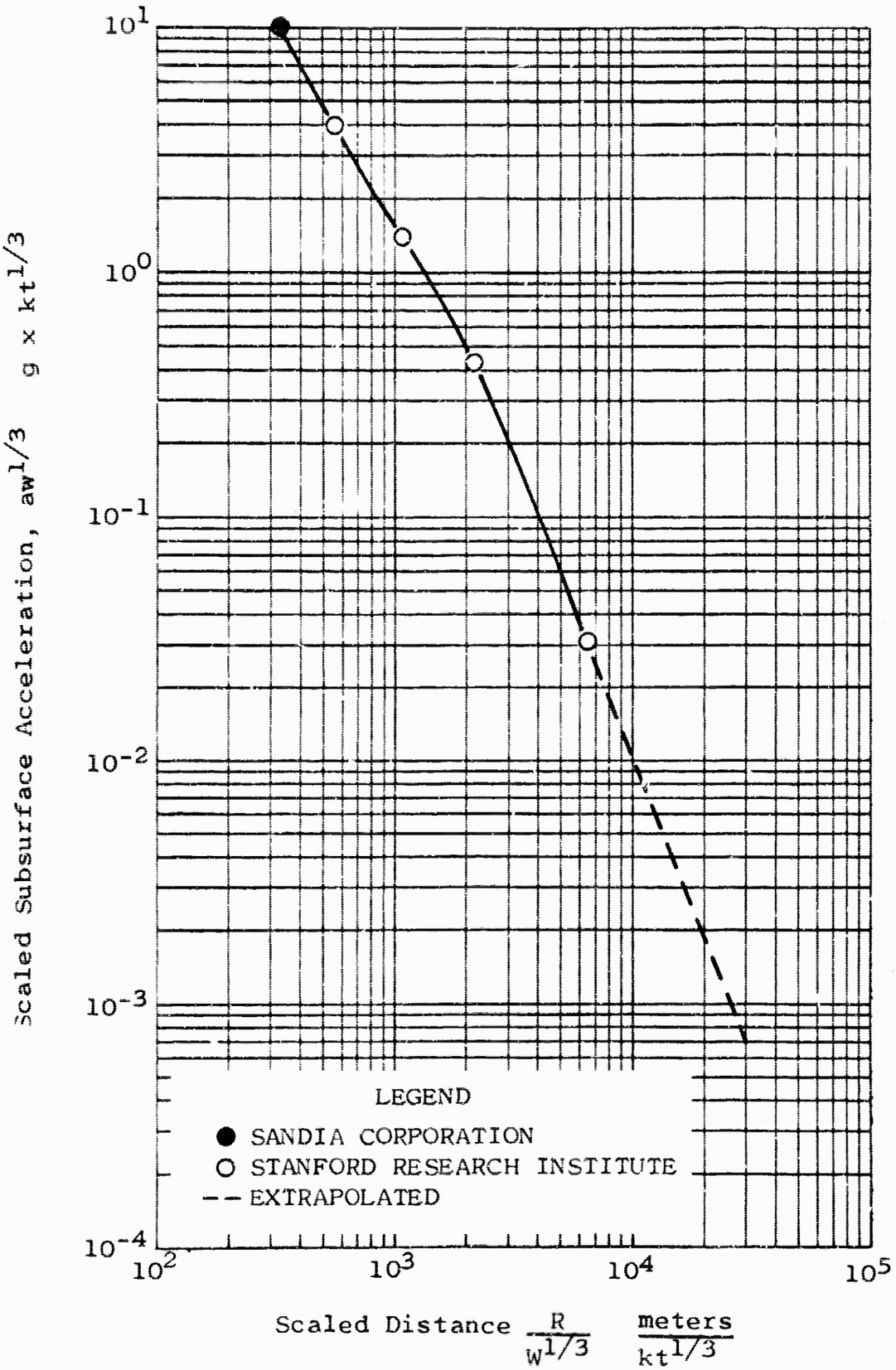

Figure 2.10 Scaled Subsurface Acceleration Observed at GNOME Versus Scaled Distance

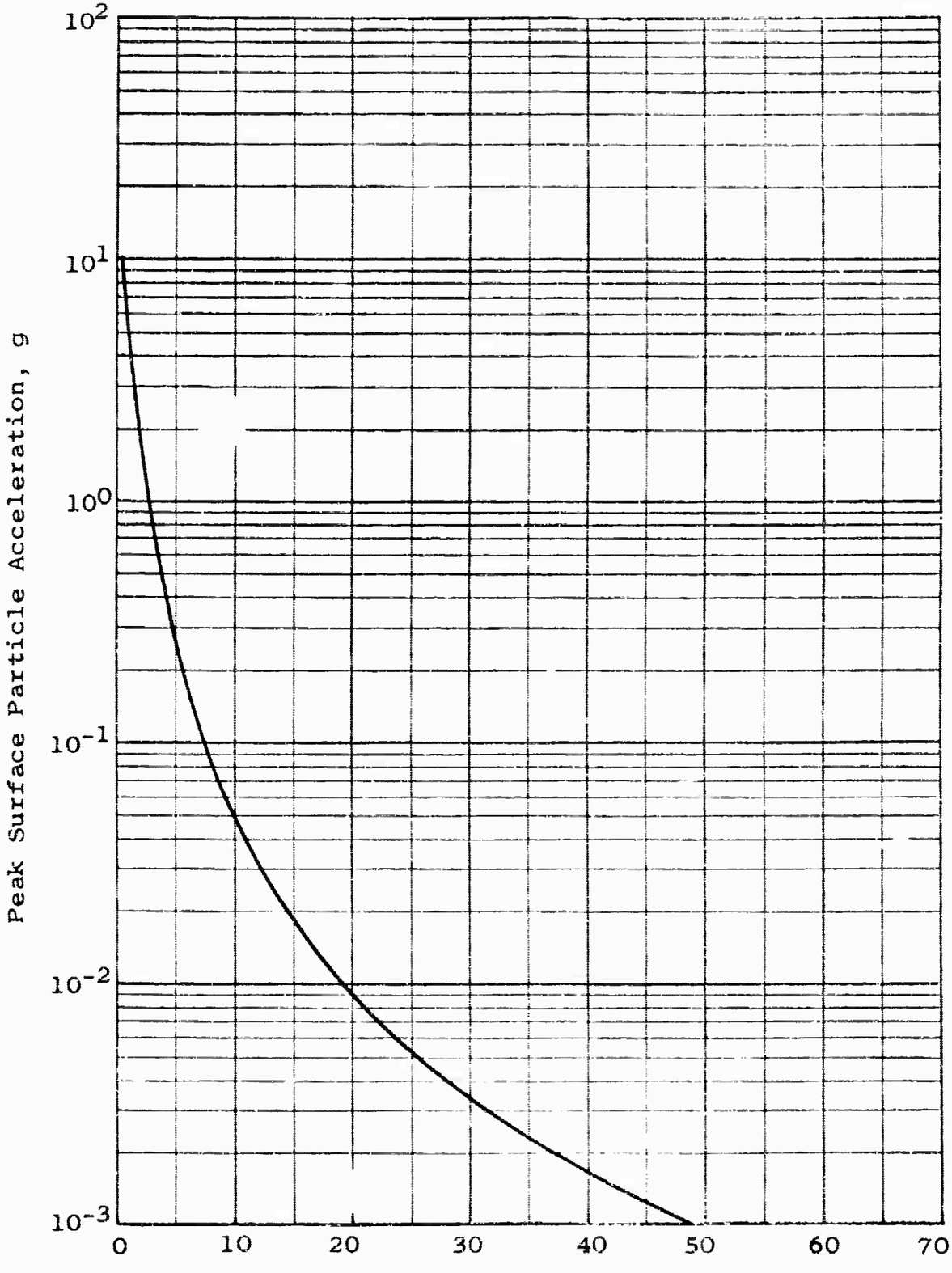

Figure 2.11 Predicted Surface Acceleration versus Horizontal Distance, Salmon Event.

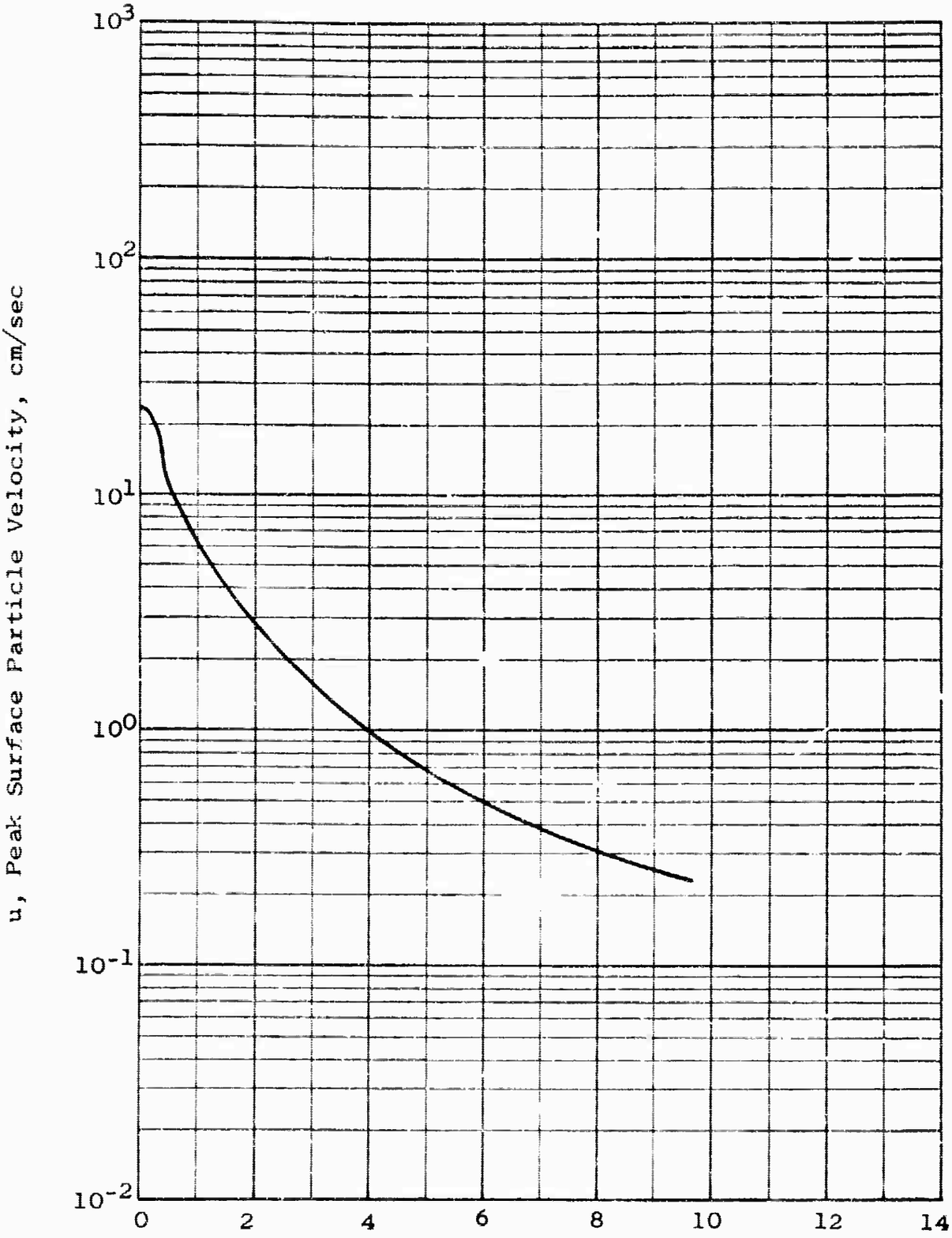

Figure 2.12 Predicted Surface Particle Velocity versus Horizontal Distance, Salmon Event.

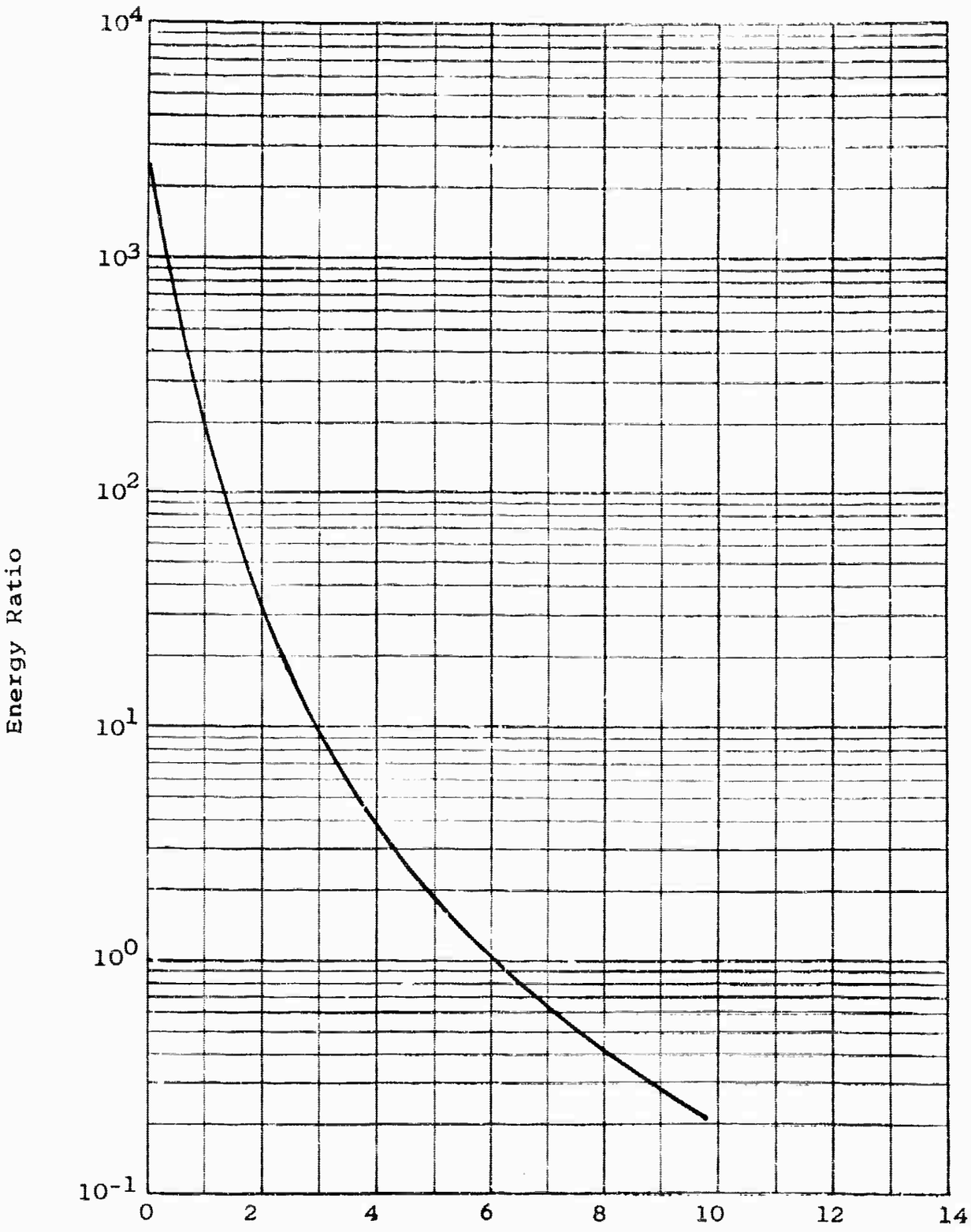

Figure 2.13 Predicted Energy Ratio versus Horizontal Distance, Salmon Event.

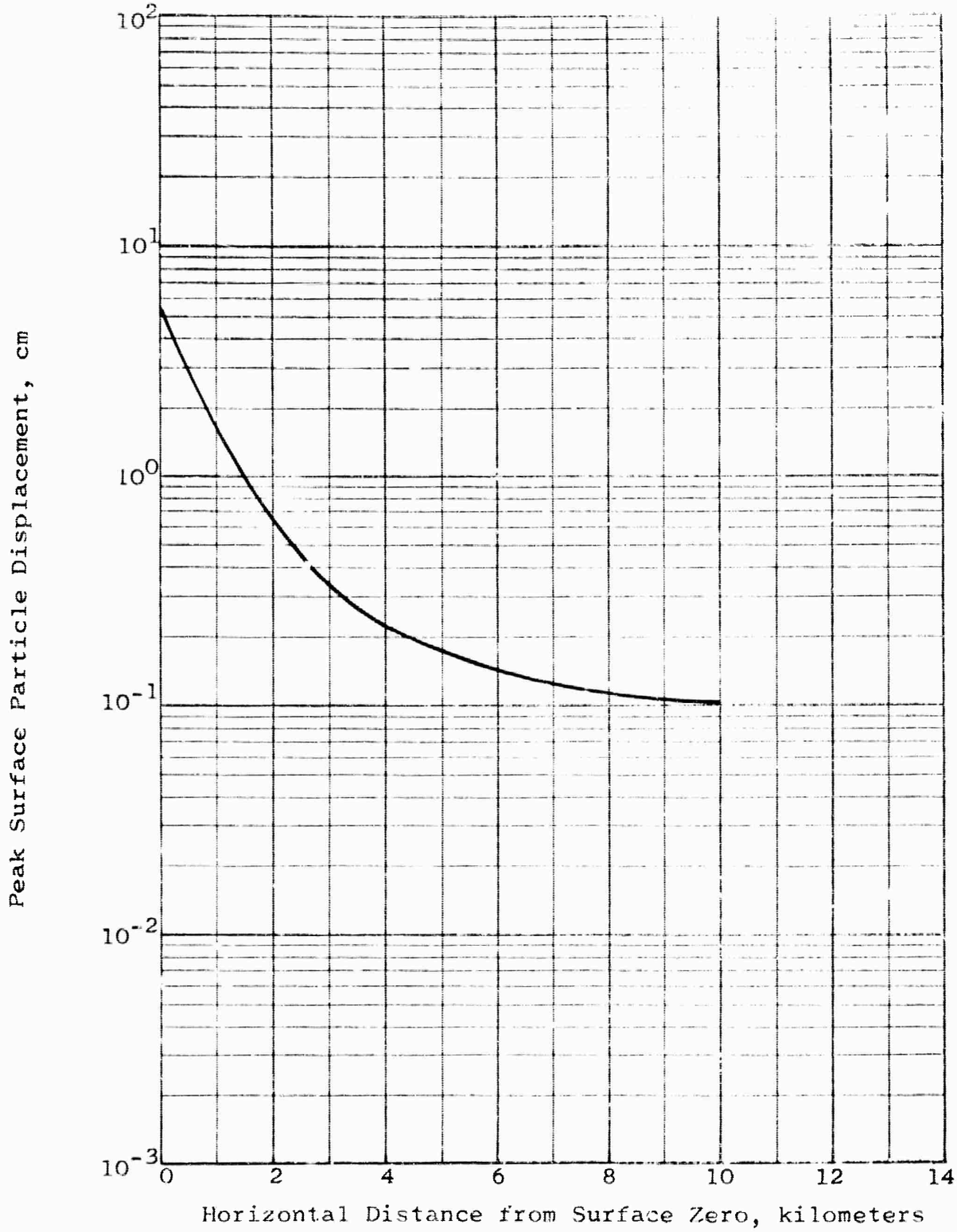

Figure 2.14 Predicted Surface Particle Displacement versus Horizontal Distance, Salmon Event

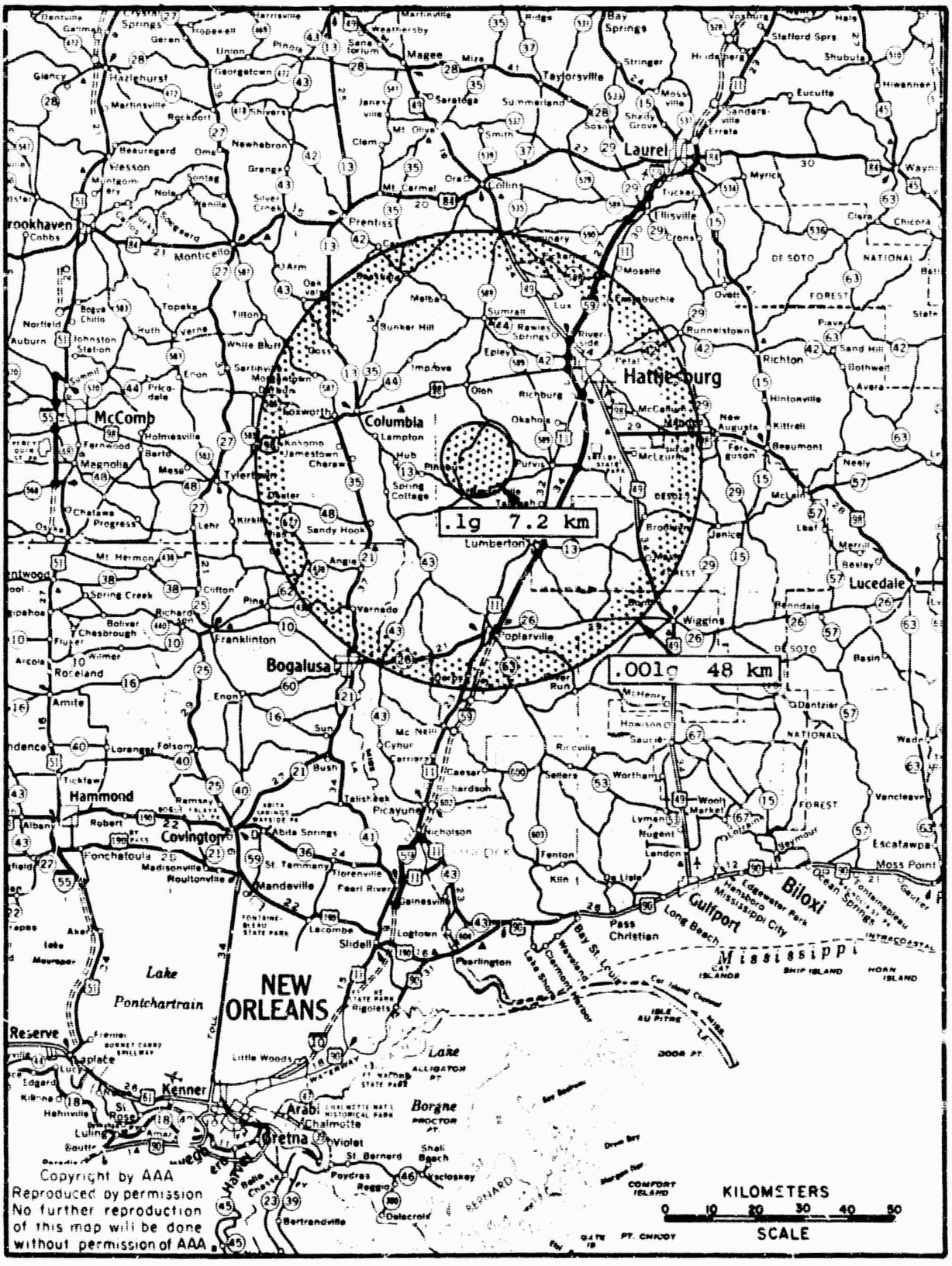

Figure 2.15 Area Map Showing Predicted Distances to Significant Ground Motions, Salmon Event.

CHAPTER 3

ANALYSIS AND INTERPRETATION

3.1 PHENOMENOLOGY AND CONTAINMENT

A prediction of effects and an evaluation of containment were made for the purpose of operational safety. The primary result of the Salmon event was that it was satisfactorily contained as predicted. This prediction of containment was based on an estimation and analysis of the individual effects anticipated and the interrelation of one to another with respect to containment. The results of post-shot exploration programs permit a comparison of some of these predicted quantities with observed data. The absence of a final yield figure necessitates the use of the values predicted on the basis of the planned yield of 5.0 kt.

3.1.1 Cavity Radius

Reference 3.1 states that the horizontal radius of the post-shot cavity for the Salmon event was found to be approximately 16.8 meters. The vertical dimension was less since the top to bottom height was decreased by the melted salt that flowed to the floor. The predicted most probable radius (section 2.2.1) was 19 meters which is seen to be in good agreement with the observed value.

3.1.2 Chimney Height

If the cavity collapsed, the maximum probable chimney height predicted in Section 2.2.4 would be 85 meters. It was not anticipated, however, that major collapse of the cavity would occur. This conclusion has been verified by the results of Salmon, where post-shot exploration indicates the cavity has remained essentially intact (Reference 3.1).

3.1.3 Cracking Radius

Reference 3.2 states that the macrofracture radius (planes or fracture zones that cut across samples and exist on large scale) extended to 45-60 meters from the shot point; the microfracture radius (deformational failures occurring within individual crystals on a small scale) extended to 90-120 meters.

Our prediction of the anticipated cracking radius was based on observed fractures at Gnome and an evaluation of the ultimate strain at failure from tests of Dribble cores (see Section 2.2.2). These data, particularly the ultimate strain at failure, are associated with macrofracturing which would be preceded by microfracturing. On this basis the most probable outer limit of cracking was predicted to be 58 meters. This agrees excellently with the observed value of 45-60 meters and tends to substantiate the method used to arrive at the predicted radius.

3.1.4 Radius of Radiation Injection into Cracks by Particulates and Condensates

In Section 2.2.3 the predicted radius of radiation injection into cracks by particulates and condensates, was computed by two means. The first indicated an anticipated radius of 46 meters, the second, a radius of 39 meters. Reference 3.2 states that the melt injection radius was a minimum of 37 meters below the shot point. The predicted values were therefore consistant with each other and with the observed data.

Reference 3.2 also states that gaseous injection was inferred to a radius of 64 meters.

This would indicate that even though solid particulate do not occur at the outer limit of fractures a path exists for the transport of radioactive gases.

3.1.5 Depth of Spalling

Predictions of the depth of spalling anticipated were made by means of a single spall analysis which indicated the depth should be 10 meters. The displacement at surface zero was also calculated and was predicted to be 0.14 meters. Based on Reference 3.3 the maximum depth of spall at surface zero was 12 meters and the vertical displacement or gap was 0.1 meters. Both of these values agree remarkably well with

the predicted quantities in light of the assumptions necessary in any analysis of the spalling phenomena.

The above mentioned effects were all used to arrive at the conclusion that the Salmon event would be contained. Additionally, an evaluation of the stemming plans for emplacement and satellite holes showed them to be adequate. The good agreement between the predicted and observed effects is very encouraging in addition to the main conclusion of containment which was completely substantiated.

3.2 SEISMIC EFFECTS

3.2.1 Processing of Seismic Data

As detailed in Chapter 1, surface motions resulting from the Salmon event were recorded at various locations with acceleration, displacement, and/or velocity-sensitive instruments. With the exception of the recordings at the three stations employed by Wiss, Janney, Elstner and Associates and the six Wood-Anderson stations of the USC&GS, all recordings have been corrected for the frequency response characteristics of the particular instrument.

The corrected acceleration and displacement records were integrated and differentiated to obtain partial velocity, and the corrected records from velocity meters were integrated and differentiated to obtain particle displacement and

acceleration. Additionally amplitude-frequency relationships were obtained from the USC&GS strong motion accelerograph and NC-21 velocity meter data.

Peak values of surface particle motion and their arrival times were determined from the corrected records. In addition, the available components at each station were analyzed simultaneously in order to determine the absolute value of peak motion received at the station. The values are designated as peak resultant vectors. A detailed discussion of the data processing procedures used on the Salmon records may be found in references 3.4 and 3.5.

The peak values of observed surface motion are given in Tables 3.1 through 3.5. These data, with the exception of the Wood-Anderson data and the long-range AFTAC data, are graphically displayed on Figures 3.1 through 3.12 along with the least squares regression lines, their equations, and the standard error of estimate which were fitted to these data.

A comparison of predictions with observed motions is shown on Figures 3.13 through 3.15. On these graphs only the regression lines of the peak resultant vectors are compared with predictions because this was the basis on which the predictions were made. The predictions of acceleration are

seen to agree quite well (Figure 3.13) with the observed accelerations to distances of about 10 kilometers. Beyond this distance the observed motions did not decrease as rapidly with distance as was predicted. Nevertheless, at the point of largest deviation between observed and predicted acceleration, a distance of 50 km (30 miles) the predicted acceleration is only a factor of 2 below the observed. With the standard error of observed acceleration being a factor of 1.6, the predictions of acceleration are considered to have been reasonably accurate. The predictions of particle velocity compare excellently with the observed data (see Figure 3.14). Although particle velocity predictions were made only to about 10 kilometers (6 miles), extrapolation of the predictions to greater distances would also have provided very accurate values. Particle displacement shows the greatest deviation between predicted and observed. See Figure 3.15. As with velocity, displacement predictions were made only to 10 kilometers. The predicted values are consistently lower than the regression line by a factor of about 2. As previously stated, particle displacement was predicted using simply harmonic motion assumptions. Therefore, it was not surprising that displacement predictions show the poorest comparison with observed results.

In order to explain possible sources of the scatter which is seen in th data (Figures 3.1 through 3.12), contour maps were drawn to check for azimuthal variations in energy propagation. Maps of the radial and transverse components of velocity and displacement are shown on Figures 3.16 through 3.19. These components provided the best areal coverage and therefore are the only ones shown. Distinct variations of ground motion with azimuth are seen on these maps and in general these four components tend to show a consistent pattern of variation. A relatively high level of ground motion is seen to the northeast toward Hattiesburg and with less consistency to the south. The level of motion to the east toward Purvis and to the north was consistently lower than in other directions. As a possible explanation of this azimuthal variation the effect of the shape of Tatum Dome was explored. Figure 3.20 shows the variation in the longitudinal plane wave transmission coefficient at the edge of the dome at shot level. Also shown is the outline of the dome. The pattern of the coefficient shows the azimuthal variation which could be expected due solely to the shape of the dome at shot level only. Comparison of this figure with the ground motion contour maps shows that there is some relationship between the shape of the dome and the azimuthal variation of ground motion.

The distance to 0.1 g was predicted to be 7250 meters (4.5 miles). From the regression line on Figure 3.13 it is seen that on the average the distance was actually about 8000 meters (about 5 miles). However, because of the azimuthal variations it is known to have extended to greater distances in some directions. For instance, station 2N at a distance of 16.6 km measured a vertical acceleration of .063 g (Table 3.1). Extrapolating this value back to 0.1 g (using the slope for vertical acceleration as shown in figure 3.1) the distance to 0.1 g could be about 14 km (8.7 miles). Because most of the instruments were located along two radial lines, the asymmetry can not be precisely defined. It is estimated that about 16 km (10 miles) is a reasonable maximum probable distance to 0.1 g.

Figures 3.21 through 3.23 show the results of an analysis of the amplitude- frequency composition of the individual components of the peak ground motions recorded at stations 10S, 20S, 160SW and 272SW. These graphs show the variation with distance of amplitude, frequency, and time duration of the particle velocity at the time of peak displacement, velocity, and acceleration, respectively. Figures 3.24 and 3.35 show the areal variation of the amplitude of the individual components of surface particle velocity at different frequency bandwidths. These results have been extracted from Fourier spectra. They are, however, similar

to the results extracted from the band-pass filtered data. This has permitted the inclusion of particle velocity amplitudes for similar frequency bandwidths extracted by band-pass filtering with the data extracted from the Fourier spectra. The reader should note, however, that an adjustment in the measured band-pass data (recorded in tabular form on Figures 3.30 through 3.35) for stations 10S and 20S is required to insure compatability with the Fourier data. Tabular values for these stations were adjusted so that the number of cycles would approximately equal those of nearby stations--assuming the average amplitude times the number of cycles was constant. The adjusted values were contoured. Figures 3.36 through 3.38 show the areal variation of the frequency having greatest Fourier or band-pass amplitude for vertical, radial, and transverse components of velocity. Additional information on these analyses is given in Appendices B and C.

Corrected data recorded with USC&GS strong motion and velocity instruments show no evidence of low-frequency ground motion. This is not, however, sufficient basis for concluding that no low-frequency ground motion was present. Recovery of low-frequency information through use of frequency compensation is limited by the signal-noise ratio. Outside the designed range of frequency response, currently used recording instruments very quickly reduce the signal

level to that of the background noise.

Some insight into the probable low-frequency character of the ground motions at short distances from Salmon is provided by the data recorded with long and short period displacement meters located at Jena and Eutaw, the closest (243 kilometers) AFTAC-LRSM stations (see Table 3.2). When compensated for the transducer's non-linear amplitude response across the frequency spectrum, the analyzable frequency range of these data covers periods ranging from 3.3 to 0.1 and 33.3 to 3.7 seconds.

These data show that the lowest frequency particle displacement was associated with surface waves of 13.7 second period. This period is the exception, however, as the longest periods of most of the particle displacement data are less than 10.0 seconds. Closer than 243 kilometers from Salmon the lowest frequency particle displacements must have had shorter periods owing to wave dispersion. A measure of the amount of this dispersion is provided by the difference in periods between Jena and Grapevine and between Eutaw and Cumberland Plateau. If the wave dispersion for these distances is diagnostic of the entire transmission path, the lowest frequency of the particle displacements at short distances from Salmon could not have been too different from those recorded at Jena and Eutaw. On the

basis of the above data it would appear that the recording instruments located at short distances from Salmon did not record low-frequency ground motions although such motions were probably present.

Additional support for the thesis that low-frequency ground motion was present near Salmon is provided by the 0.7 to 7.9 seconds periods of the water level fluctuations recorded at Well HT-2 by the USGS. The longer period water level fluctuations of 6.25 and 7.9 seconds at HT-2 are commensurate with those which would be expected for the surface waves recorded at Jena and Eutaw at the distance of this well from ground zero (1,884 meters). The principal discrepancy in available water level fluctuation data is that no long period fluctuations were recorded at Wells HT-3, HT-5, and E-9 located closer to ground zero than HT-2. A possible explanation for the absence of long period water level fluctuations in these wells is that they were located too close to the explosion.

There is a theoretical minimum for the distance from the shot at which Rayleigh waves can appear. (Reference 3.6). At this distance the Rayleigh wave amplitude is a minimum For a theoretical shot buried 824 meters (the depth of Salmon) beneath the surface of an isotropic, elastic medium this

distance is 516 meters. (For a shot in real media this distance must be modified). Wells HT-3, HT-5, and E-9 were 543, 549, and 518 meters, respectively, from ground zero. Well HT-2, which did exhibit long period water level fluctuations, was 1,884 meters from ground zero. This suggests that low frequency Rayleigh waves were generated by Salmon.

3.2.2 Hazards to Existing Subsurface Facilities

As detailed in Section 2.3.2, an evaluation was made of the possibility of damage to several subsurface facilities including the United Gas Line, Olin Mathieson facilities at McIntosh and the Sand shaft. The conclusion reached was that no damage was anticipated. Based on current knowledge this conclusion has been substantiated.

TABLE 3.1

PEAK PARTICLE ACCELERATION

Station	Component	Slant Range (Meters)	Acceleration (g's)	Arrival Time of Peak Acceleration (sec)
USC&GS				
1 East	Z	1,460	1.50×10^{0}	.35
	R	"	7.08×10^{-1}	.84
	T	"	3.84×10^{-1}	.33
	Vector	"	1.50×10^{0}	.35
1 East	Z	1,460	-	-
	R	"	7.32×10^{-1}	.88
	T	"	3.27×10^{-1}	.36
	Vector	"	7.37×10^{-1}	.88
2 East	Z	1,980	1.16×10^{0}	.92
	R	"	5.13×10^{-1}	1.19
	T	"	1.79×10^{-1}	1.47
	Vector	"	1.16×10^{0}	.92
3 East	Z	2,150	1.46×10^{0}	.68
	R	"	6.39×10^{-1}	1.53
	T	"	1.49×10^{-1}	1.26
	Vector	"	1.52×10^{0}	.68
4 East	Z	3,110	4.94×10^{-1}	2.18
	R	"	1.17×10^{0}	2.20
	T	"	1.73×10^{-1}	2.19
	Vector	"	1.20×10^{0}	2.20
5 East	Z	4,080	3.94×10^{-1}	1.69
	R	"	3.16×10^{-1}	2.36
	T	"	6.81×10^{-2}	2.41
	Vector	"	3.95×10^{-1}	1.69
6 East	Z	6,060	3.13×10^{-1}	2.16
	R	"	1.99×10^{-1}	3.11
	T	"	8.07×10^{-2}	5.02
	Vector	"	3.17×10^{-1}	2.16
Purvis	Z	14,500	4.29×10^{-2}	6.86
	R	"	2.00×10^{-2}	6.73
	T	"	1.08×10^{-2}	13.00
	Vector	"	4.31×10^{-2}	6.86
1 South	Z	1,460	-	-
	R	"	-	-
	T	"	-	-
	Vector	"	-	-

TABLE 3.1 CONTINUED

PEAK PARTICLE ACCELERATION

Station	Component	Slant Range (Meters)	Acceleration (g's)	Arrival Time of Peak Acceleration (sec)
1 South	Z	1,460	4.38×10^{0}	.33
	R	"	1.16×10^{0}	.81
	T	"	-	-
	Vector	"	4.89×10^{0}	.33
2 South	Z	1,980	8.78×10^{-1}	.38
	R	"	4.18×10^{-1}	1.00
	T	"	2.58×10^{-1}	1.31
	Vector	"	8.86×10^{-1}	.38
3 South	Z	2,160	5.94×10^{-1}	.55
	R	"	6.19×10^{-1}	1.45
	T	"	2.71×10^{-1}	1.44
	Vector	"	6.71×10^{-1}	1.45
4 South	Z	3,110	4.98×10^{-1}	1.74
	R	"	3.65×10^{-1}	2.22
	T	"	1.31×10^{-1}	2.20
	Vector	"	5.19×10^{-1}	1.74
5 South	Z	4,080	2.79×10^{-1}	1.62
	R	"	2.02×10^{-1}	2.33
	T	"	8.69×10^{-2}	2.56
	Vector	"	2.81×10^{-1}	1.62
6 South	Z	6,060	2.66×10^{-1}	2.25
	R	"	1.09×10^{-1}	3.70
	T	"	4.78×10^{-2}	4.85
	Vector	"	2.71×10^{-1}	2.25
10 South	Z	17,800	3.42×10^{-2}	8.60
	Z	18,100	3.64×10^{-2}	8.50
	Z	18,400	2.68×10^{-2}	8.60
	R	17,800	2.28×10^{-2}	8.70
	T	"	8.54×10^{-3}	14.10
	Vector	"	3.30×10^{-2}	8.50
20 South	Z	30,800	1.02×10^{-2}	13.30
	Z	31,400	1.20×10^{-2}	14.20
	R	31,700	9.43×10^{-3}	14.50
	T	"	4.69×10^{-3}	15.60
	Vector	"	1.23×10^{-2}	14.40

TABLE 3.1 CONTINUED

PEAK PARTICLE ACCELERATION

Station	Component	Slant Range (Meters)	Acceleration (g's)	Arrival Time of Peak Acceleration (sec)
Baxterville Oil Field	Z	9,680	5.81×10^{-2}	2.90
	R	"	-	-
	T	"	7.96×10^{-2}	4.60
	Vector	"	-	-
Lumberton	Z	17,700	2.24×10^{-2}	8.62
	R	"	2.62×10^{-2}	8.69
	T	"	1.58×10^{-2}	8.68
	Vector	"	3.30×10^{-2}	8.69
Gulf Oil Refinery	Z	18,683	-	-
	R	"	-	-
	T	"	-	-
	Vector	"	-	-
Columbia	Z	27,852	-	-
	R	"	-	-
	T	"	-	-
	Vector	"	-	-
Hattiesburg	Z	32,663	-	-
	R	"	-	-
	T	"	-	-
	Vector	"	-	-
160 Southwest	Z	272,700	1.05×10^{-4}	45.20
	Z	273,000	1.09×10^{-4}	47.10
	Z	273,300	7.86×10^{-5}	45.30
	Z	273,600	6.29×10^{-5}	45.00
	R	273,000	7.46×10^{-5}	55.20
	T	"	6.45×10^{-5}	83.70
	Vector	"	1.05×10^{-4}	47.10
272 Southwest	Z	450,700	1.46×10^{-5}	64.60
	Z	451,000	1.46×10^{-5}	64.60
	Z	451,300	1.34×10^{-5}	64.70
	Z	451,600	1.29×10^{-5}	64.70
	R	451,000	1.13×10^{-5}	84.30
	T	"	8.90×10^{-6}	120.00
	Vector	"	1.46×10^{-5}	64.60

TABLE 3.1 CONTINUED

PEAK PARTICLE ACCELERATION

Station	Component	Slant Range (Meters)	Acceleration (g's)	Arrival Time of Peak Acceleration (sec)
Wiss, Janney, Elstner, & Assoc.				
1N	Z	8,800	-	-
	R	"	-	-
	T	"	-	-
2N	Z	16,600	6.30×10^{-2}	.14
	R	"	3.70×10^{-2}	.15
	T	"	4.00×10^{-2}	.15
3N	Z	30,200	-	-
	R	"	-	-
	T	"	-	-

TABLE 3.2

PEAK PARTICLE DISPLACEMENT

Station	Component	Slant Range (Meters)	Displacement (cm)	Arrival Time of Peak Displacement (sec)
USC&GS				
1 East	Z	1,460	1.97×10^{0}	.26
	R	"	1.47×10^{0}	.85
	T	"	2.79×10^{-1}	1.54
	Vector	"	1.97×10^{0}	.26
1 East	Z	1,460	-	-
	R	"	1.40×10^{0}	.88
	T	"	2.35×10^{-1}	1.51
	Vector	"	1.40×10^{0}	.88
2 East	Z	1,980	7.62×10^{-1}	.46
	R	"	8.50×10^{-1}	1.20
	T	"	1.21×10^{-1}	3.18
	Vector	"	8.62×10^{-1}	1.20
3 East	Z	2,160	8.29×10^{-1}	.58
	R	"	8.38×10^{-1}	2.11
	T	"	1.66×10^{-1}	4.57
	Vector	"	8.38×10^{-1}	2.11
4 East	Z	3,110	1.21×10^{-1}	1.41
	R	"	6.39×10^{-1}	1.96
	T	"	1.16×10^{-1}	6.06
	Vector	"	6.41×10^{-1}	1.96
5 East	Z	4,080	4.80×10^{-1}	1.67
	R	"	5.45×10^{-1}	2.37
	T	"	8.69×10^{-2}	4.09
	Vector	"	5.61×10^{-1}	2.37
6 East	Z	6,060	4.75×10^{-1}	2.04
	R	"	2.11×10^{-1}	3.02
	T	"	6.46×10^{-2}	5.03
	Vector	"	4.84×10^{-1}	2.04
Purvis	Z	14,500	-	-
	R	"	-	-
	T	"	2.39×10^{-2}	16.42
	Vector	"	-	-

TABLE 3.2 CONTINUED

PEAK PARTICLE DISPLACEMENT

Station	Component	Slant Range (Meters)	Displacement (cm)	Arrival Time of Peak Displacement (sec)
1 South	Z	1,460	-	-
	R	"	1.14×10^{0}	1.00
	T	"	6.61×10^{-1}	.91
	Vector	"	1.15×10^{0}	1.00
1 South	Z	1,460	-	-
	R	"	1.14×10^{0}	.99
	T	"	6.01×10^{-1}	.91
	Vector	"	1.14×10^{0}	.99
2 South	Z	1,980	9.39×10^{-1}	.35
	R	"	8.90×10^{-1}	.99
	T	"	5.94×10^{-1}	1.29
	Vector	"	1.05×10^{0}	1.29
3 South	Z	2,160	-	-
	R	"	5.72×10^{-1}	1.47
	T	"	-	-
	Vector	"	-	-
4 South	Z	3,110	-	-
	R	"	5.39×10^{-1}	2.07
	T	"	1.67×10^{-1}	2.93
	Vector	"	5.40×10^{-1}	2.07
5 South	Z	4,080	1.66×10^{-1}	1.62
	R	"	3.98×10^{-1}	2.32
	T	"	1.13×10^{-1}	6.92
	Vector	"	4.00×10^{-1}	2.32
6 South	Z	6,060	-	-
	R	"	1.53×10^{-1}	7.60
	T	"	5.96×10^{-2}	5.60
	Vector	"	1.53×10^{-1}	7.60
10 South	Z	17,800	1.02×10^{-1}	11.10
	Z	18,100	3.24×10^{-1}	11.20
	Z	18,400	8.92×10^{-2}	11.50
	R	17,800	7.81×10^{-2}	12.00
	T	"	2.23×10^{-2}	9.80
	Vector	"	1.06×10^{-1}	11.40

TABLE 3.2 CONTINUED

PEAK PARTICLE DISPLACEMENT

Station	Component	Slant Range (Meters)	Displacement (cm)	Arrival Time of Peak Displacement (sec)
20 South	Z	30,800	2.55×10^{-2}	14.10
	Z	31,400	2.65×10^{-2}	14.60
	R	31,700	2.60×10^{-2}	19.30
	T	"	1.25×10^{-2}	17.30
	Vector	"	3.00×10^{-2}	14.60
Baxterville Oil Field	Z	9,680	1.28×10^{-1}	4.05
	R	"	3.23×10^{-2}	10.29
	T	"	9.32×10^{-2}	4.78
	Vector	"	1.28×10^{-1}	4.05
Lumberton	Z	17,700	-	-
	R	"	6.25×10^{-2}	8.54
	T	"	5.73×10^{-2}	8.54
	Vector	"	8.48×10^{-2}	8.54
Gulf Oil Refinery	Z	18,683	1.12×10^{-1}	7.40
	R	"	5.99×10^{-2}	27.09
	T	"	3.66×10^{-2}	10.27
	Vector	"	-	-
Columbia	Z	27,852	-	-
	R	"	2.02×10^{-2}	14.02
	T	"	2.08×10^{-2}	18.47
	Vector	"	-	-
Hattiesburg	Z	32,663	-	-
	R	"	2.18×10^{-2}	16.72
	T	"	4.20×10^{-2}	16.48
	Vector	"	-	-
160 Southwest	Z	272,700	2.12×10^{-4}	138.80
	Z	273,000	3.81×10^{-4}	139.10
	Z	273,300	2.96×10^{-4}	44.70
	Z	273,600	3.21×10^{-4}	138.70
	R	273,000	4.02×10^{-4}	101.40
	T	"	2.96×10^{-4}	149.00
	Vector	"	4.76×10^{-4}	138.50

TABLE 3.2 CONTINUED

PEAK PARTICLE DISPLACEMENT

Station	Component	Slant Range (Meters)	Displacement (cm)	Arrival Time of Peak Displacement (sec)
272 Southwest	Z	450,700	1.14×10^{-4}	88.50
	Z	451,000	8.04×10^{-5}	84.10
	Z	451,300	7.19×10^{-5}	84.70
	Z	451,600	7.61×10^{-5}	84.70
	R	451,000	1.10×10^{-4}	168.50
	T	"	1.14×10^{-4}	162.20
	Vector	"	1.14×10^{-4}	168.50
Wiss, Janney, Elstner, & Assoc.				
1N	Z	8,800	1.13×10^{-1}	.44
	R	"	1.04×10^{-1}	.28
	T	"	5.44×10^{-2}	.28
2N	Z	16,600	7.24×10^{-2}	.22
	R	"	3.05×10^{-2}	.44
	T	"	3.30×10^{-2}	.44
3N	Z	30,200	4.75×10^{-2}	.32
	R	"	3.81×10^{-2}	.29
	T	"	1.45×10^{-2}	.29
AFTAC				
Eutaw (Benioff)	Z	242,000	3.68×10^{-4}	90.00
	R	"	8.18×10^{-4}	112.00
	T	"	7.02×10^{-4}	112.00
Eutaw (Sprengnether)	Z	242,000	3.60×10^{-4}	141.00
	R	"	1.10×10^{-4}	141.00
	T	"	3.5×10^{-4}	228.00
Jena (Benioff)	Z	243,000	4.20×10^{-4}	110.00
	R	"	4.86×10^{-4}	95.00
	T	"	6.15×10^{-4}	80.00
Jena (Sprengnether)	Z	243,000	3.80×10^{-4}	166.00
	R	"	11.40×10^{-4}	169.00
	T	"	3.50×10^{-4}	194.00
Cumberland Plateau (Benioff)	Z	618,000	-	-
	N	"	1.11×10^{-4}	183.00
	E	"	1.34×10^{-4}	187.00

TABLE 3.2 CONTINUED

PEAK PARTICLE DISPLACEMENT

Station	Component	Slant Range (Meters)	Displacement (cm)	Arrival Time of Peak Displacement (sec)
Cumberland Plateau (Sprengether)	Z	618,000	6.00×10^{-5}	228.00
	N	"	4.30×10^{-5}	228.00
	E	"	-	-
Grapevine (Sprengnether)	Z	728,000	6.00×10^{-5}	407.00

TABLE 3.3

PEAK PARTICLE VELOCITY - DIRECTLY MEASURED

Station	Component	Slant Range (Meters)	Velocity (cm/sec)	Arrival Time of Peak Velocity (sec)
USC&GS				
10 South	Z	17,800	1.12×10^{0}	8.30
	Z	18,100	1.38×10^{0}	8.50
	Z	18,400	9.15×10^{-1}	8.50
	R	17,800	8.70×10^{-1}	8.70
	T	"	3.35×10^{-1}	14.00
	Vector	"	1.14×10^{0}	8.20
20 South	Z	30,800	4.40×10^{-1}	13.40
	Z	31,400	4.90×10^{-1}	14.20
	R	31,700	4.60×10^{-1}	17.30
	T	"	1.70×10^{-1}	19.30
	Vector	"	5.40×10^{-1}	14.50
160 Southwest	Z	272,700	3.25×10^{-3}	43.10
	Z	273,000	3.33×10^{-3}	43.20
	Z	273,300	2.93×10^{-3}	45.20
	Z	273,600	2.22×10^{-3}	51.60
	R	273,000	4.28×10^{-3}	55.20
	T	"	2.77×10^{-3}	83.80
	Vector	"	4.36×10^{-3}	84.00
272 Southwest	Z	450,700	8.24×10^{-4}	77.50
	Z	451,000	6.81×10^{-4}	84.50
	Z	451,300	6.49×10^{-4}	84.60
	Z	451,600	6.49×10^{-4}	84.50
	R	451,000	6.55×10^{-4}	91.00
	T	"	5.54×10^{-4}	161.00
	Vector	"	8.39×10^{-4}	84.50
Wiss, Janney, Elstner, & Assoc..				
1N	Z	8,800	1.07×10^{0}	.12
	R	"	1.86×10^{0}	.15
	T	"	5.26×10^{-1}	.10

TABLE 3.4

PEAK PARTICLE VELOCITY - DERIVED FROM ACCELERATION

Station	Component	Slant Range (Meters)	Velocity (cm/sec)	Arrival Time of Peak Velocity (sec)
USC&GS				
1 East	Z	1,460	3.01×10^{1}	.25
	R	"	2.05×10^{1}	.83
	T	"	4.87×10^{0}	.28
	Vector	"	3.09×10^{1}	.25
1 East	Z	1,460	-	-
	R	"	1.96×10^{1}	.87
	T	"	5.23×10^{0}	1.37
	Vector	"	1.97×10^{1}	.87
2 East	Z	1,980	2.36×10^{1}	.40
	R	"	2.07×10^{1}	1.07
	T	"	4.21×10^{0}	.34
	Vector	"	2.40×10^{1}	.40
3 East	Z	2,160	2.52×10^{1}	.72
	R	"	1.67×10^{1}	2.05
	T	"	2.92×10^{0}	1.77
	Vector	"	2.62×10^{1}	.72
4 East	Z	3,110	6.58×10^{0}	1.19
	R	"	2.02×10^{1}	2.87
	T	"	3.57×10^{0}	2.15
	Vector	"	2.03×10^{1}	2.87
5 East	Z	4,080	9.07×10^{0}	1.66
	R	"	9.87×10^{0}	2.42
	T	"	2.15×10^{0}	4.12
	Vector	"	9.89×10^{0}	2.42
6 East	Z	6,060	8.42×10^{0}	2.13
	R	"	6.13×10^{0}	3.09
	T	"	1.54×10^{0}	4.98
	Vector	"	8.64×10^{0}	2.13
Purvis	Z	14,500	1.14×10^{0}	5.97
	R	"	7.54×10^{-1}	6.69
	T	"	2.32×10^{-1}	13.39
	Vector	"	1.21×10^{0}	5.98

TABLE 3.4 CONTINUED

PEAK PARTICLE VELOCITY - DERIVED FROM ACCELERATION

Station	Component	Slant Range (Meters)	Velocity (cm/sec)	Arrival Time of Peak Velocity (sec)
1 South	Z	1,460	-	-
	R	"	-	-
	T	"	-	-
	Vector	"	-	-
1 South	Z	1,460	3.91×10^{1}	.32
	R	"	2.55×10^{1}	.91
	T	"	-	-
	Vector	"	4.21×10^{1}	.32
2 South	Z	1,980	1.68×10^{1}	.39
	R	"	1.56×10^{1}	1.57
	T	"	7.74×10^{0}	1.46
	Vector	"	1.73×10^{1}	.39
3 South	Z	2,160	1.45×10^{1}	.48
	R	"	1.30×10^{1}	1.42
	T	"	3.99×10^{0}	1.19
	Vector	"	1.48×10^{1}	.48
4 South	Z	3,110	1.27×10^{1}	1.64
	R	"	1.04×10^{1}	2.12
	T	"	2.46×10^{0}	2.74
	Vector	"	1.39×10^{1}	1.64
5 South	Z	4,080	5.03×10^{0}	1.82
	R	"	7.19×10^{0}	2.38
	T	"	1.82×10^{0}	6.86
	Vector	"	7.42×10^{0}	2.38
6 South	Z	6,060	8.44×10^{0}	2.19
	R	"	2.82×10^{0}	3.74
	T	"	1.23×10^{0}	5.51
	Vector	"	8.58×10^{0}	2.19
Baxterville Oil Field	Z	9,680	1.43×10^{0}	3.62
	R	"	-	-
	T	"	1.65×10^{0}	5.25
	Vector	"	-	-

TABLE 3.4 CONTINUED

PEAK PARTICLE VELOCITY - DERIVED FROM ACCELERATION

Station	Component	Slant Range (Meters)	Velocity (cm/sec)	Arrival Time of Peak Velocity (sec)
Lumberton	Z	17,000	8.00×10^{-1}	8.67
	R	"	1.01×10^{0}	8.49
	T	"	5.84×10^{-1}	8.47
	Vector	"	1.22×10^{0}	8.65
Gulf Oil Refinery	Z	18,682	-	-
	R	"	-	-
	T	"	-	-
	Vector	"	-	-
Columbia	Z	27,852	-	-
	R	"	-	-
	T	"	-	-
	Vector	"	-	-
Hattiesburg	Z	32,663	-	-
	R	"	-	-
	T	"	-	-
	Vector	"	-	-

TABLE 3.5

PEAK PARTICLE VELOCITY - DERIVED FROM DISPLACEMENT

Station	Component	Slant Range (Meters)	Velocity (cm/sec)	Arrival Time of Peak Velocity (sec)
USC&GS				
1 East	Z	1,460	5.99×10^{1}	.23
	R	"	2.30×10^{1}	.82
	T	"	5.85×10^{0}	1.57
	Vector	"	6.01×10^{1}	.23
1 East	Z	1,460	-	-
	R	"	2.17×10^{1}	.83
	T	"	4.73×10^{0}	1.68
	Vector	"	2.17×10^{1}	.83
2 East	Z	1,980	2.00×10^{1}	.43
	R	"	1.59×10^{1}	1.38
	T	"	3.76×10^{0}	1.41
	Vector	"	2.02×10^{1}	.43
3 East	Z	2,160	2.19×10^{1}	.64
	R	"	1.26×10^{1}	2.00
	T	"	3.44×10^{0}	1.75
	Vector	"	2.22×10^{1}	.64
4 East	Z	3,110	3.73×10^{0}	1.24
	R	"	1.78×10^{1}	2.00
	T	"	2.89×10^{0}	2.23
	Vector	"	1.80×10^{1}	2.00
5 East	Z	4,080	8.75×10^{0}	1.70
	R	"	1.23×10^{1}	2.42
	T	"	2.11×10^{0}	4.15
	Vector	"	1.24×10^{1}	2.42
6 East	Z	6,060	1.28×10^{1}	1.92
	R	"	6.25×10^{0}	3.08
	T	"	1.93×10^{0}	4.99
	Vector	"	1.28×10^{1}	1.92
Purvis	Z	14,500	-	-
	R	"	-	-
	T	"	2.96×10^{-1}	13.42
	Vector	"	-	-

TABLE 3.5 CONTINUED

PEAK PARTICLE VELOCITY - DERIVED FROM DISPLACEMENT

Station	Component	Slant Range (Meters)	Velocity (cm/sec)	Arrival Time of Peak Velocity (sec)
1 South	Z	1,460	-	-
	R	"	2.63×10^{1}	.89
	T	"	1.21×10^{1}	1.00
	Vector	"	2.71×10^{1}	.89
1 South	Z	1,460	-	-
	R	"	3.88×10^{1}	.88
	T	"	1.81×10^{1}	.98
	Vector	"	4.04×10^{1}	.77
2 South	Z	1,980	2.19×10^{1}	.32
	R	"	1.55×10^{1}	1.03
	T	"	7.43×10^{0}	1.25
	Vector	"	2.21×10^{1}	.32
3 South	Z	2,160	-	-
	R	"	1.53×10^{1}	1.42
	T	"	-	-
	Vector	"	-	-
4 South	Z	3,110	-	-
	R	"	1.21×10^{1}	2.12
	T	"	2.55×10^{0}	2.88
	Vector	"	1.21×10^{1}	2.12
5 South	Z	4,080	5.90×10^{0}	1.84
	R	"	6.59×10^{0}	2.39
	T	"	1.65×10^{0}	2.52
	Vector	"	6.86×10^{0}	2.38
6 South	Z	6,060	-	-
	R	"	3.25×10^{0}	3.08
	T	"	1.29×10^{0}	3.11
	Vector	"	3.26×10^{0}	3.08
Baxterville Oil Field	Z	9,680	2.77×10^{0}	4.09
	R	"	8.67×10^{-1}	5.87
	T	"	2.75×10^{0}	4.84
	Vector	"	3.05×10^{0}	4.84

TABLE 3.5 CONTINUED

PEAK PARTICLE VELOCITY - DERIVED FROM DISPLACEMENT

Station	Component	Slant Range (Meters)	Velocity (cm/sec)	Arrival Time of Peak Velocity (sec)
Lumberton	Z	17,700	-	-
	R	"	1.10×10^{0}	8.63
	T	"	1.06×10^{0}	8.63
	Vector	"	1.53×10^{0}	8.63
Gulf Oil Refinery	Z	18,683	2.60×10^{0}	7.96
	R	"	1.54×10^{0}	9.84
	T	"	7.20×10^{-1}	-
	Vector	"	-	-
Columbia	Z	27,852	-	
	R	"	4.00×10^{-1}	-
	T	"	2.79×10^{-1}	18.37
	Vector	"	-	-
Hattiesburg	Z	32,663	-	-
	R	"	3.87×10^{-1}	21.00
	T	"	1.11×10^{0}	17.00
	Vector	"	-	-

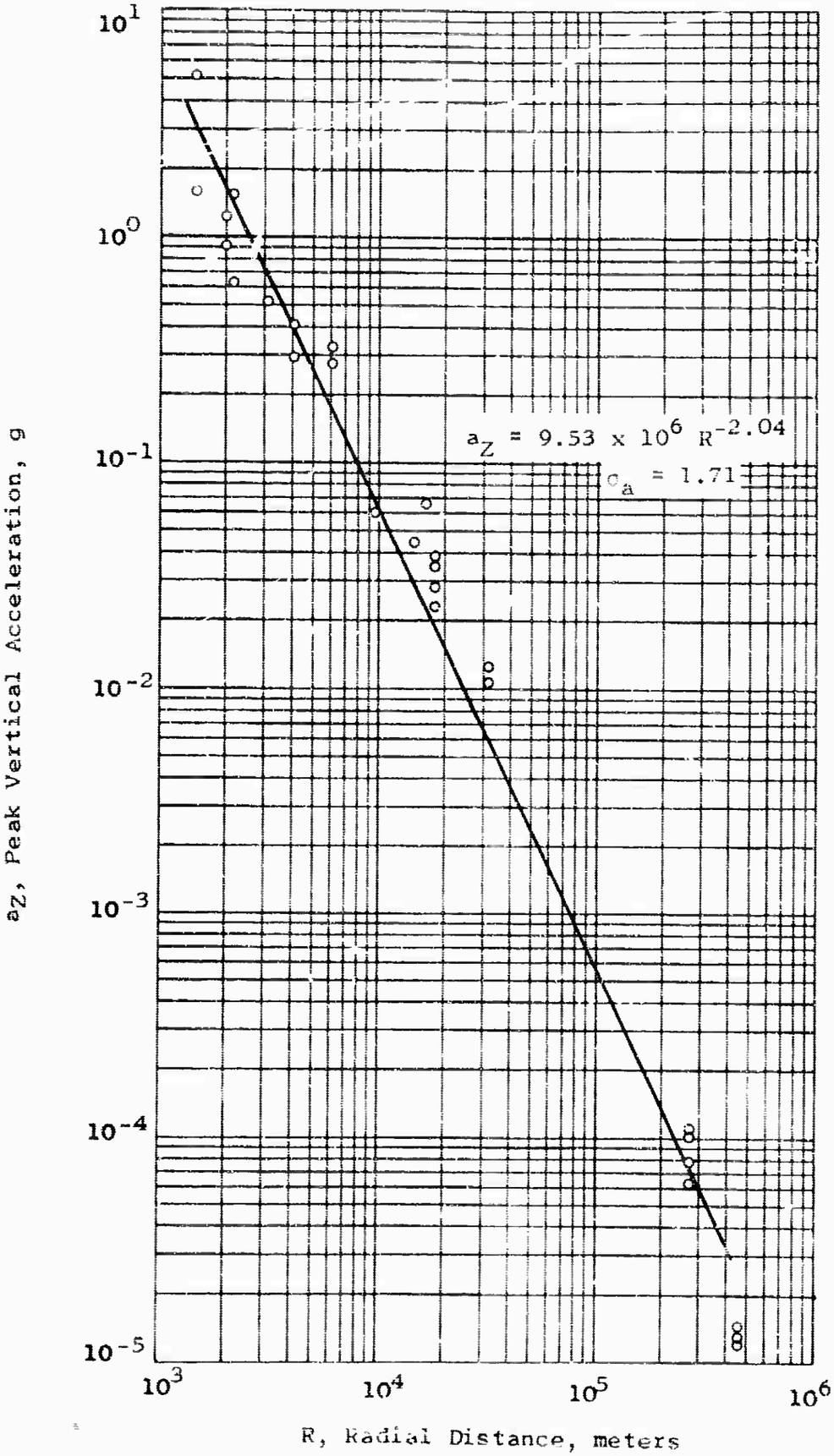

Figure 3.1 Vertical Component of Peak Surface Particle Acceleration versus Radial Distance, Salmon Event.

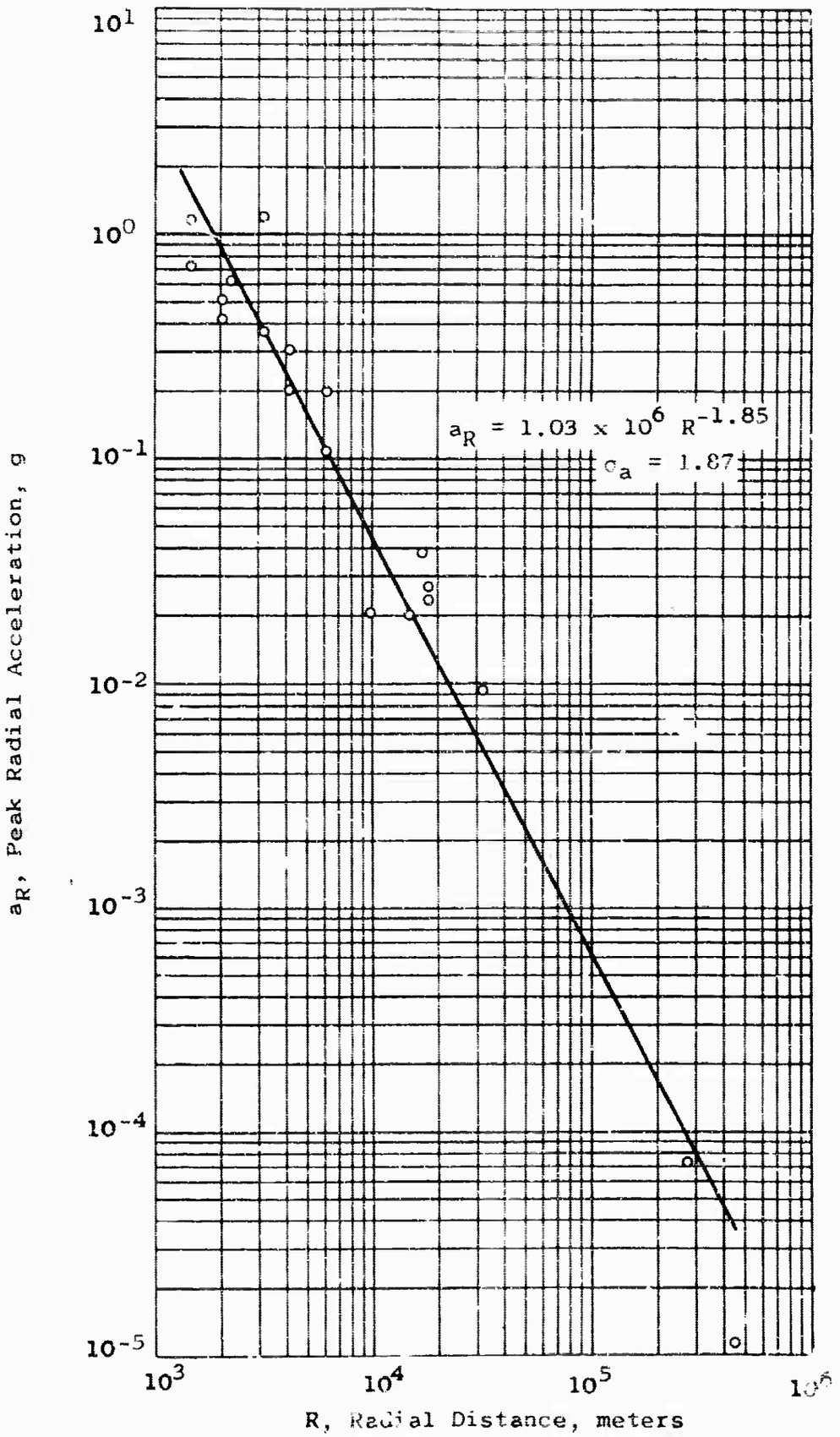

Figure 3.2 Radial Component of Peak Surface Particle Acceleration versus Radial Distance, Salmon Event.

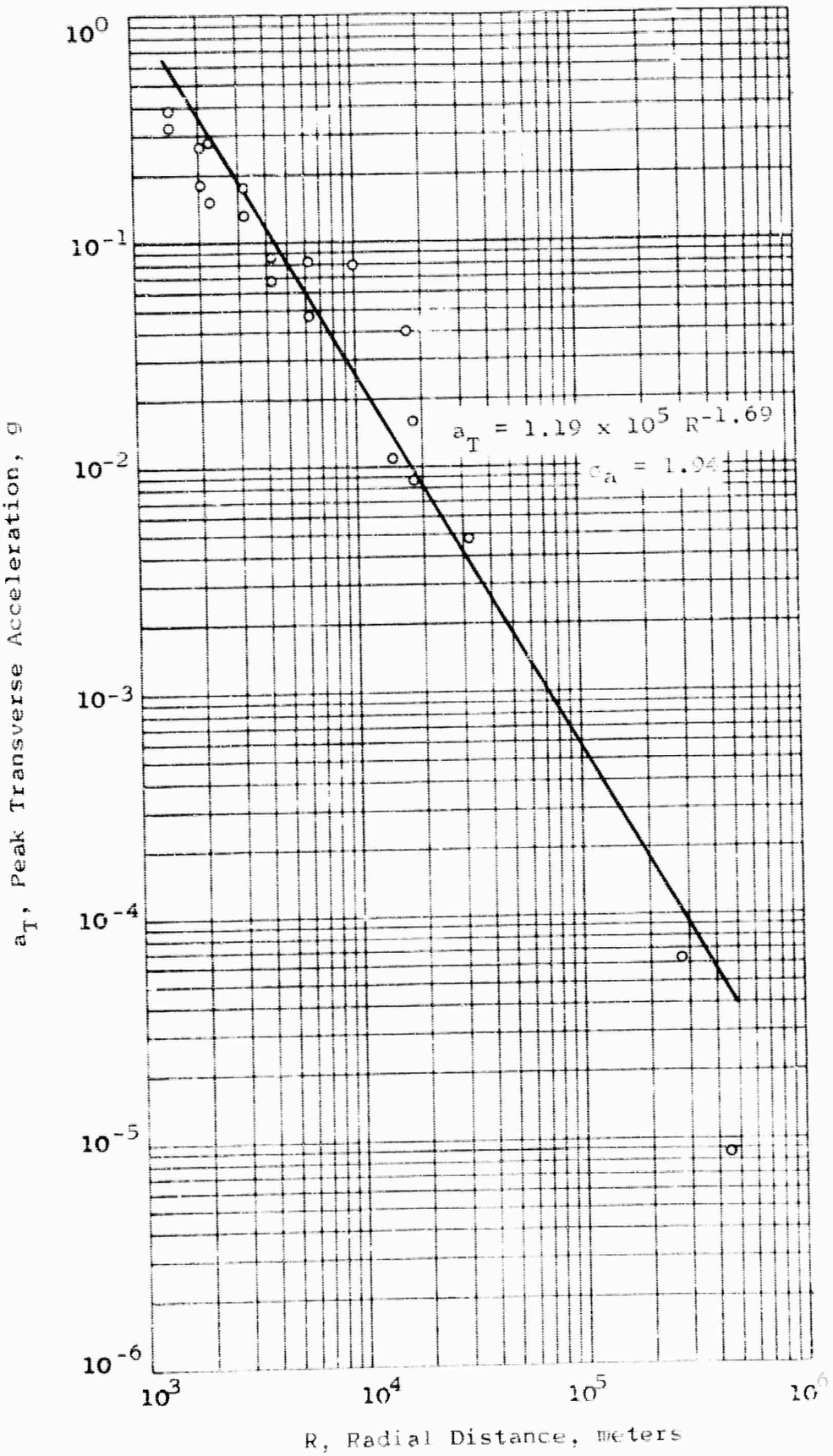

Figure 3.3 Transverse Component of Peak Surface Particle Acceleration versus Radial Distance, Salmon Event

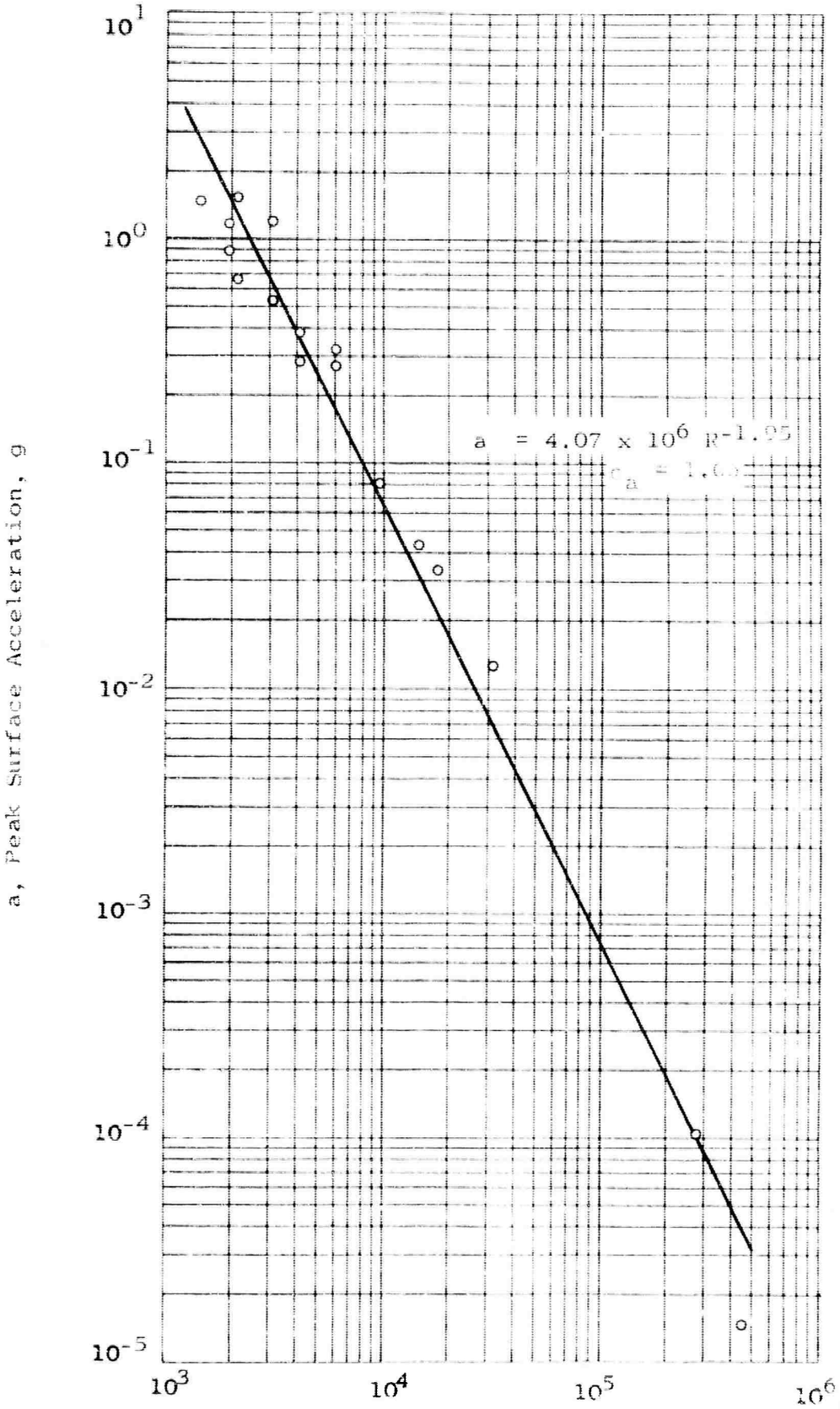

Figure 3.4 Resultant Vector of Peak Surface Particle Acceleration versus Radial Distance, Salmon Event.

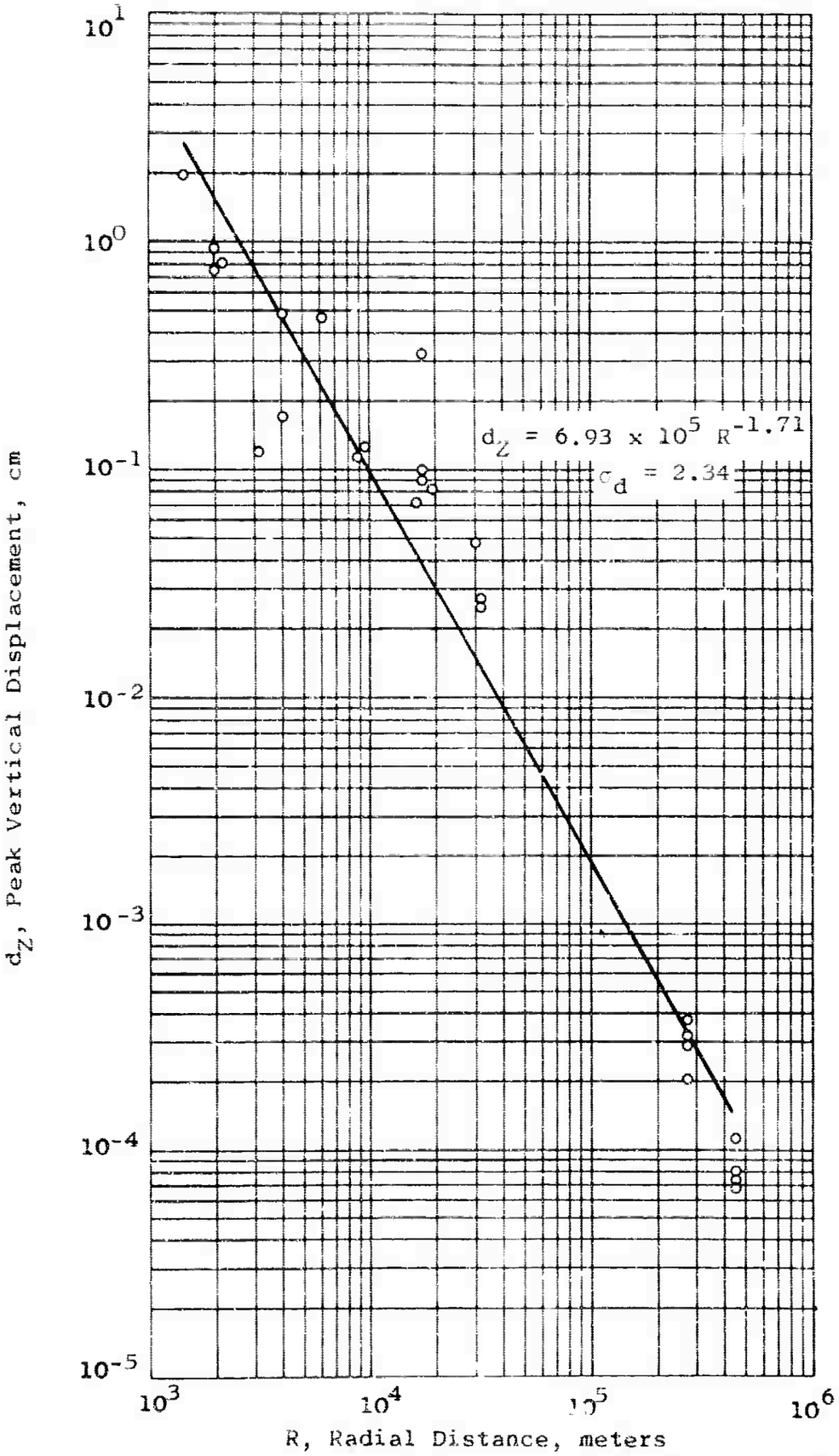

Figure 3.5 Vertical Component of Peak Surface Particle Displacement versus Radial Distance, Salmon Event.

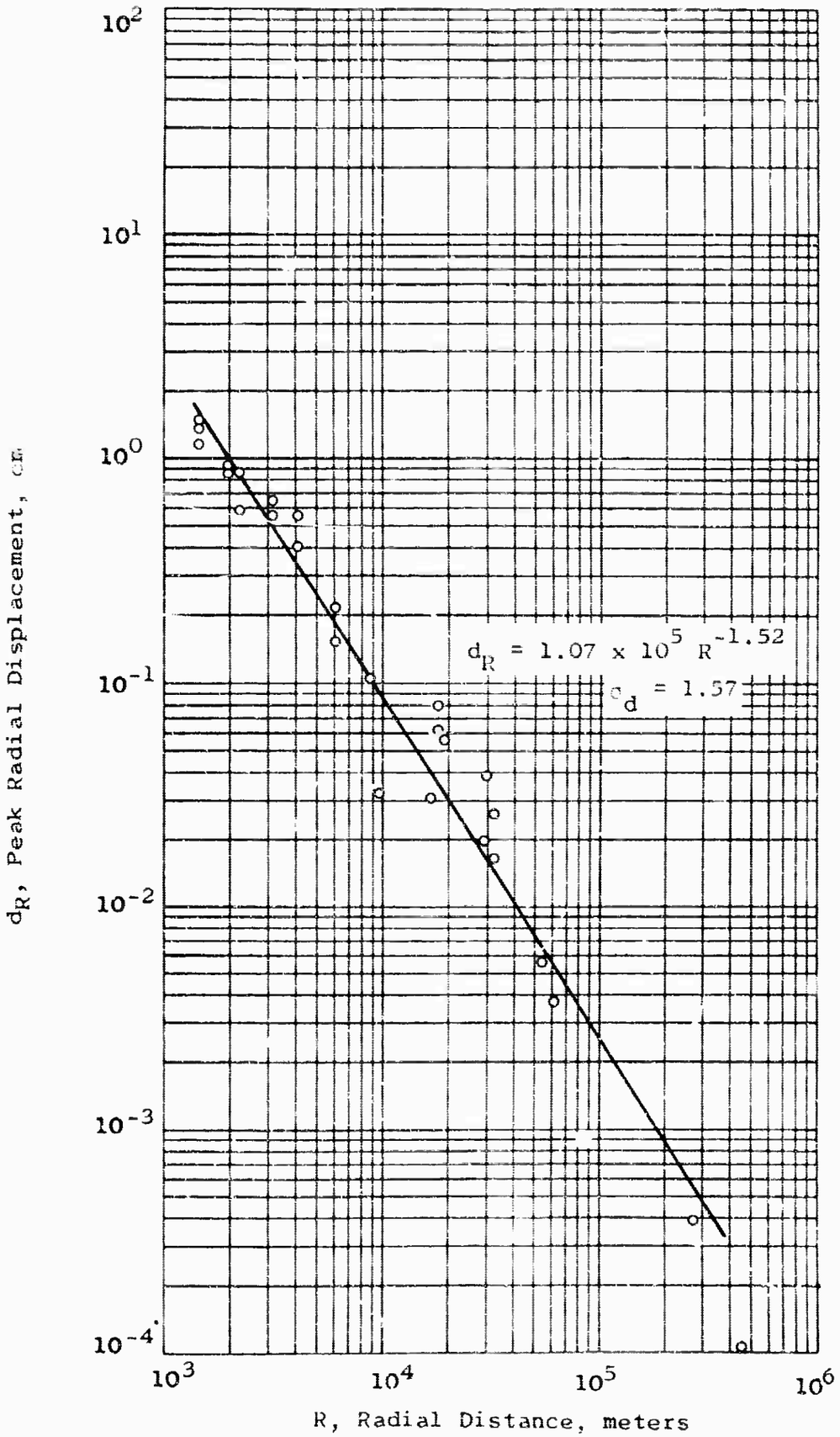

Figure 3.6 Radial Component of Peak Surface Particle Displacement versus Radial Distance, Salmon Event.

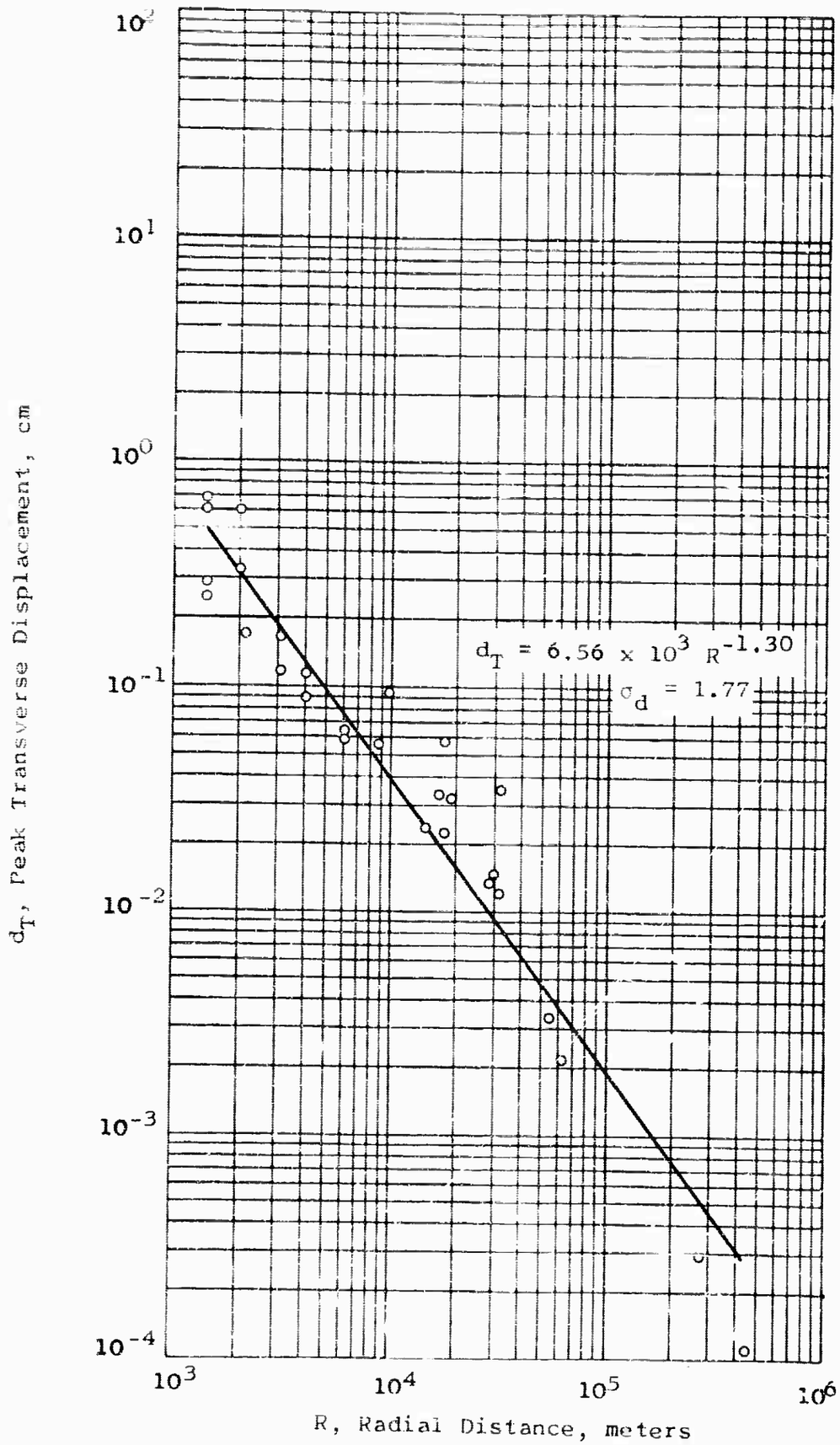

Figure 3.7 Transverse Component of Peak Surface Particle Displacement versus Radial Distance, Salmon Event.

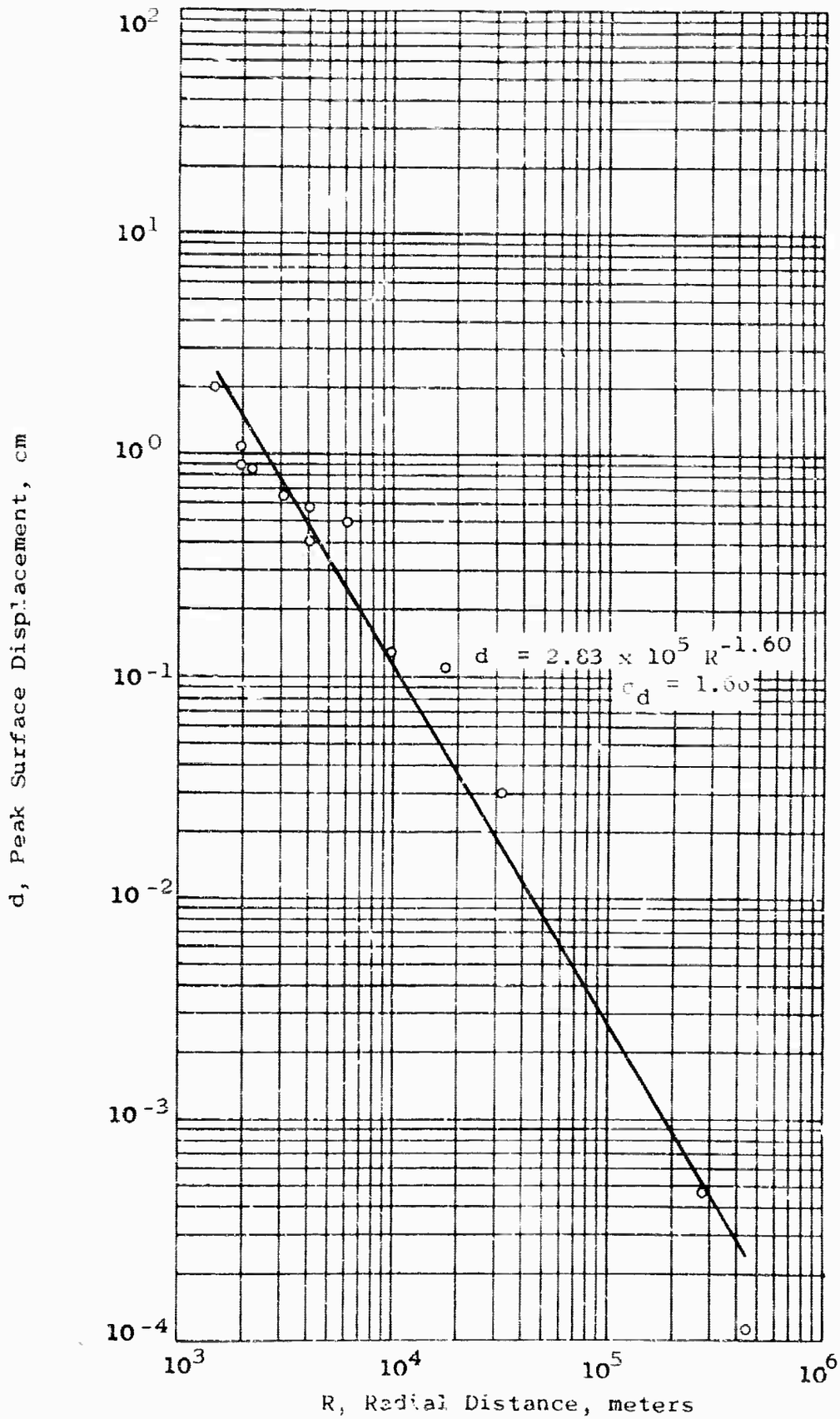

Figure 3.8 Resultant Vector of Peak Surface Particle Displacement versus Radial Distance, Salmon Event.

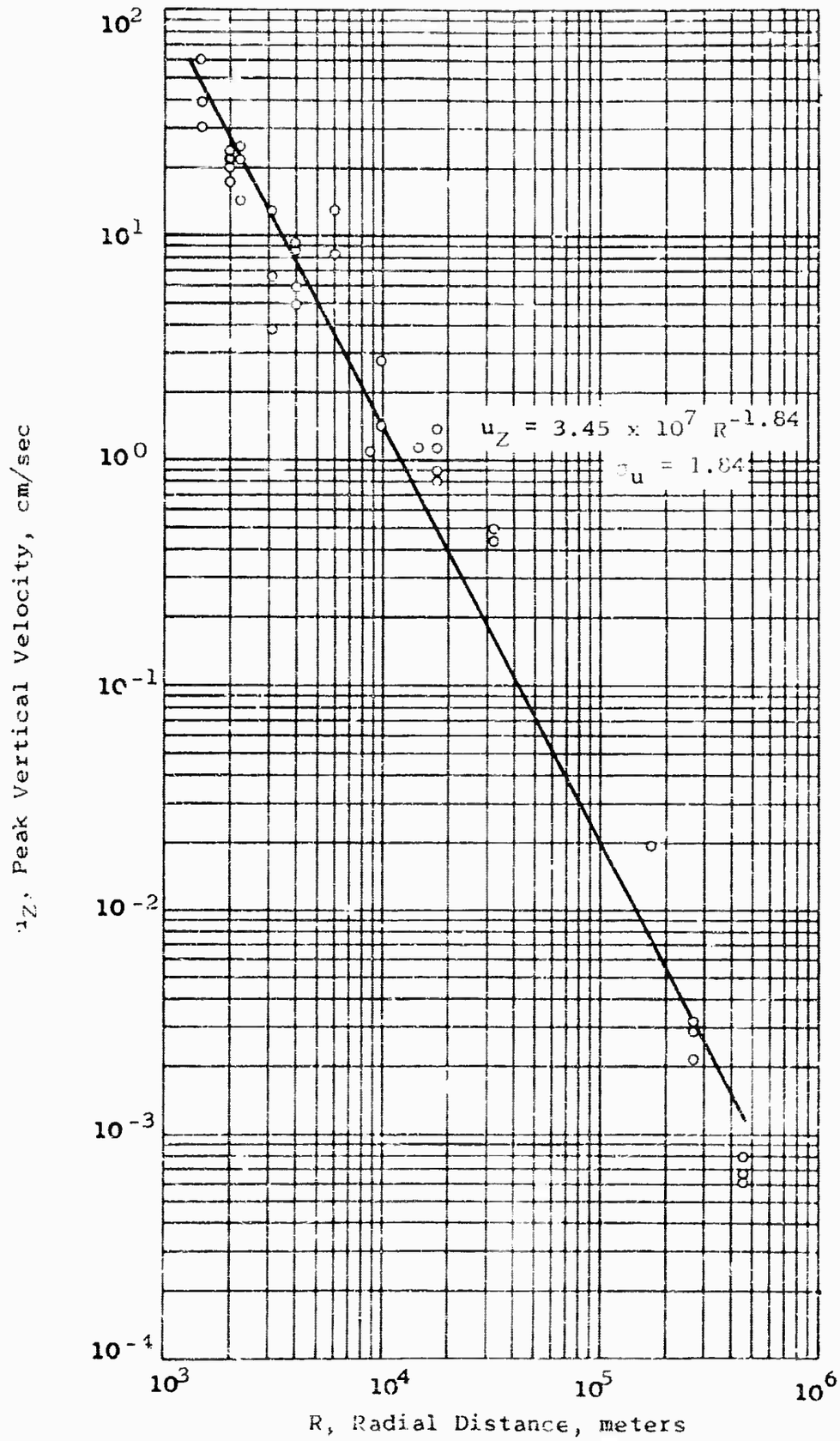

Figure 3.9 Vertical Component of Peak Surface Particle Velocity versus Radial Distance, Salmon Event.

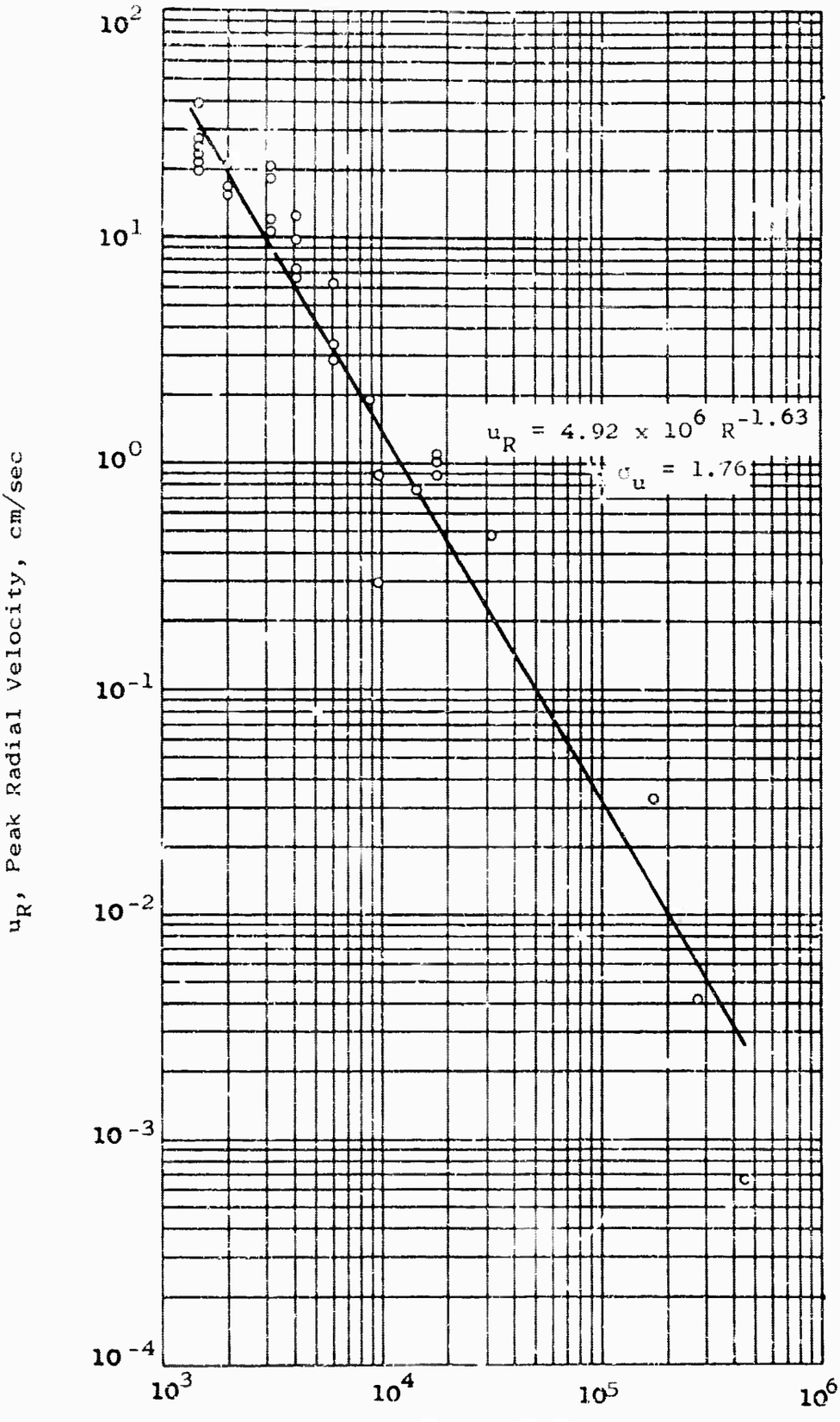

Figure 3.10 Radial Component of Peak Surface Particle Velocity versus Radial Distance, Salmon Event.

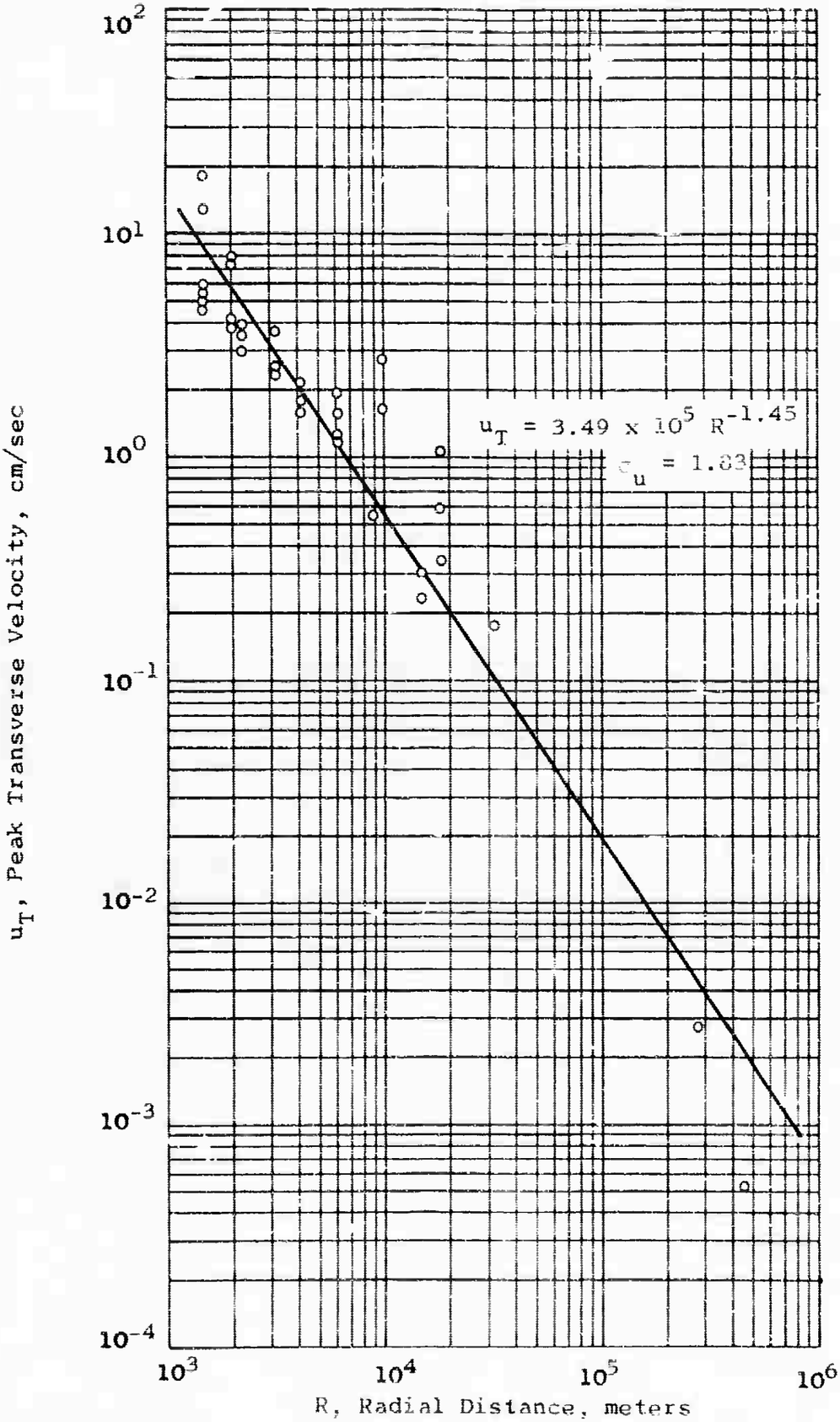

Figure 3.11 Transverse Component of Peak Surface Particle Velocity versus Radial Distance, Salmon Event.

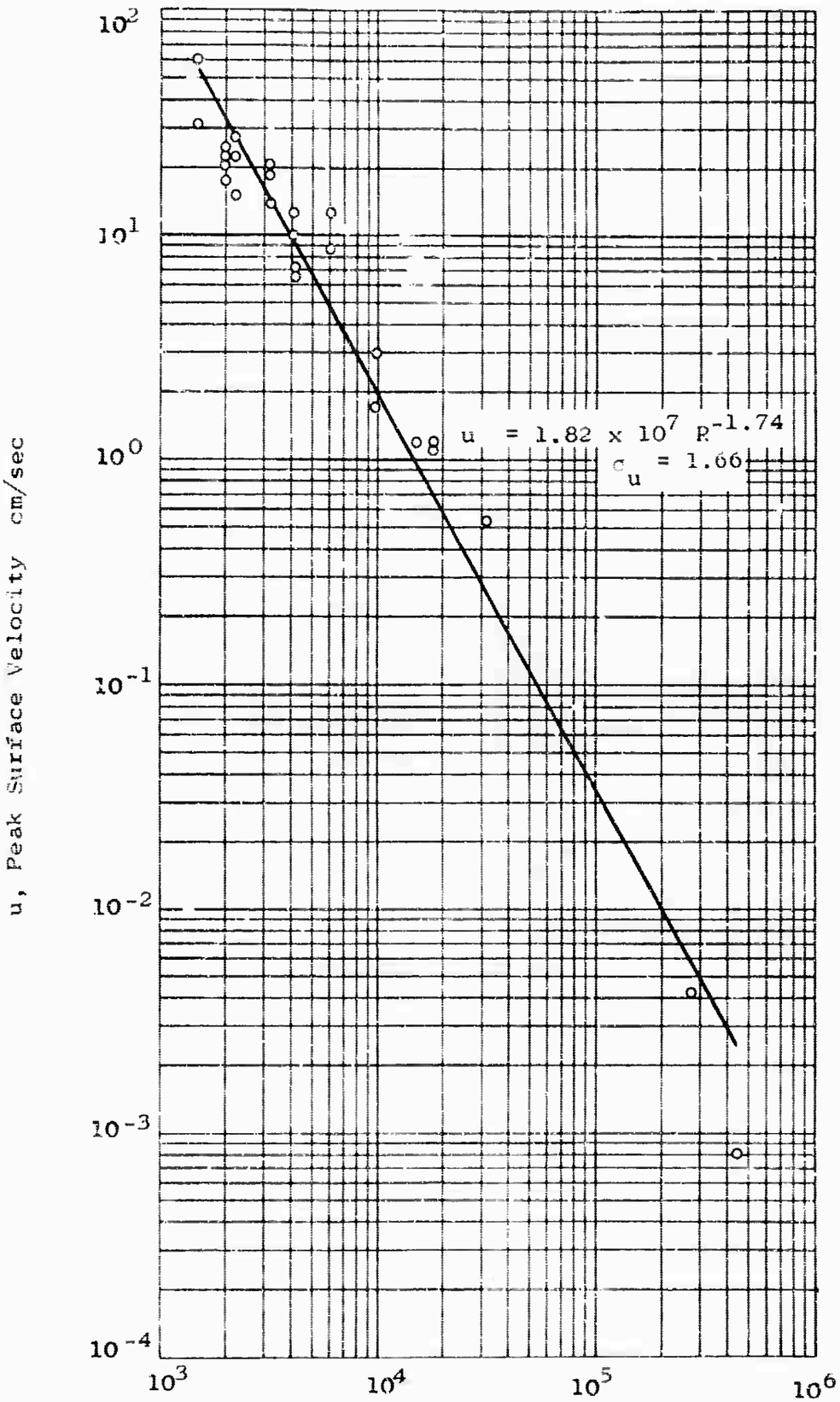

Figure 3.12 Resultant Vector of Peak Surface Particle Velocity versus Radial Distance, Salmon Event.

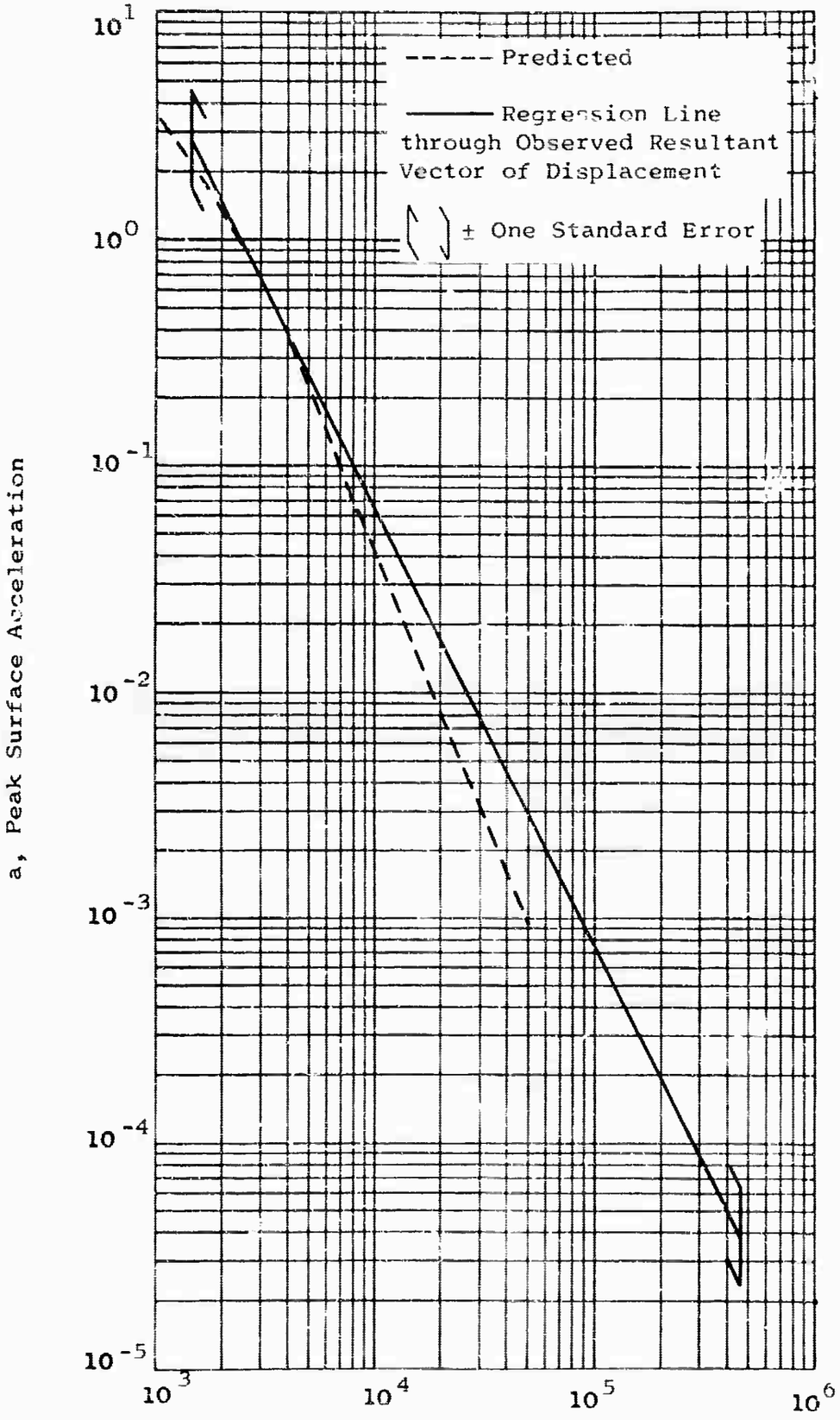

Figure 3.13 Comparison of Predicted and Observed Surface Particle Acceleration

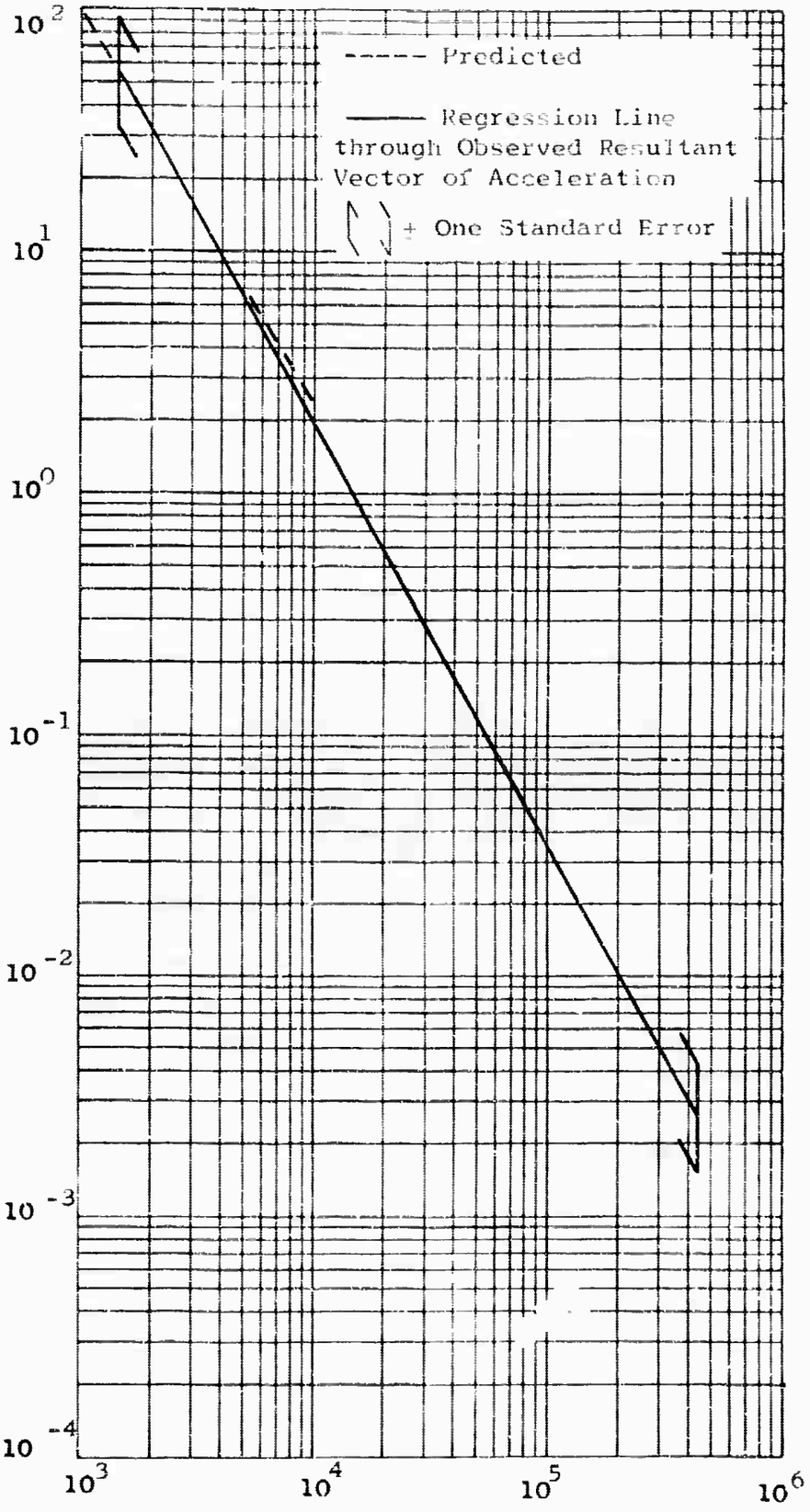

Figure 3.14 Comparison of Predicted and Observed Surface Particle Velocity

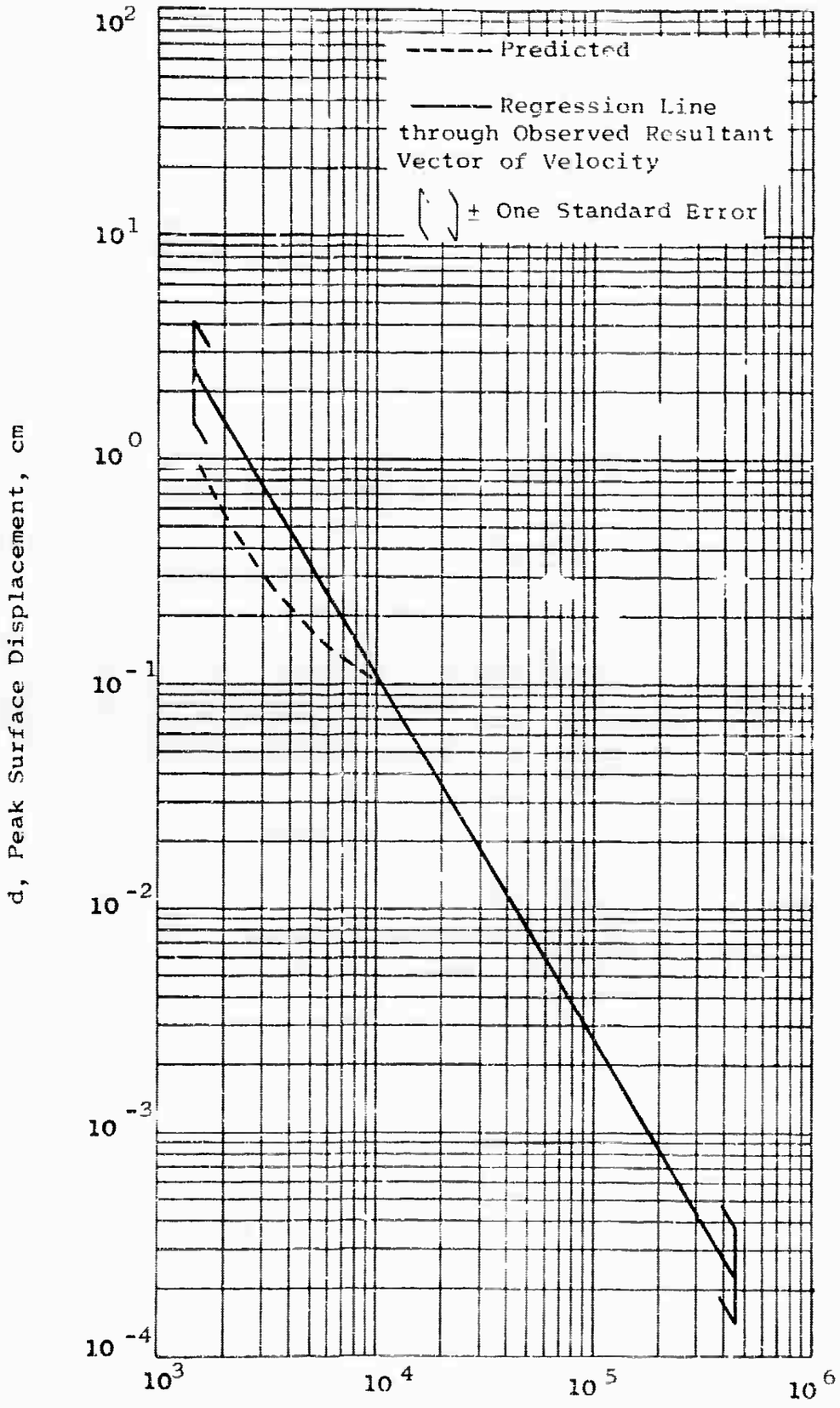

Figure 3.15 Comparison of Predicted and Observed Surface Particle Displacement

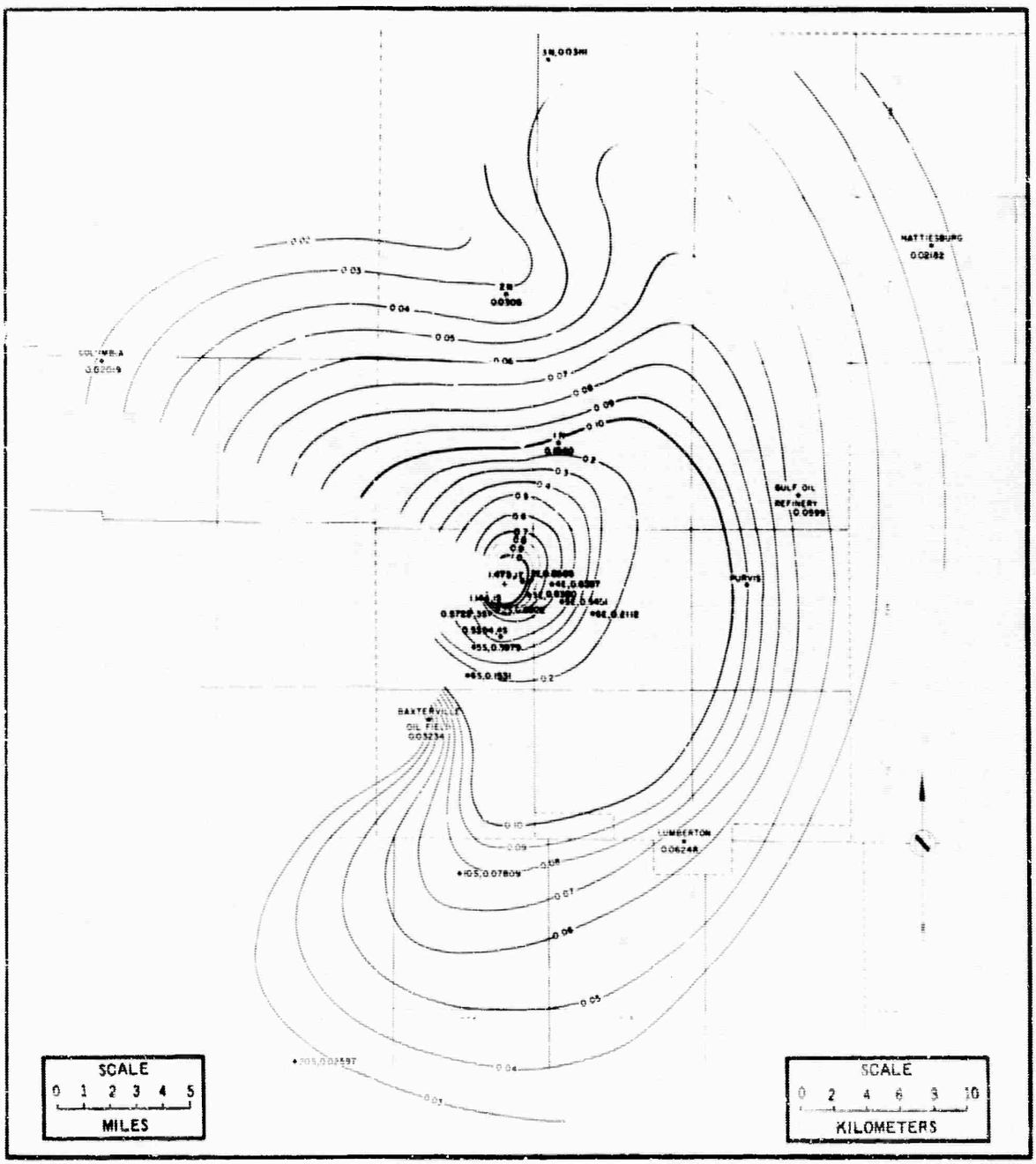

Figure 3.16 Contour Map of Radial Component of Peak Particle Displacement (cm)

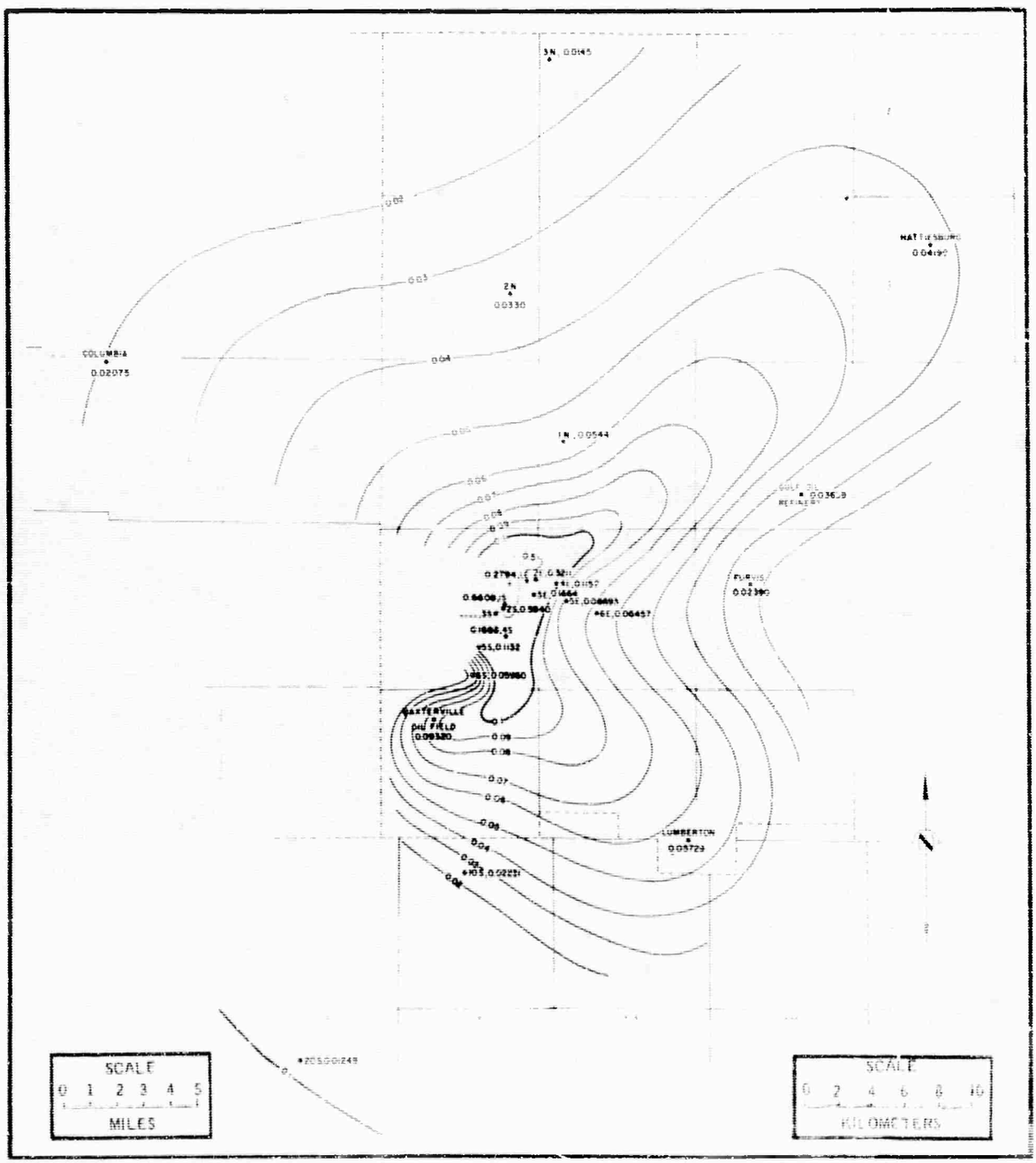

Figure 3.17 Contour Map of Transverse Component of Peak Particle Displacement (cm)

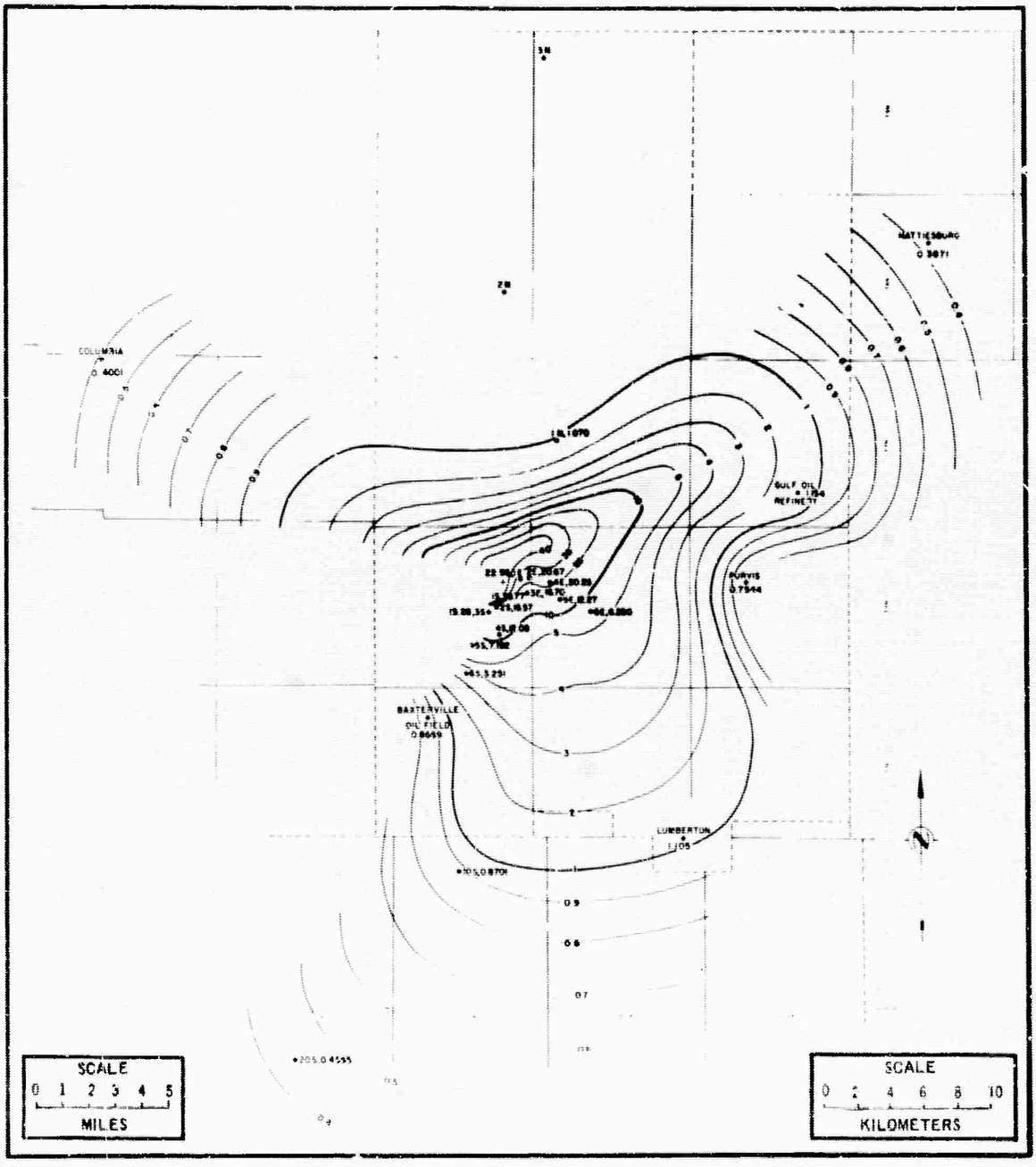

Figure 3.18 Contour Map of Radial Component of Peak Particle Velocity (cm/sec)

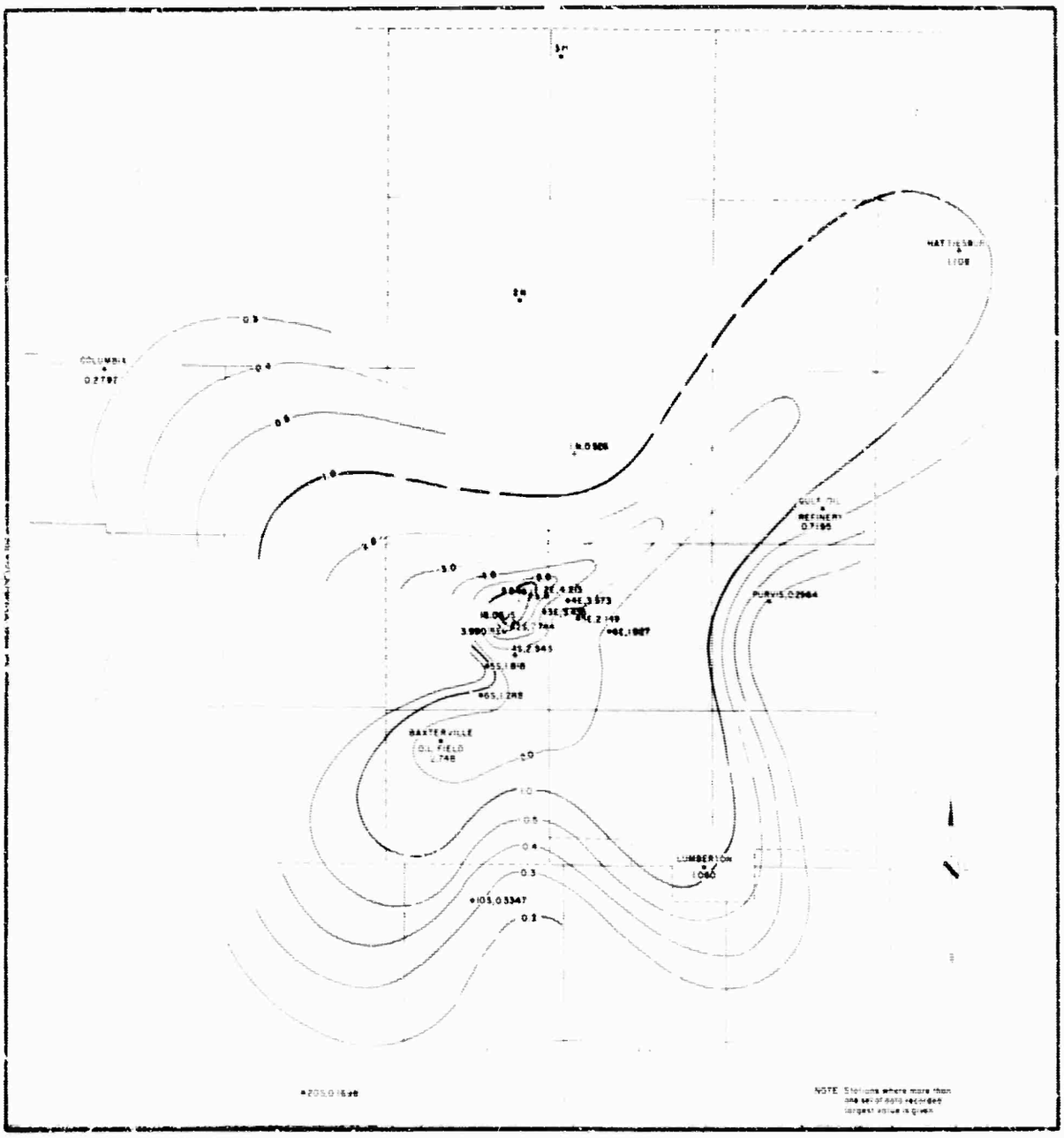

Figure 3.19 Contour Map of Transverse Component of Peak Particle Velocity (cm/sec)

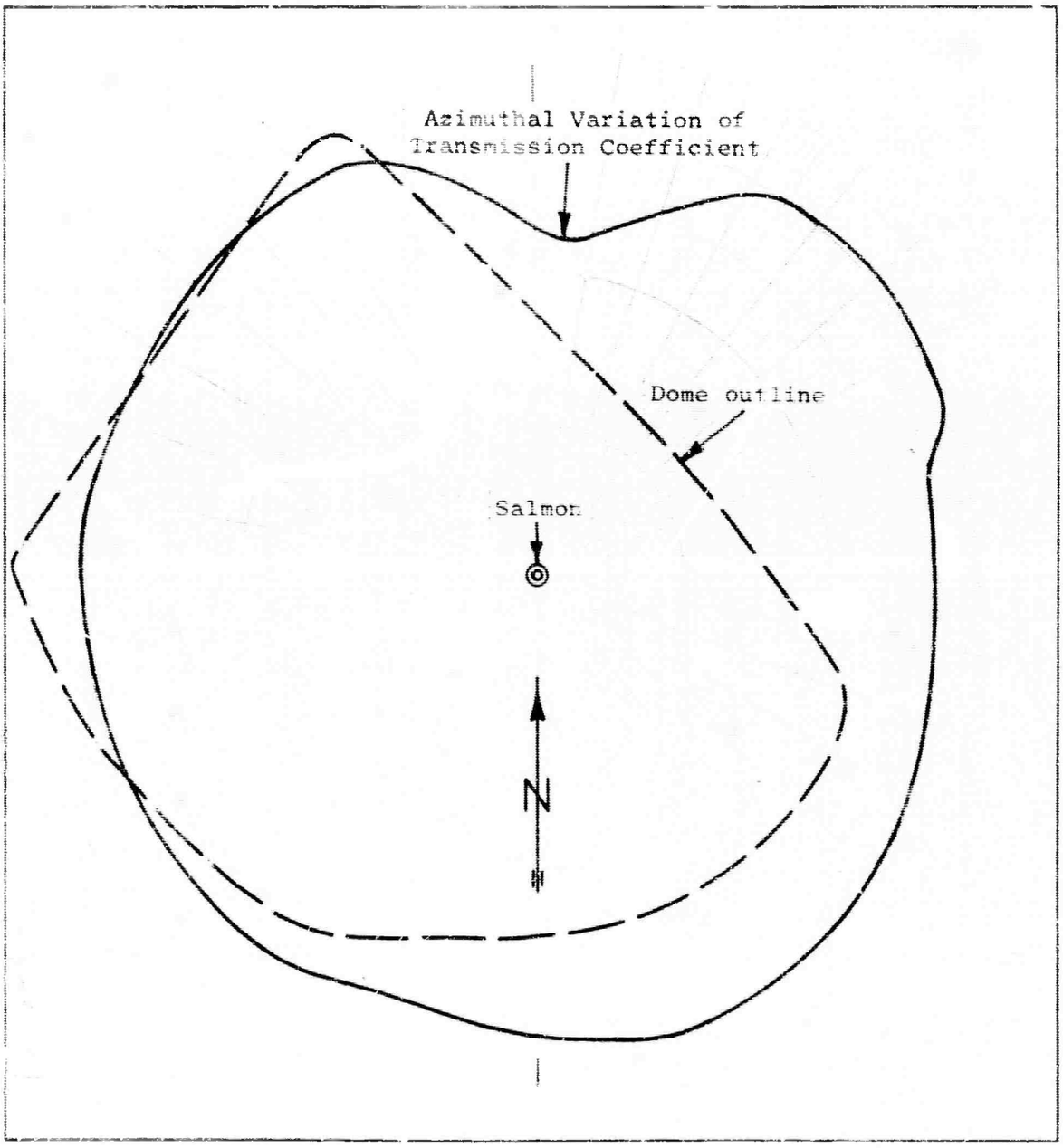

Figure 3.20 Variation in the Longitudinal Plane Wave Transmission Coefficient at the Edge of the Tatum Salt Dome at Shot Level

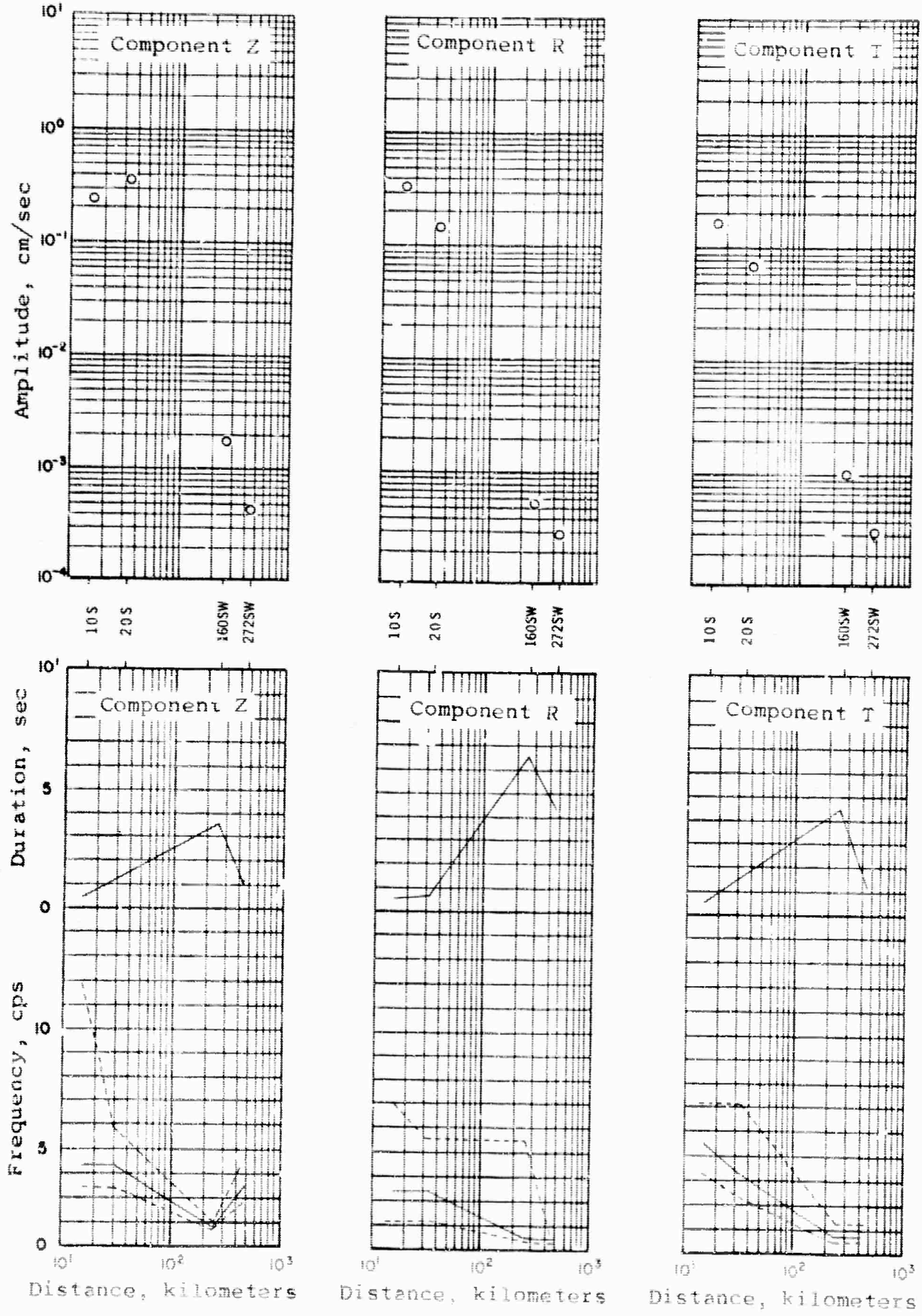

Figure 3.21 Variation with Distance of Amplitude, Frequency, and Time Duration of Particle Velocity at the Time of Peak Displacement.

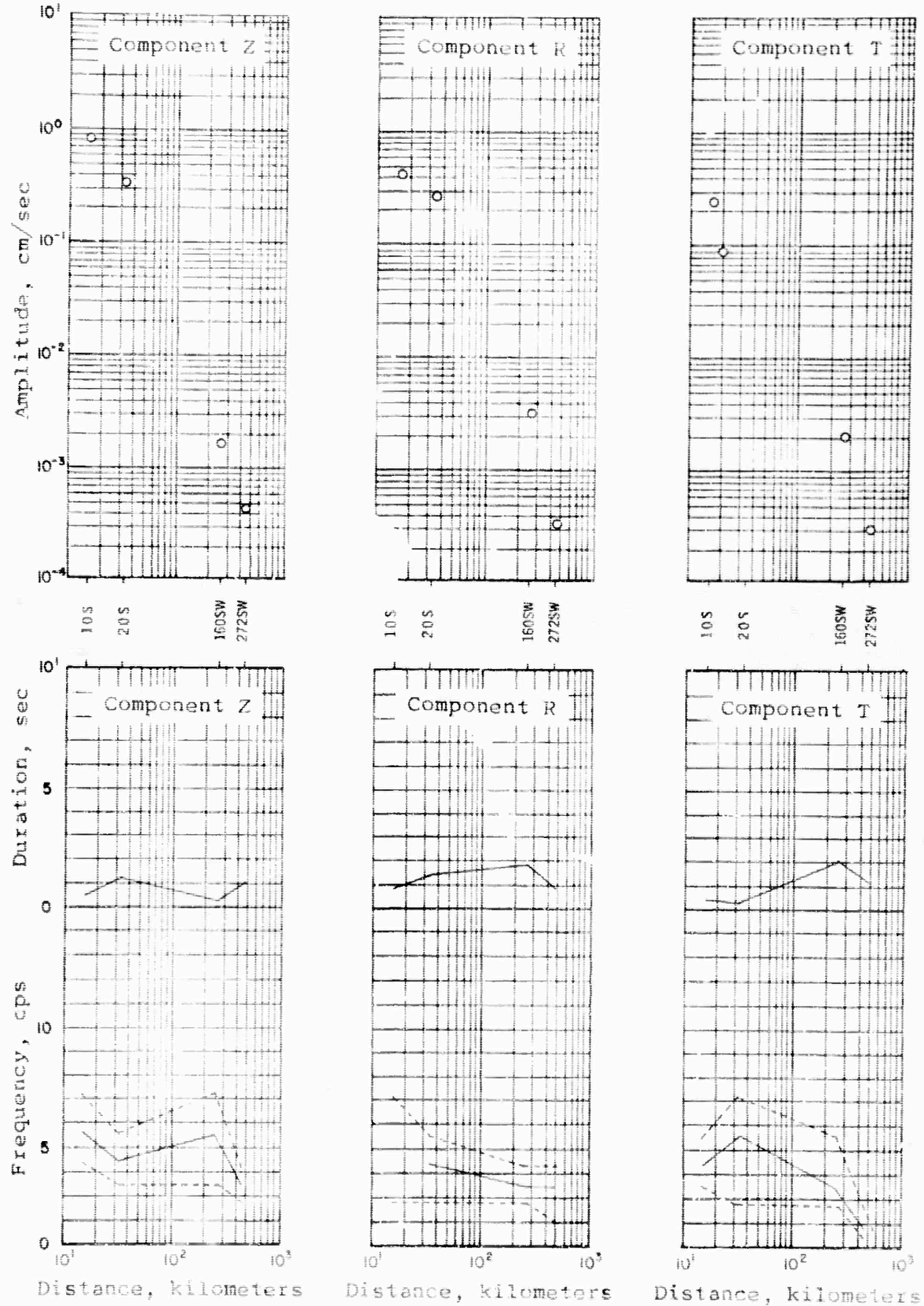

Figure 3.22 Variation with Distance of Amplitude, Frequency, and Time Duration of Particle Velocity at the Time of Peak Velocity.

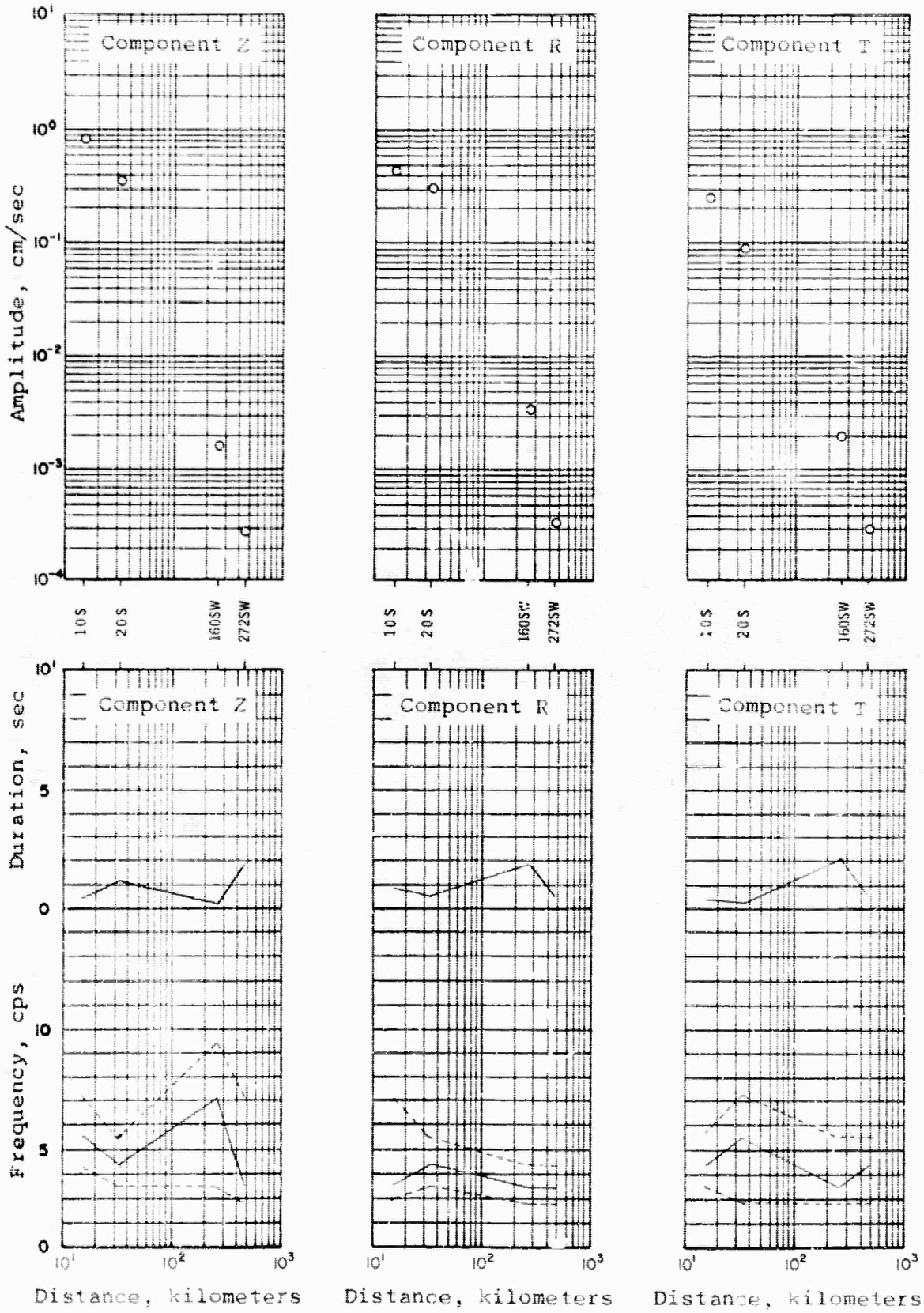

Figure 3.23 Variation with Distance of Amplitude, Frequency and Time Duration of Particle Velocity at the Time of Peak Acceleration.

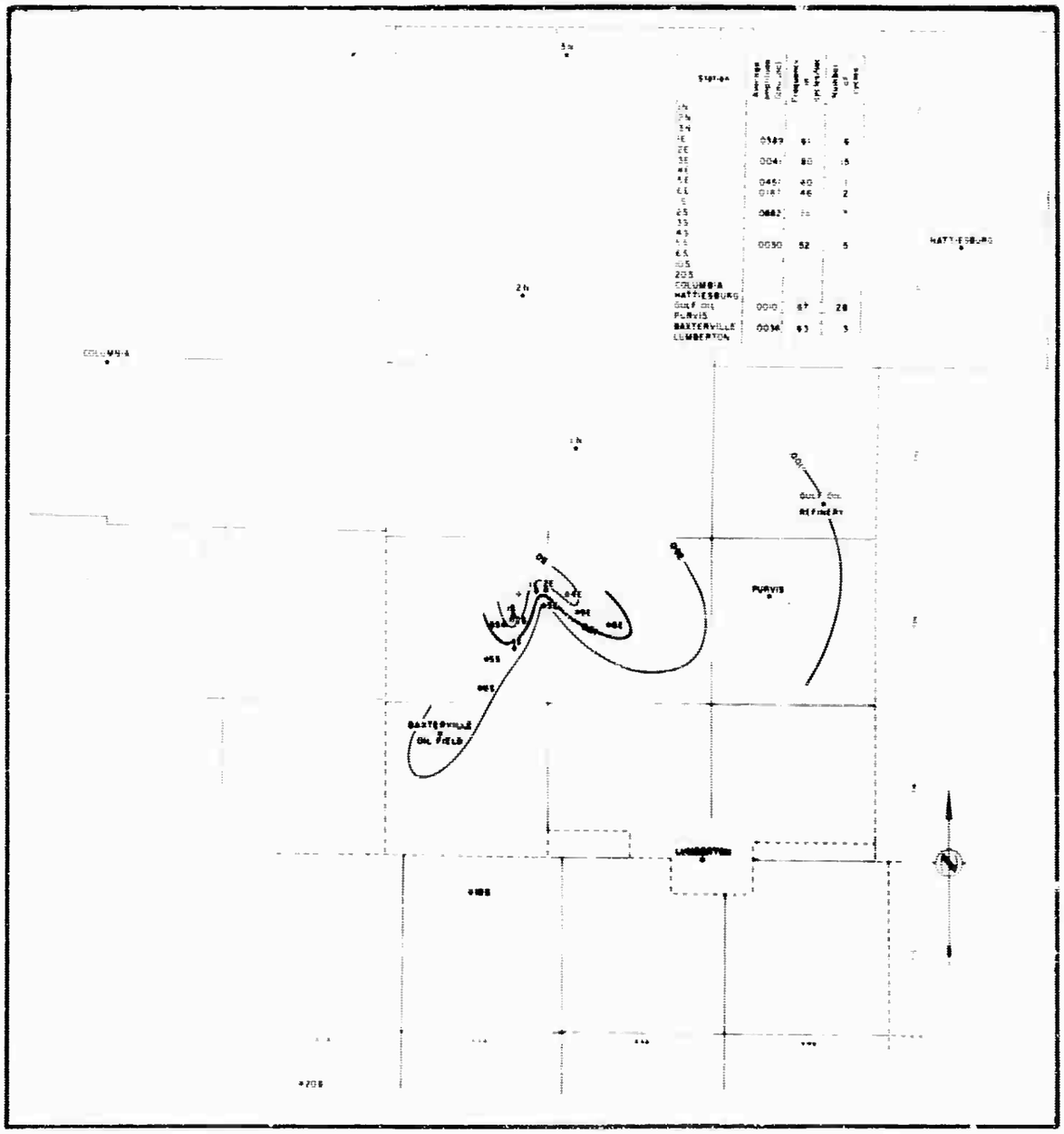

Figure 3.24 Average Vertical Velocity Contours in cm/sec from .35 to .86 cycles/sec.

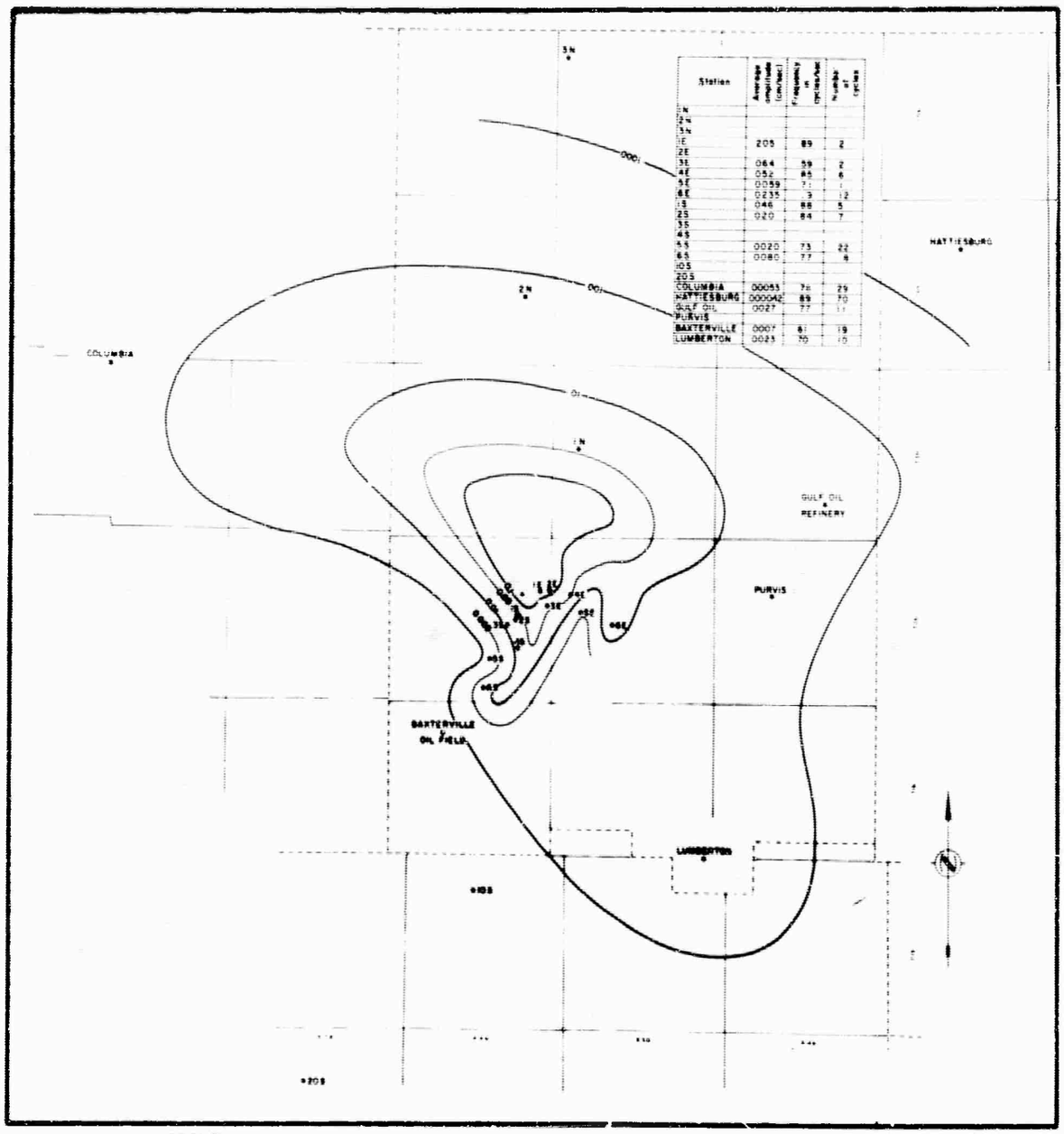

Figure 3.25 Average Radial Velocity Contours in cm/sec from .35 to .86 cycles/sec.

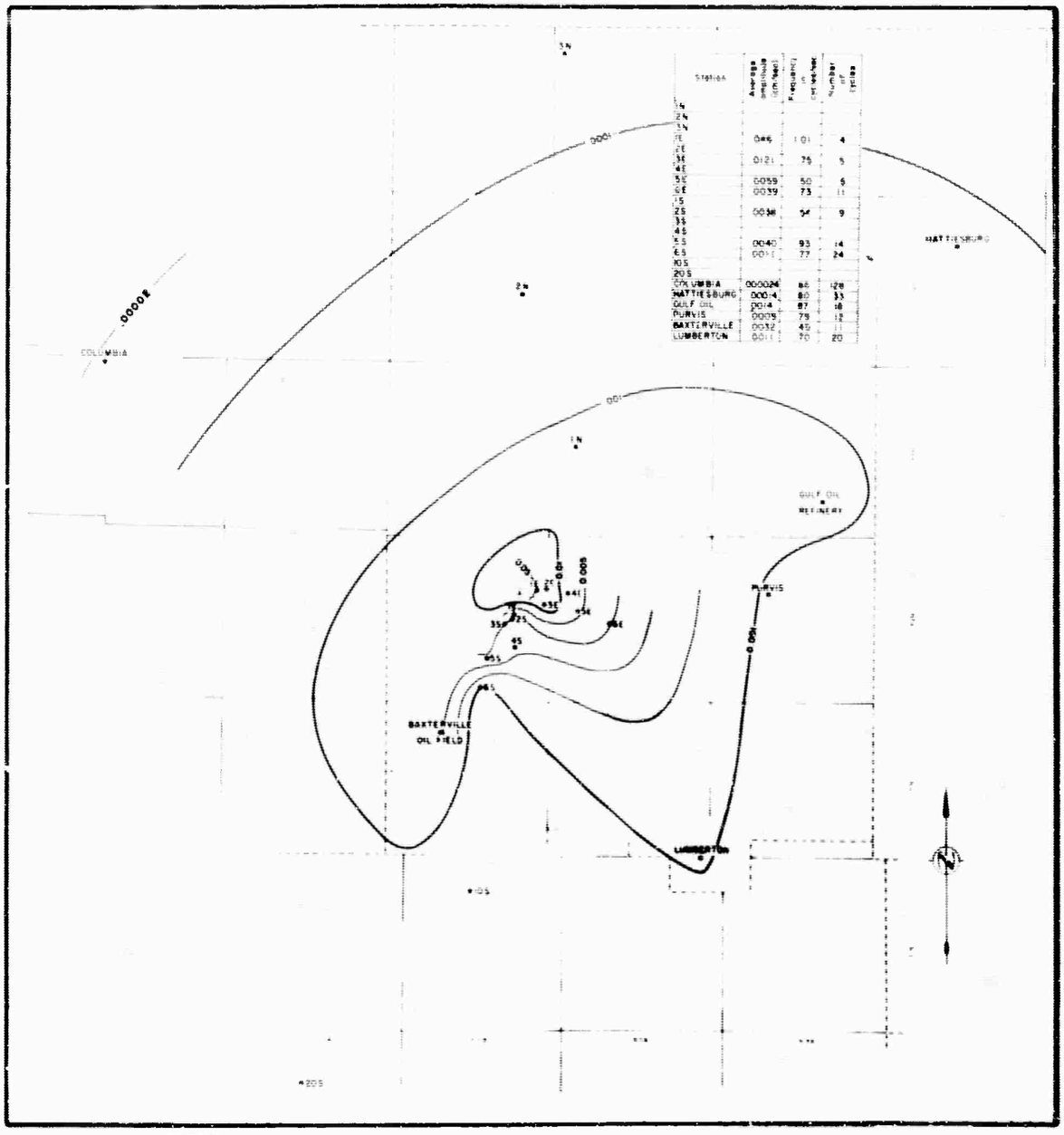

Figure 3.26 Average Transverse Velocity contours in cm/sec from .35 to .86 cycles/sec.

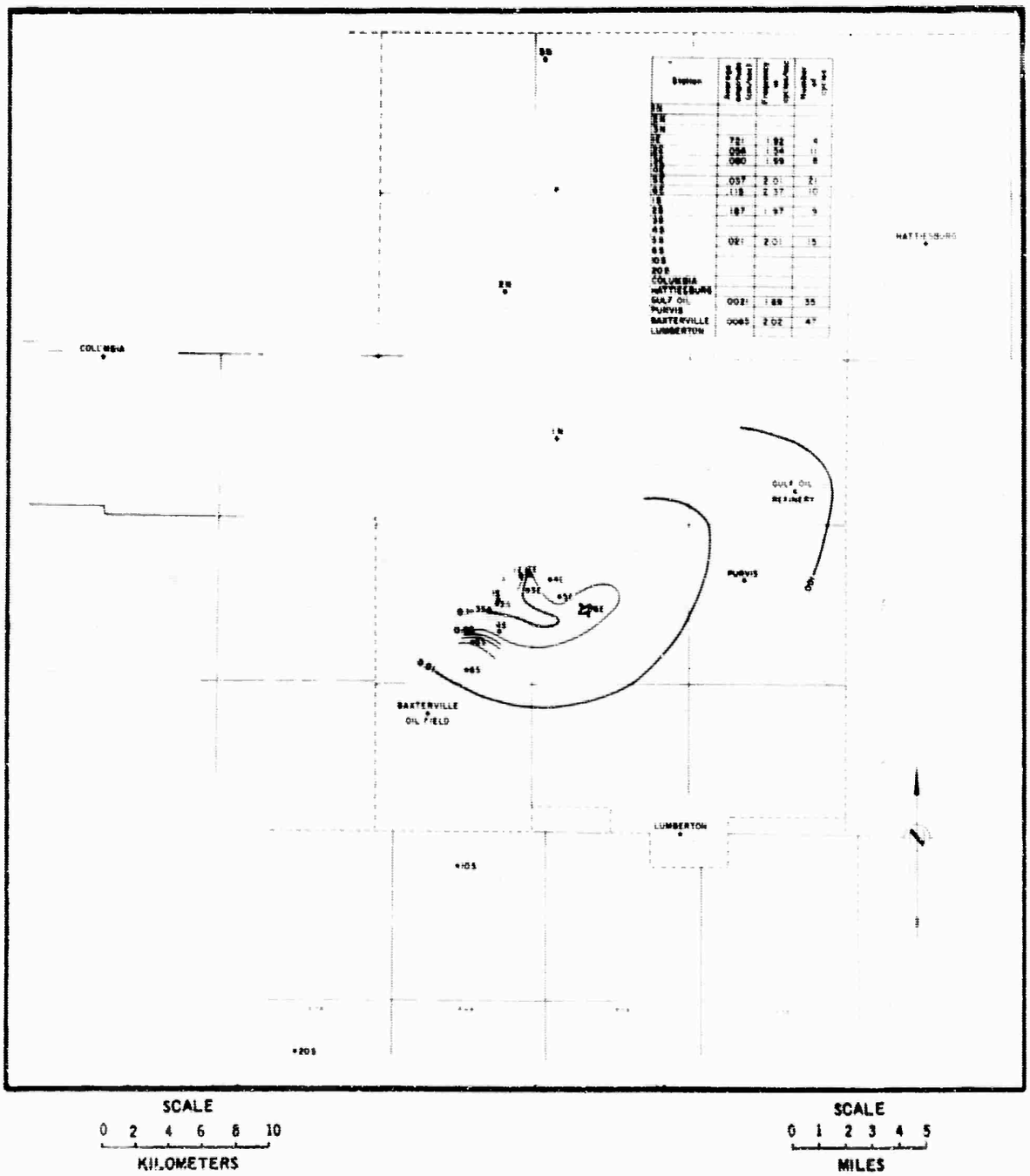

Figure 3.27 Average Vertical Velocity Contours in cm/sec from .86 to 2.14 cycles/sec.

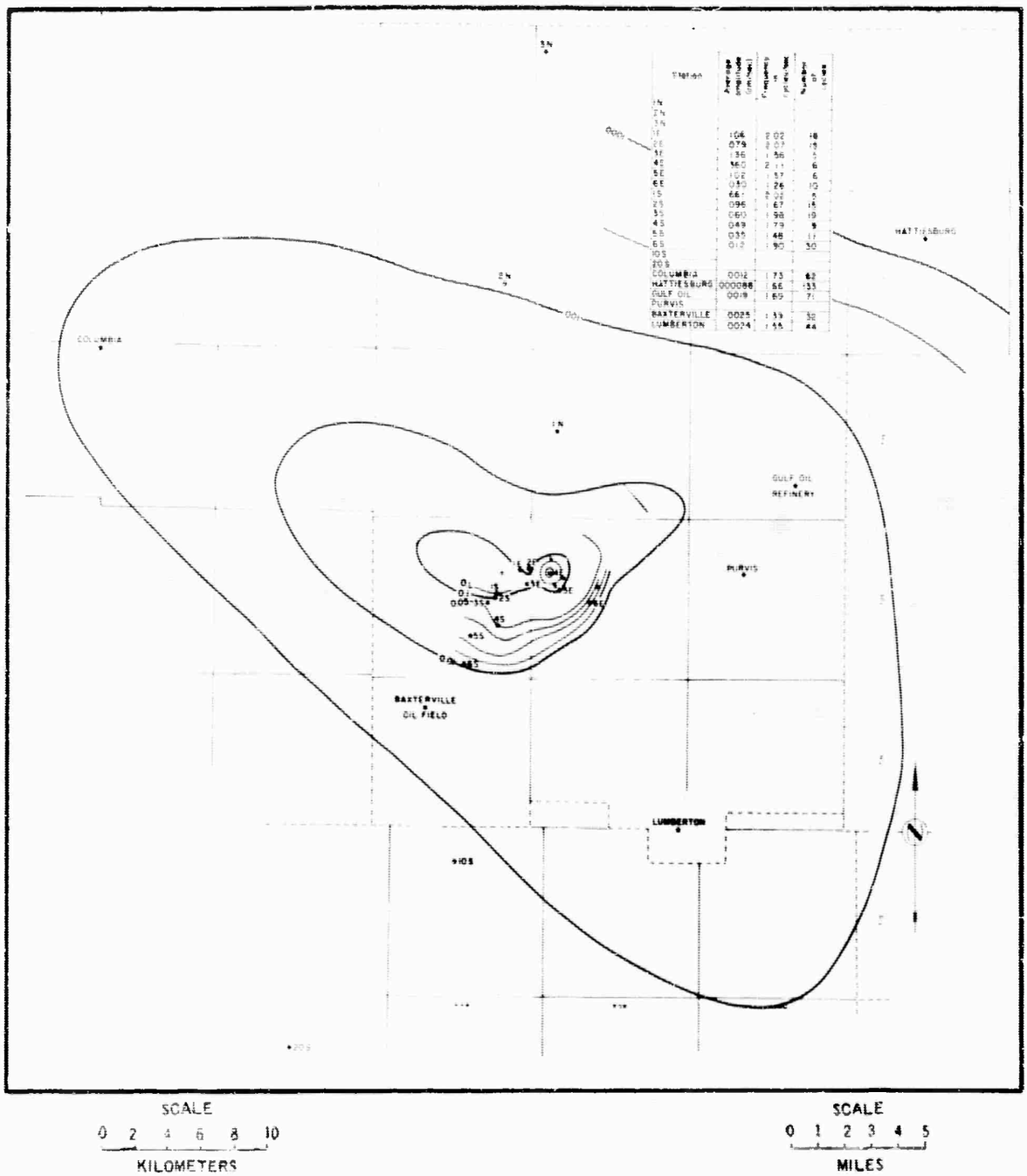

Figure 3.28 Average Radial Velocity Contours in cm/sec from .86 to 2.14 cycles/sec.

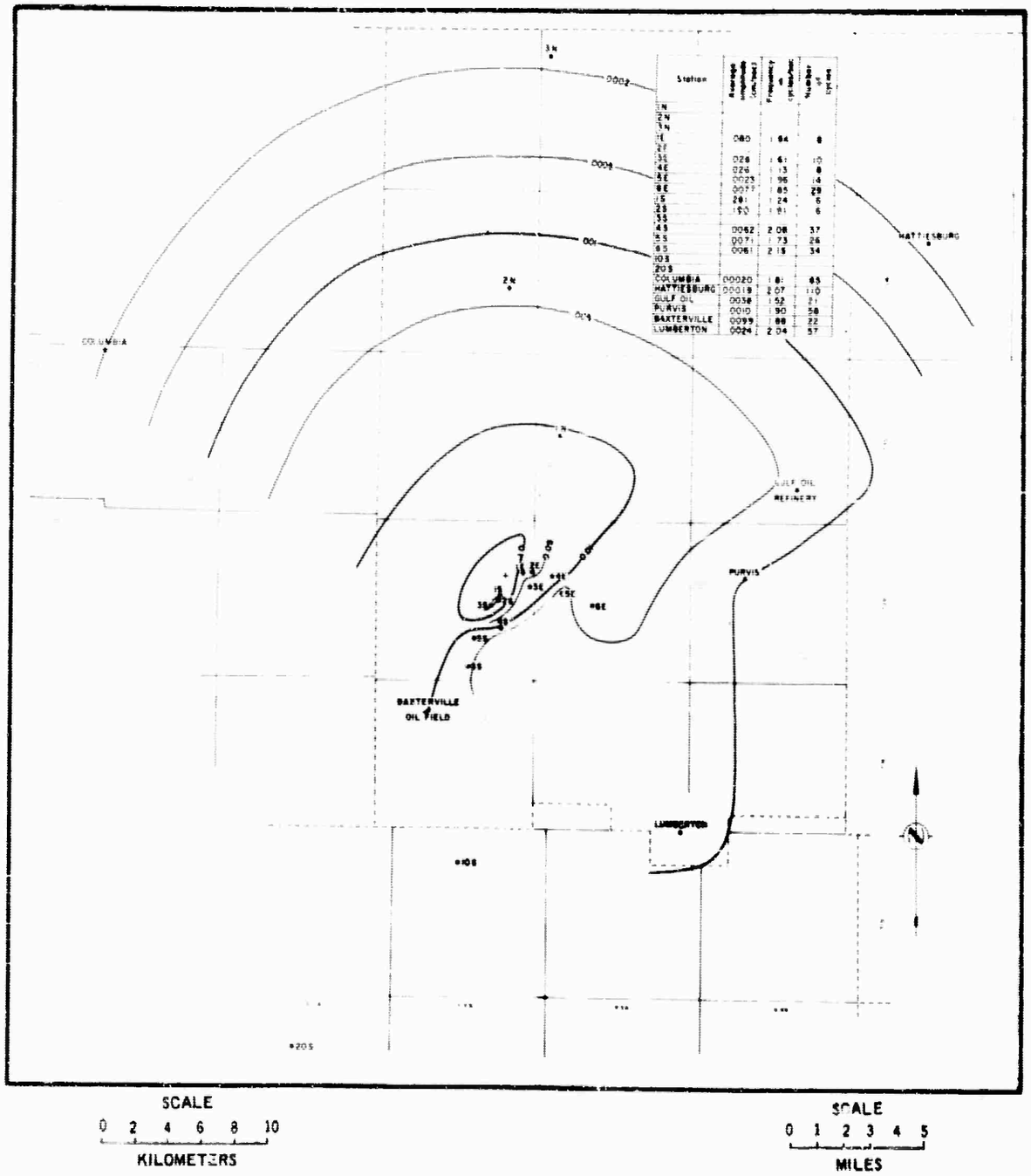

Figure 3.29 Average Transverse Velocity Contours in cm/sec from .86 to 2.14 cycles/sec.

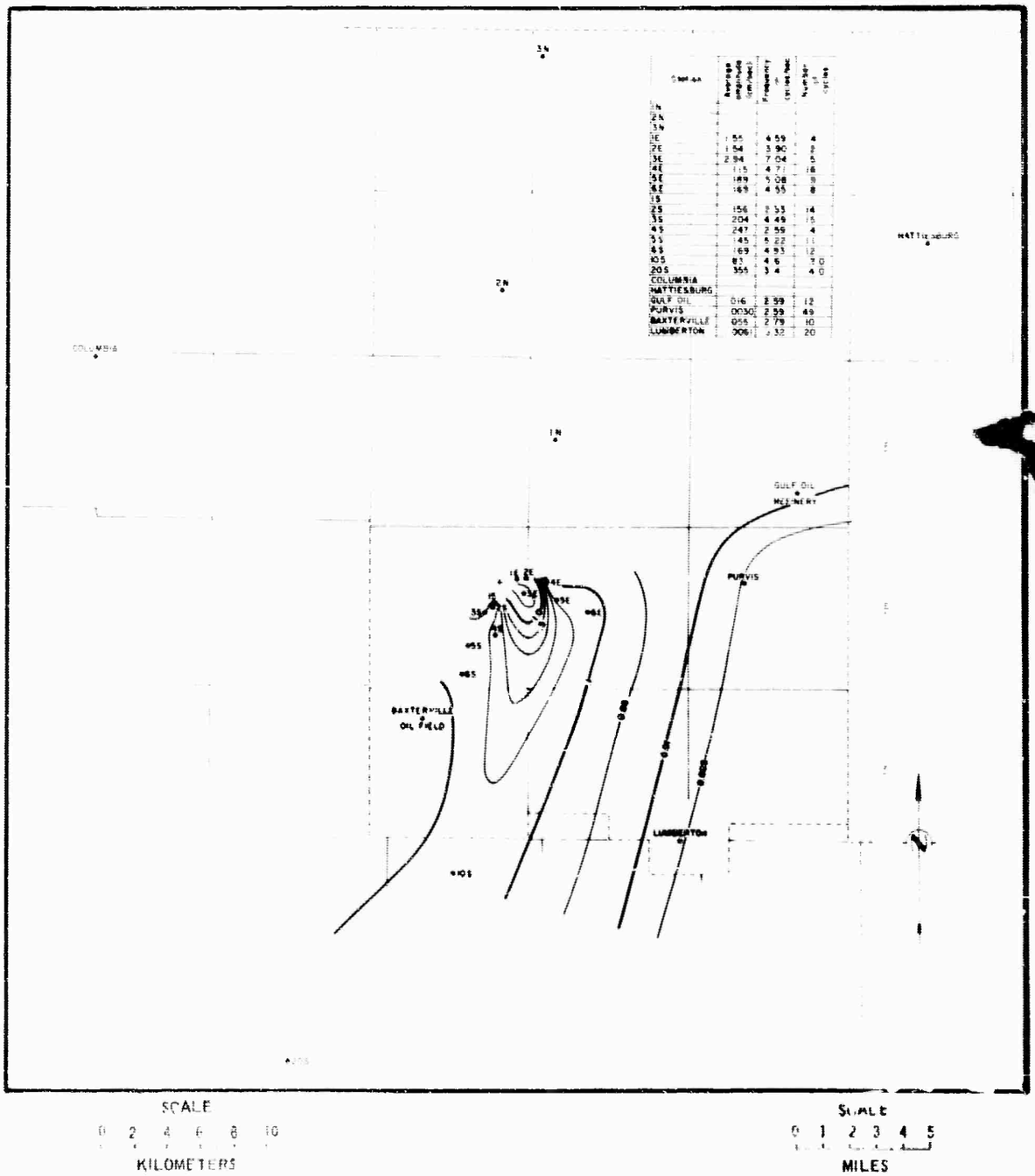

Figure 3.30 Average Vertical Velocity Contours in cm/sec from 2.14 to 5.34 cycles/sec.

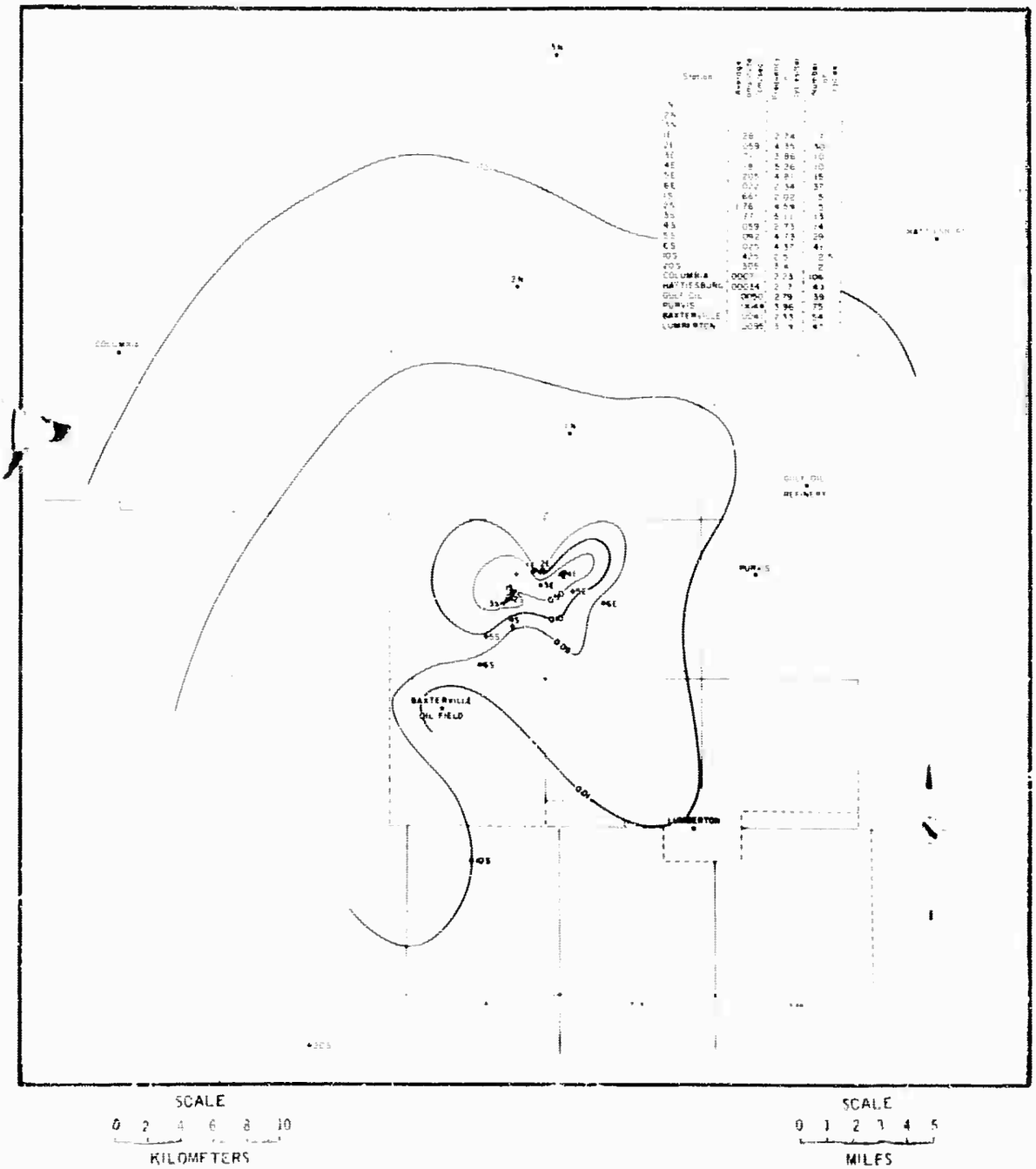

Figure 3.31 Average Radial Velocity Contours in cm/sec from 2.14 to 5.34 cycles/sec.

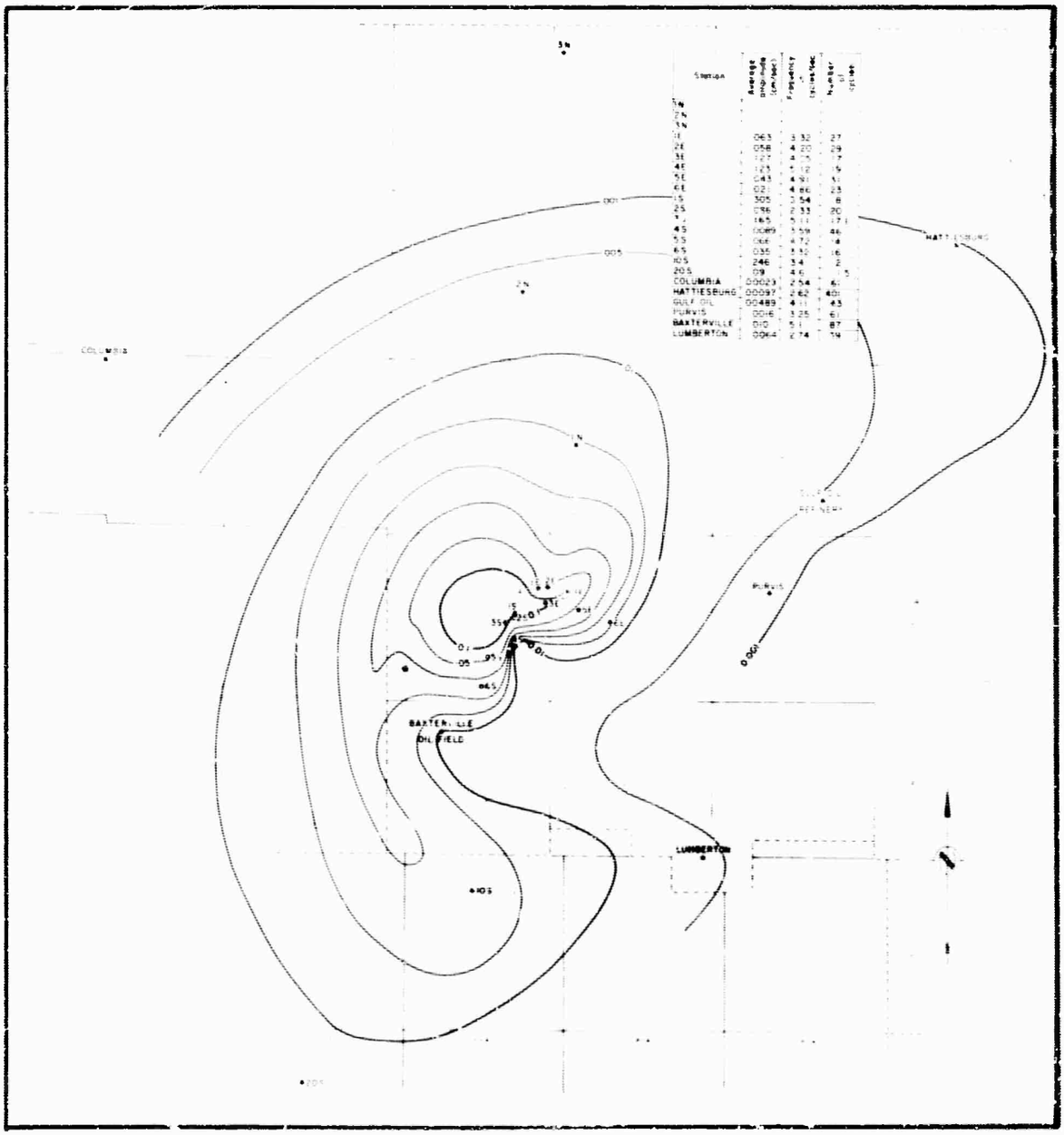

Figure 3.32 Average Transverse Velocity Contours in cm/sec from 2.14 to 5.34 cycles/sec.

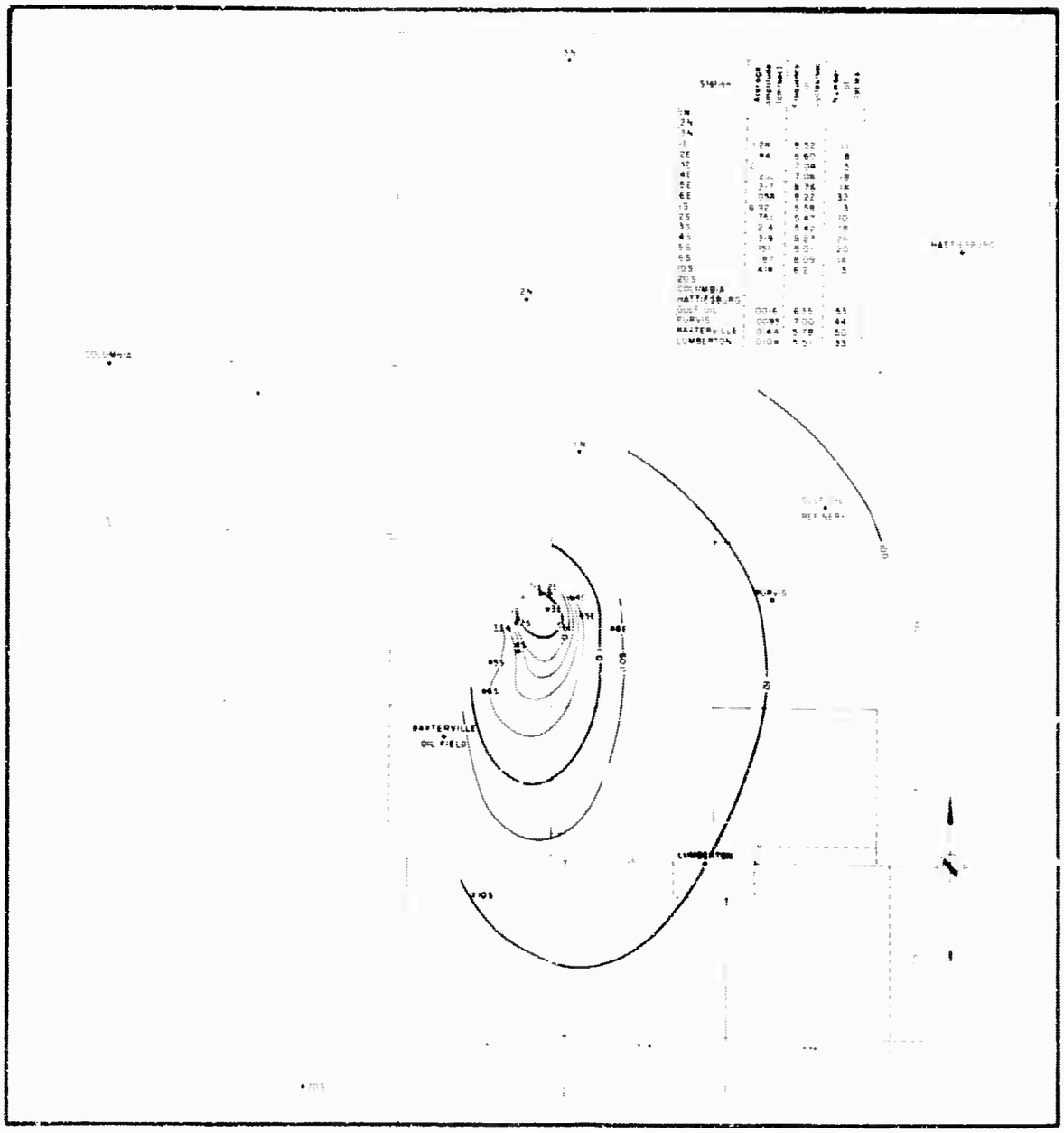

Figure 3.33 Average Vertical Velocity Contours in cm/sec above 5.34 cycles/sec.

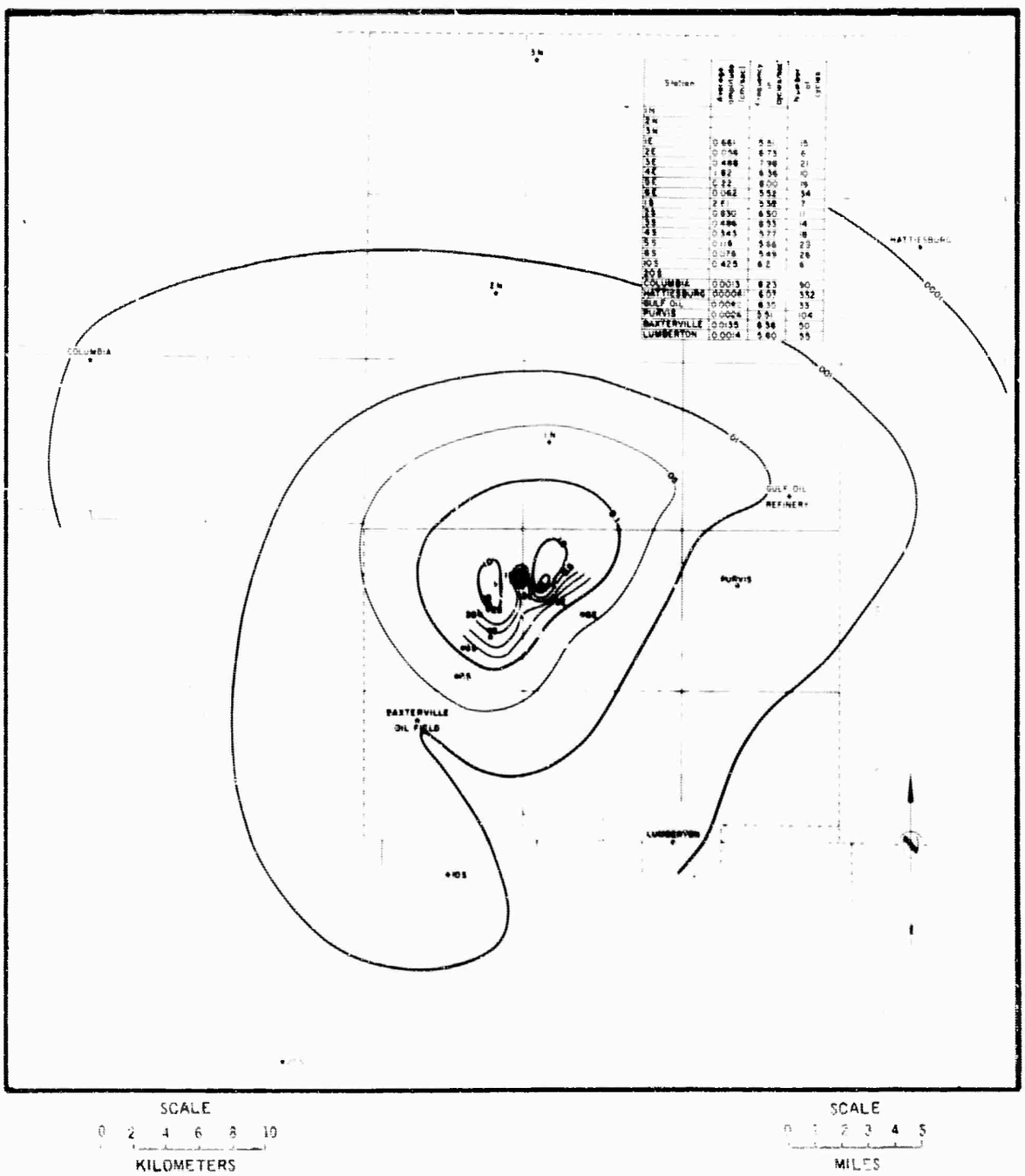

Figure 3.34 Radial Velocity Contours in cm/sec above 5.34 cycles/sec

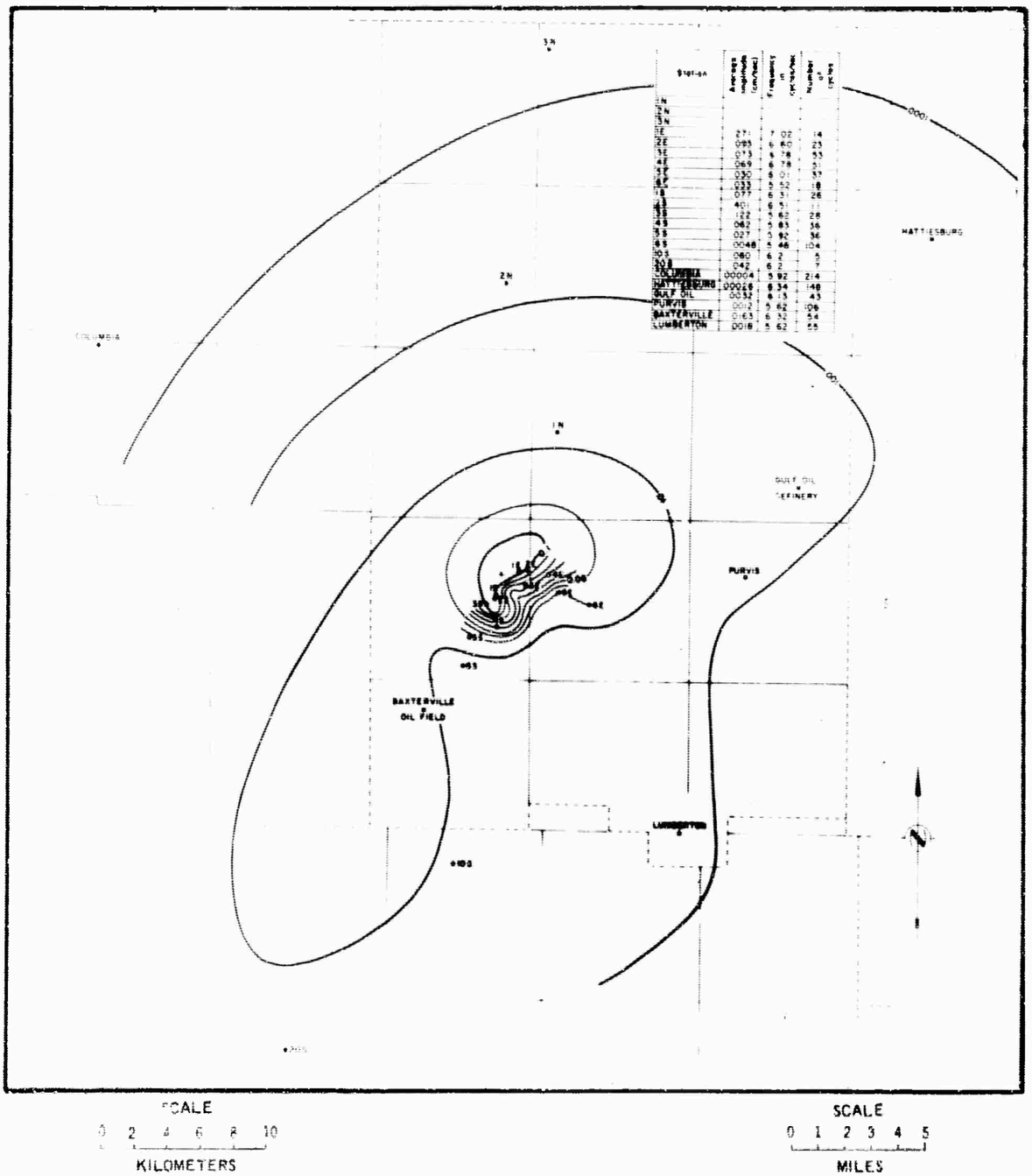

Figure 3.35 Transverse Velocity Contours in cm/sec above 5.34 cycles/sec.

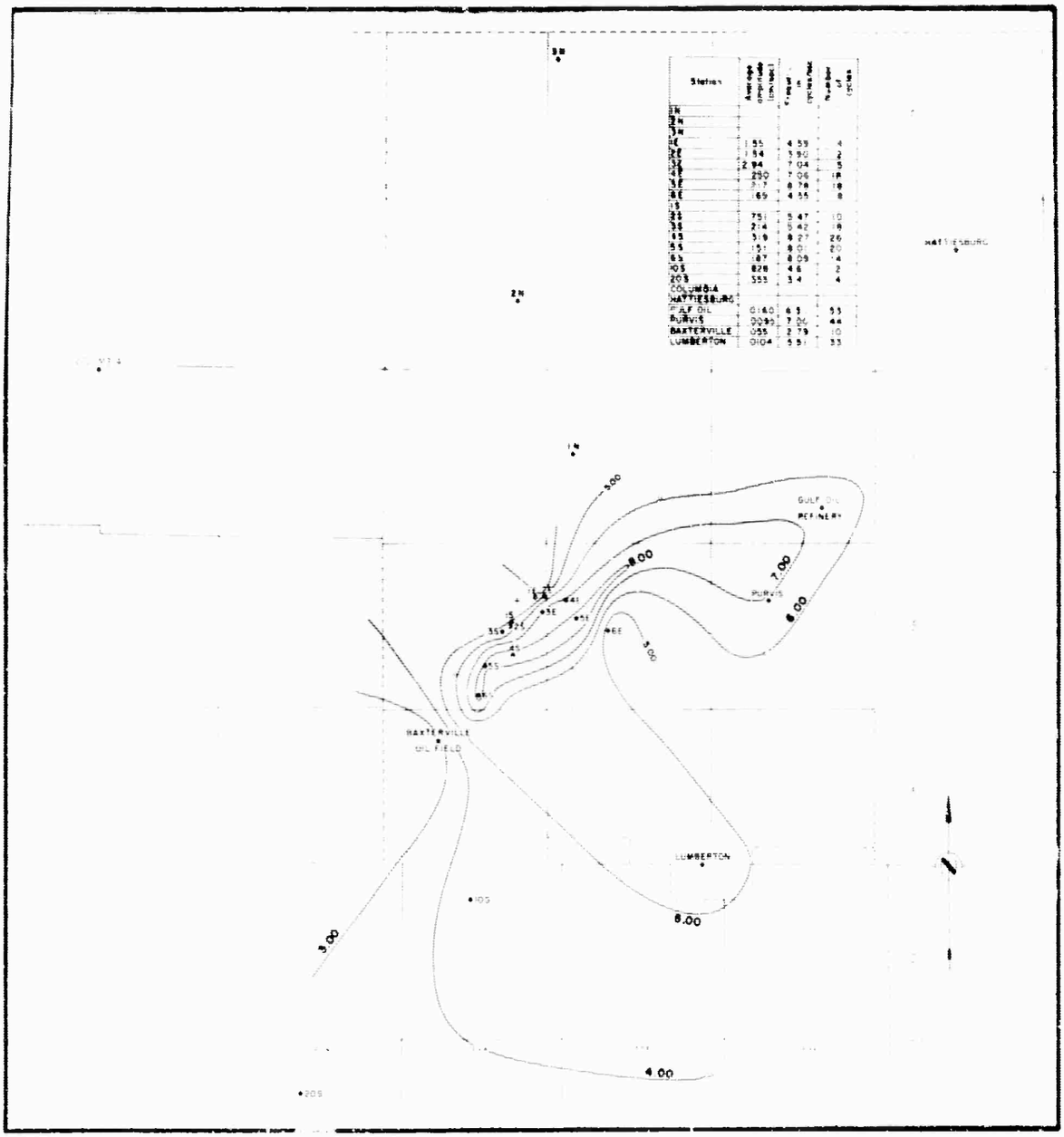

Figure 3.36 Contours of all Vertical Frequencies, cps.

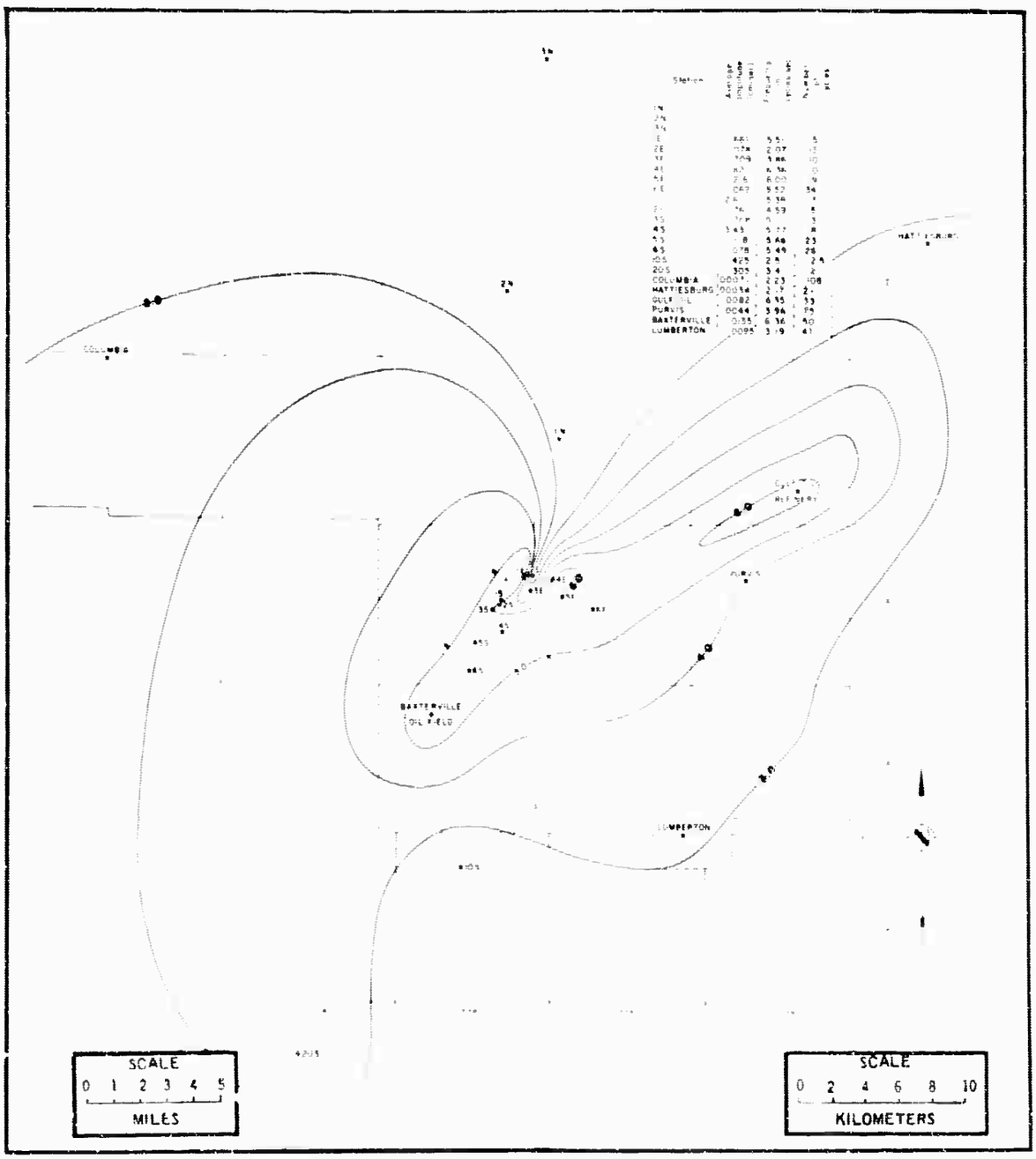

Figure 3.37 Contours of all Radial Frequencies (cps)

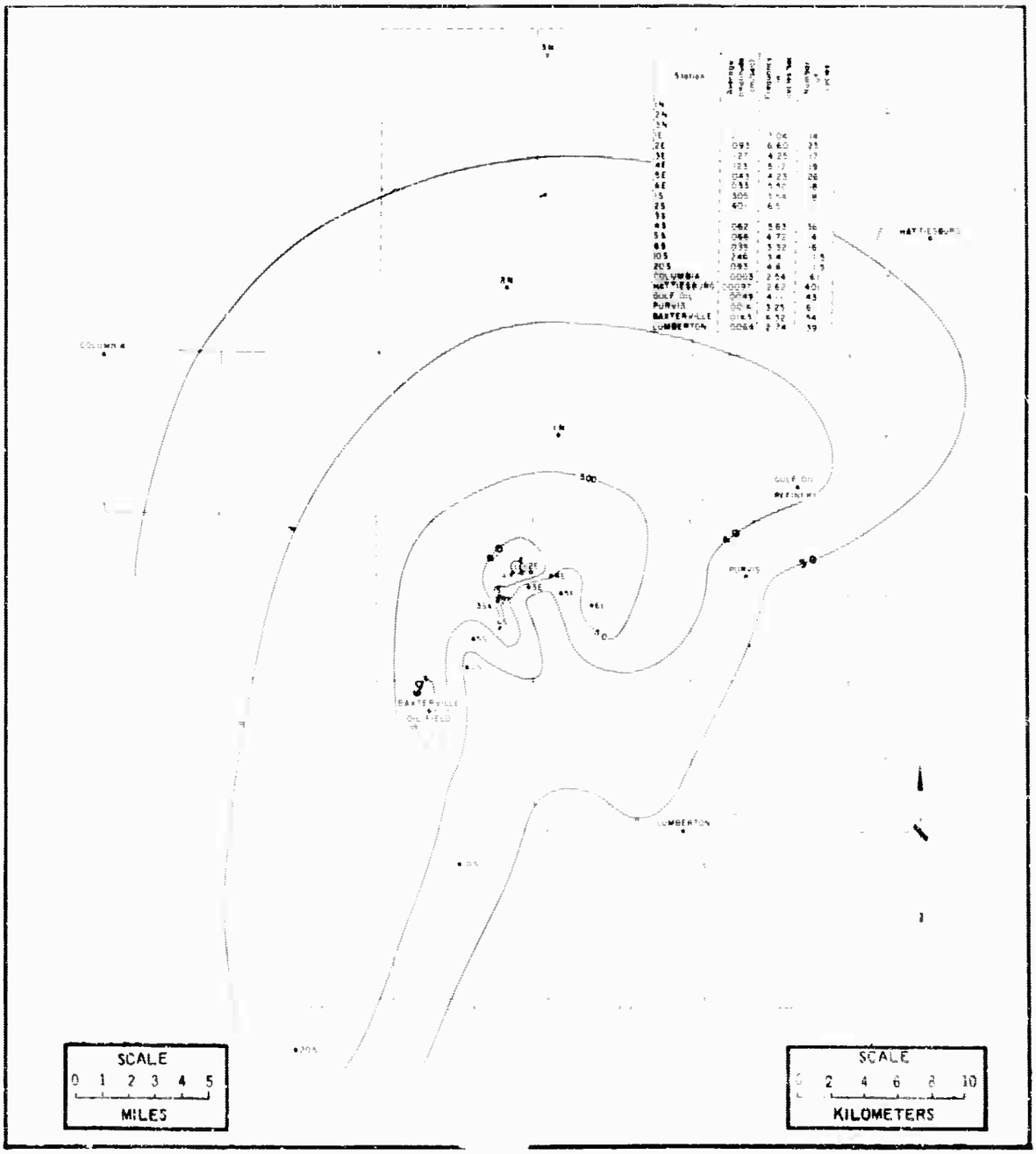

Figure 3.38 Contours of all Transverse Frequencies (cps)

CHAPTER 4

CONCLUSIONS AND RECOMMENDATIONS

4.1 GROUND MOTIONS

Detonation of the 5 ± kt Salmon event in halite provided a great deal of useful information on seismic effects relating to public safety. However, the large number of claims of damage to structures extending out to a distance of 40 kilometers from surface zero raised serious questions. The more important question was the criterion of damage in terms of ground motion. However, this is beyond the scope of this report. The second question, related to the first, is the amplitude of the ground motions that caused the damage.

While the measurements of ground motion on lines to the east and south with USC&GS strong motion instruments compared favorably with predictions, this fact has limited significance. Motions along other azimuths are essentially unknown and there are indications that large azimuthal variations in ground motions occurred, which probably originated at the source. The observed distance to 0.1 g based on all available measurements was on the average about 8 kilometers compared to 7.2 predicted. However, because of azimuthal variations 0.1 g may have been experienced out to a distance of 16 kilometers.

The other great uncertainty is the amplitude of motions because of their low frequency. Long period waves beyond the capabilities of the instruments were probably present. The amplitudes of these waves may have exceeded the amplitudes of observed motion. Their significance in causing damage is, therefore, also uncertain.

4.2 CONTAINMENT

The depth of the event was such that there was little question that it would be adequately contained except for uncertainties in regard to the condition of the event hole and satellite holes. The drilling and grouting of holes was difficult, and it was not certain that adequate seals had been provided. On the basis of the verbal assurances of the Project Officer, USAEC, Hattiesburg, Miss., that construction had been accomplished in accordance with plans and specifications, approval was recommended to the Manager, NVOO.

The predictions of overall containment and adequacy of stemming were substantiated. Post-shot exploration programs permitted comparisons of predicted and observed values for the cavity radius, chimney height, crack and radioactive crack radius, spall depth and spall replacement. These com-

parisons showed good agreement and indicate the validity of the methods employed.

4.3 EFFECTS OF GROUND MOTION ON SUBSURFACE FACILITIES

It was predicted that there would be no physical damage to aquifers, the oil and gas facilities near Baxterville and the Olin Mathieson operation near McIntosh, Alabama. There was no reported damage to any of these facilities.

4.4 RECOMMENDATIONS

In view of the difficulties in making an adequate analysis of the ground motion from Salmon, it is strongly recommended that more comprehensive instrumentation be employed for any future off-site event. An instrumentation plan will be required on the minimum number of lines necessary to determine azimuthal variations indicated by geologic considerations. Instruments should be capable of recording long period motions, preferably down to a frequency of 0.03 cps.

APPENDIX A

ANALYSIS OF SPALLING MECHANISM

Spalling is herein defined as the fracturing of a solid by tensional stress produced when a seismic pulse is reflected from a free face. The conversion of a compressional pulse to a tensional one is considered to be perfectly elastic with no loss of energy into the atmosphere at the solid-air interface.

The problem is to analyze the stress situation at continuous distances back from the free face to determine if sufficient tension exists to fracture the solid. The tensional stress arises only from the reflected pulse, whereas those forces resisting fracturing are that portion of the compressional pulse waveform which has not yet arrived at the interface, the tensile strength of the medium, and any overburden pressure which becomes significant when horizontal surfaces and long wave lengths are considered.

If the problem is restricted to one involving compressional pulses arising from subsurface nuclear detonations and a rock medium, generalized equations may be used to determine the stress condition at continuous depths below the surface. The equations are based on hydrodynamic considerations and machine computations;

in the form shown they are applicable at ranges of a few hundred meters. The pulse shape assumed is one with an exponential decay thus producing a maximum pressure the instant the peak reaches a point of interest. The stress condition at any point below the surface may then be given by:

$$P_{net} = P_{ovb} + P_{ts} + P_{pwf} - P_{ref.} \qquad (A.1)$$

where P_{net} = net stress at the section of interest

P_{ts} = constant - tensile strength of the medium

P_{ovb} = K (depth) - overburden stress

$P_{pwf} = P_p \left(\frac{r}{R}\right)^2$ - pressure wave form or that portion of the pulse which has not arrived at the free surface

$P_p = CR^{-1.5}$ - peak pressure

$P_{ref.} = CR^{-1.5}$ - reflected peak pressure

where R = depth of burial plus the depth of interest

r = depth of burial minus the depth of interest.

The value of each of these quantities may then be computed as functions of depth to determine if P_{net} becomes $\geq$ zero, in which case a spall is predicted to occur. When a spall occurs, the overburden pressure must be reduced to zero since the overlying strata are detached, and recomputed for further depths of interests on the basis of the newly created free surface. Additionally, the peak reflected pressure ($P_{ref.}$) must be reduced

to the value of the pressure wave form (P_{pwf}) at the new free face since the energy in the descending pulse is trapped in the spalled section. On the basis of these new values further depths of interest may be investigated to determine if additional spalls will occur.

Since actual test conditions are not similar to free field predictions for a homogeneous medium, corrections for the variation in the stratigraphic section are introduced. The transmission coefficient, or change of pressure across an interface, is given by:

$$\frac{P_2}{P_1} = \frac{2\rho_1 C_1}{\rho_1 C_1 + \rho_2 C_2} \qquad (A.2)$$

where $\rho_1 C_1$ are the density and compressional wave propagation velocity of the original medium and $\rho_2 C_2$ are those of the medium across the interface. Corrections for transmission coefficients must be introduced at all depths where they are applicable, to both the ascending and descending pulses.

The analysis as outline above is confined to the case of normal incidence only and three methods are presently available for the solution of the calculations; these are by graphical procedures, analog computer and digital computer.

POST-SHOT CHIMNEY CALCULATIONS

Calculations to determine the height to which post-shot chimney formation will occur are based on the assumption that:

1) The post-shot cavity is spherically symmetrical,

2) The chimney is cylindrical with a radius equal to that of the cavity, and

3) An increase in volume will occur upon breaking of solid material.

The volume of the cavity, or void, is

$$V_{cav.} = 4/3 \ \pi \ R^3 \qquad (A.3)$$

The volume of the chimney (Vch) is then given by $Vch = \pi R^2 h$ where (h) is the height above the shot point.

Since the chimney volume includes one half of the cavity void, the volume of solids is seen to be:

$$V_{sol} = V_{ch} - 1/2 \ V_{cav.} \qquad (A.4)$$

The original volume of solid material must then swell upon breaking to include both its original volume and the volume of the existing void

$$(n) \ V_{sol} = V_{cav.} + V_{sol} \qquad (A.5)$$

where (n) is the swell factor for the medium being considered.

Then $n \left[\pi R^2 h - 2/3 \pi R^3 \right] = 4/3 \pi R^3 + \pi R^2 h - 2/3 \pi R^3$

and $n (h - 2/3 R) = 2/3 R + h$

yielding $n = \frac{h + 2/3 R}{h - 2/3 R}$ and $h = \frac{2/3 R (1+n)}{n-1}$. (A.6)

The value of (n) may then be determined for mediums in which experience is available and subsequently be used to determine the chimney height for future events, in the same medium, based on the predicted cavity radius.

PERMANENT DISPLACEMENT AND STRAIN CALCULATIONS

With the detonation of an underground nuclear explosion a post-shot cavity results which is larger than the original shot chamber. The expansion of this cavity to its final size entails the vaporization, melting and deformation of the material surrounding the original chamber. The major portion of the material is displaced radially from the source. The difference in position between an original point in the medium and its final location, as measured upon re-entry, is termed the permanent radial displacement of the point.

EQUATION DERIVATION

Given the initial chamber radius and final cavity size, the assumption can be made that the medium has behaved as an incompressible material and no loss of volume of material has occurred through vaporization or melting. The volume of material which originally occupied the post-shot cavity must therefore be distributed throughout the medium. Assuming spherical symmetry the following equation may be derived:

Given: R_1 = radius of original shot chamber

R_1' = radius of post-shot cavity.

R_2 = original radius to point of interest

R_2' = final radius to point of interest

If the original and final volumes are equal, then

$$4/3\ \pi \left[(R_2)^3 - (R_1)^3\right] = 4/3\ \pi \left[(R_2')^3 - (R_1')^3\right] \qquad (A.7)$$

and $(R_2')^3 = (R_2)^3 - (R_1)^3 + (R_1')^3$ yielding $\Delta R_2 = R_2' - R_2$ (A.8)

which is the permanent radial displacement of a point whose initial position was R_2.

Given the predicted radial permanent displacements, the tangential strains may be computed by considering the change in circumference at any radius of interest.

The compressive strain due to a radial displacement is obtained by plotting the displacement versus distance,

and fitting an equation to that segment of interest.

At distances relevant to radial fracturing, this portion of the curve may be approximated by the equation $D = CR^{-1.9}m$.

The radial strain is then $\frac{dD}{dR} = -1.9\ CR^{-2.9}m/m$.

APPENDIX B

ANALYSIS OF BAND-PASS FILTERED DATA

Magnetic tape seismograms from NC-21 stations 10S, 20S, 160SW and 272SW were band-pass filtered and displayed as described on pages 31-36 of Reference 3.1. Center band frequencies used for this analysis were 0.41, 0.55, 0.75, 1.0, 1.35, 1.85, 2.5, 3.4, 4.6, 6.2, 8.4 and 11.3 cycles per second.

Peak acceleration, velocity and displacement were determined from unfiltered records. The corresponding peaks were noted on the filtered records allowing for the 1.0 to 1.5 cycle delay of this filter. These peaks were associated with an event on each of the filtered records, the maximum amplitude of the associated events being noted. The largest maximum amplitude and the corresponding frequency was recorded from the filtered record with the corresponding-associated-event of largest maximum amplitude.

The event containing this largest maximum amplitude was terminated by being bordered in both increasing and decreasing time by two successive peaks or troughs of amplitude less than the maximum amplitude of the event. As no internal succession of two peaks or troughs less

than the maximum amplitude were allowed, the event was defined. The beginning and end of the event were chosen as the zero crossing following and preceding the early and late bordering low amplitude peaks and troughs respectively. The starting time, duration and number of cycles of the event were recorded and the apparent frequency (equal to the number of cycles divided by the duration) was calculated and recorded.

APPENDIX C

ANALYSIS OF FOURIER FREQUENCY DATA

Velocity spectra, the square of which is directly related to the energy spectra, were calculated from strong-motion seismographs and vibration meter recordings.

Velocity was obtained by differentiating displacement and by integrating acceleration. The Fourier transform of velocity from displacement was used to analyze frequencies below 3.00 cycles per second (cps) and the Fourier transform of velocity from acceleration was used to analyze frequencies above 3.00 cps. Where acceleration records were not available the Fourier transforms of velocity from displacement were used both above and below 3.00 cps.

The peak values, $\hat{Y}(f)$, of the Fourier transform of velocity and the frequency, f, at which they occurred were recorded in four frequency ranges: 0.351 to 0.861 cps, 0.861 to 2.14 cps, 2.14 to 5.34 cps and 5.34 to 13.2 cps. The width of the associated pulse was taken as the difference between the two frequencies, on either side of the peak, at which the amplitude of the pulse was equal to 0.7 times the peak amplitude (the amplitudes between these two frequencies being greater than 0.7 times the

peak amplitude). Note that the root-mean-square (RMS) value of a sine (or cosine) wave is 0.707 = sin 45°.

This pulse can be associated with the Fourier spectrum of a single characteristic frequency as discussed on pages 18-24 of Reference C.1. Using Figure C5 on page 24 of this reference one notes that the pulse width, measured from the 0.49 maximum amplitude points[1], is approximately 0.92 times the fundamental frequency. Hence the duration in time, Δt, of the single characteristic frequency to be associated with the measured peak pulse is

$$\Delta t = (\text{fundamental frequency})^{-1} = \frac{(0.92)}{(\text{Pulse Width})} \qquad (C.1)$$

The amplitude, Y_o, associated with this single characteristic frequency can be computed as follows. Let

f = frequency associated with peak values of Fourier transform (cps).

---

[1] $0.49 = (0.7)^2$, as Figure C5 represents a squared Fourier spectrum.

Δt = duration (sec) of frequency f

$$g(t) = \begin{cases} Y_o \cos(2\pi ft), & t \in [o, \Delta t] \\ o, & t \notin [o, \Delta t] \end{cases}$$

$\hat{Y}(f)$ = amplitude of Fourier transform at frequency f

then

$$\hat{Y}(f) = Y_o \int_o^{\Delta t} \cos^2 (2\pi ft)\, dt = Y_o \left(\frac{\Delta t}{2}\right) \qquad (C.2)$$

provided $(f\Delta t)$ is an integer.

$$Y_o = \left(\frac{2}{\Delta t}\right) \hat{Y}(f) \qquad (C.3)$$

Y_o, the amplitude associated with $\hat{Y}(f)$, the peak Fourier amplitude, was contoured on maps. The frequency f and its duration (no. of cycles) was noted.

Errata: A consistent error has been discovered which is within the margin of error of the measurements. For the sake of accuracy the values in the tables and

on the maps should be multiplied by the following in order to obtain the best approximation to these values:

Multiply duration values in time and number of cycles by .88.

Multiply average amplitude by 1.14.

Note: This error is very small in light of other uncertainties. Therefore, considering the magnitude of work involved in revising the tables and graphs, no corrections have been made for this report.

REFERENCES

2.1 "Salt Disposal Study, Project DRIBBLE, Tatum Dome Area, Lamar County, Mississippi"; July 1962; U. S. Bureau of Mines, Washington, D.C.

2.2 C. J. Harvey and R. V. Chafin; "Geology and Hydrology of the Tatum Salt Dome, Lamar County, Mississippi"; Technical Letter DRIBBLE-34; April 29, 1963; U.S.G.S., Department of the Interior, Washington, D.C.

2.3 R. V. Chafin, et al; "Log of Exploratory Hole 1, Tatum Dome, Lamar County, Mississippi; Technical Letter DRIBBLE-8; October 26, 1961; U.S.G.S., Department of the Interior, Washington, D.C.

2.4 D. H. Eargle; "Geology of Core Hole WP-4, Tatum Dome, Lamar County, Mississippi"; Technical Letter DRIBBLE-19, April 25, 1962; U.S.G.S., Department of the Interior, Washington, D.C.

2.5 Glenn C. Werth and Roland F. Herbst; "Comparison of Amplitudes of Seismic Waves from Nuclear Explosions in Four Media"; UCRL-6962, June 1962; Lawrence Radiation Laboratory, Livermore, California.

2.6 K. L. Saucier and A. D. Buck; "Project DRIBBLE, Petrographic Examination and Physical Tests of Cores, Tatum Salt Dome, Mississippi"; Technical Report #6-614, January 1963; U. S. Waterways Experiment Station, U. S. Army Corps of Engineers, Vicksburg, Mississippi.

2.7 L. M. Gard; "Some Geologic Effects of the Gnome Nuclear Explosion"; Technical Letter GNOME-15, October 9, 1962; U.S.G.S , Department of the Interior, Washington, D.C.

2.8 G. W. Johnson, G. H. Higgins, and C. E. Violet; "Underground Nuclear Detonations"; UCRL-5626, July 1959; Lawrence Radiation Laboratory, Livermore, California

2.9 W. H. Diment, et al; "Geologic Effects of the RAINIER Underground Nuclear Explosion (A Summary Report of U. S. Geologic Survey Investigations); TEI-355, January 1959, Preliminary Draft; U.S.G.S., Department of the Interior, Washington, D.C.

REFERENCES (Cont.)

2.10 W. D. Weart; "Particle Motion Near a Nuclear Detonation in Halite, Project GNOME"; PNE-108F, September 5, 1963; Sandia Corporation, Albuquerque, New Mexico.

2.11 M. Heusinkveld et al; "Stress History Measurements with Piezoelectric Crystals, Project Gnome"; PNE-105P, March 1962; Lawrence Radiation Laboratory, Livermore, California.

2.12 "Project DRIBBLE, Critical Hole Summary" Fenix & Scisson; January 1964.

2.13 "Specifications for Station 1A, Project DRIBBLE, Part V, Technical Provisions"; Fenix & Scisson: January 1964.

2.14 NVOO letter, OSA:RAJ-3066, with attached memorandum HA:DGD-1609, L. J. Yelinek to O.H. Roehlk, Subject: 'Status of Station 1 Drill Hole, Project DRIBBLE," dated May 28, 1964.

2.15 Laboratory Drawing L6-17434A; titled: "Station 1 Emplacement, Project DRIBBLE"; Lawrence Radiation Laboratory, Livermore, California; April 17, 1964.

2.16 Laboratory Drawings L6-15354C, dated November 2, 1962 and L6-16084 and L6-16094 dated March 15, 1963; Lawrence Radiation Laboratory, Livermore, California.

2.17 Letter, Philip L. Randolph, Technical Director Project Dribble, to Otto H. Roehlk, PLR 62-113; Subject: "Salmon Stemming Plan"; March 18, 1963.

2.18 "Historical Report, E-14 Complex, Project DRIBBLE, Lamar County, Mississippi"; Fenix & Scisson; November 18, 1963.

2.19 NVOO letter, OSA:RLK-1899, Subject: "Station #3 Dribble-As-Built Drawing for Vent Shaft and Proposal for Access Shaft"; November 22, 1963.

2.20 L. M. Swift, "Intermediate Range Earth Motion Measurements"; Stanford Research Institute, Menlo Park, California; March 21, 1963.

REFERENCES (Cont.)

2.21 C. H. Higgs and Don L. Ward; "Oil and Gas Wells and Associated Facilities in the Tatum Dome Area, Lamar County, Mississippi"; January 1963; U. S. Bureau of Mines Special Report.

2.22 Karl V. Steinbrugge and Donald F. Moran; "An Engineering Study of the Southern California Earthquake of July 21, 1952 and Its Aftershocks"; Bulletin of the Seismological Society of America; Vol. 44, No. 26, April 1954.

3.1 USAEC Office of Information News Release, NU-65-24; April 2, 1965.

3.2 C. Boardman; Memorandum to Roehlk; O,AEC/NVCO, SDK 65-11; August 11, 1965; Lawrence Radiation Laboratory, Livermore, California.

3.3 J. Eisler, SRI, Telecon to S. B. Smith, RFB, Inc., August 17, 1965.

3.4 Robert Lynch; "Analog Computer Analysis of Magnetic Tape Seismograms"; NVO-1163-41; January 20, 1965; Roland F. Beers, Inc., Alexandria, Virginia.

3.5 L. B. Luhrs and F. Wabnik; "Geopnysics Analysis System for Seismogram Analysis IBM 7090 Programs"; NVO-1163-34; November 19, 1964; Roland F. Beers, Inc., Alexandria, Virginia.

3.6 W. M. Ewing, W. S. Jardetzky, and F. Press; "Elastic Waves in Layered Media"; 1957, pp 60-61; McGraw Hill, New York.

C.1 R. L. Gorman; "Analysis and Interpretation of Squared Fourier Spectra"; NVO-1163-38; January 29, 1965; Roland F. Beers, Inc., Alexandria, Virginia

Note: All of the above references are unclassified.

TECHNICAL AND SAFETY PROGRAM REPORTS SCHEDULED FOR ISSUANCE BY AGENCIES PARTICIPATING IN PROJECT DRIBBLE

SAFETY REPORTS

Agency	Report No.	Subject or Title
USWB	VUF-1020	Meteorological Documentation and Radiation Protection
USPHS	VUF-1021	Final Report of Off-site Surveillance
USBM	VUF-1022	Pre and Post-Shot Safety Inspection of Oil and Gas Facilities Near Project Dribble
USGS	VUF-1023	Analysis of Geohydrology of Tatum Salt Dome
USGS	VUF-1024	Analysis of Aquifer Response
REECo	VUF-1025	On-Site Health and Safety Report
RFB, Inc.	VUF-1026	Analysis of Dribble Data on Ground Motion and Containment - Safety Program
H-NSC	VUF-1027	Ground Water Supply
FAA	VUF-1028	Federal Aviation Agency Airspace Advisory
H&N	VUF-1029	Summary of Pre and Post-Shot Structural Survey Reports
JAB	VUF-1030	Structural Response of Residential-Type Test Structures in Close Proximity to an Underground Nuclear Detonation
JAB	VUF-1031	Structural Response of Tall Industrial and Residential Structures to an Underground Nuclear Detonation.

NOTE: The Seismic Safety data will be included in the USC&GS Technical Report VUF-3014

TECHNICAL REPORTS

Agency	Report No.	Subject or Title
SL	VUF-3012	Free-Field Particle Motions from a Nuclear Explosion in Salt - Part I
SRI	VUF-3013	Free-Field Particle Motions from a Nuclear Explosion in Salt - Part II
USC&GS	VUF-3014	Earth Vibration from a Nuclear Explosion in a Salt Dome
UED	VUF-3015	Compressional Velocity and Distance Measurements in a Salt Dome

LRL	VUF-3016	Design and Operation of a Chemical Processing Plant for Controlled Release of a Radioactive Gas from the Cavity of a Nuclear Explosion in Salt
LRL	PNE-3002 *	Response of Test Structures to Ground Motion from an Underground Nuclear Explosion
SRI	VUF-3017	Feasibility of Cavity Pressure and Temperature Measurements for a Decoupled Nuclear Explosion
LRL	VUF-3018	Background Engineering Data and Summary of Instrumentation for a Nuclear Test in Salt
WES	VUF-3019	Laboratory Design and Analyses and Field Control of Grouting Mixtures Employed at a Nuclear Test in Salt
LRL	VUF-3020	Geology and Physical and Chemical Properties of the Site for a Nuclear Explosion in Salt
EG&G	VUF-3021	Timing and Firing

* This report number was assigned by SAN

In addition to the reports listed above as scheduled for issuance by the Project DRIBBLE test organization, a number of papers covering interpretation of the SALMON data are to be submitted to the American Geophysical Union for publication. As of February 1, 1965, the list of these papers consists of the following:

Title	Author(s)	Agency(s)
Shock Wave Calculations of Salmon	L. A. Rogers	LRL
Nuclear Decoupling, Full and Partial	D. W. Patterson	LRL
Calculation of P-Wave Amplitudes for Salmon	D. L. Springer and W. D. Hurdlow	LRL
Travel Times and Amplitudes of Salmon Explosion	J. N. Jordan W. V. Mickey W. Helterbran	USC&GS AFTAC UED
Detection, Analysis and Interpretation of Teleseismic Signals from the Salmon Event	A. Archambeau and E. A. Flinn	SDC
Epicenter Locations of Salmon Event	E. Herrin and J. Taggart	SMU USC&GS
The Post-Explosion Environment Resulting from the Salmon Event	D. E. Rawson and S. M. Hansen	LRL
Measurements of the Crustal Structure in Mississippi	D. H. Warren J. H. Healy W. H. Jackson	USGS

All but the last paper in the above list will be read at the annual meeting of the American Geophysical Union in April 1965.

LIST OF ABBREVIATIONS FOR TECHNICAL AGENCIES

BR LTD	Barringer Research Limited Rexdale, Ontario, Canada
ERDL	Engineering Research Development Laboratory Fort Belvoir, Virginia
FAA	Federal Aviation Agency Los Angeles, California
GIMRADA	U. S. Army Geodesy, Intelligence and Mapping Research and Development Agency Fort Belvior, Virginia
H-NSC	Hazleton-Nuclear Science Corporation Palo Alto, California
H&N, INC	Holmes & Narver, Inc. Los Angeles, California Las Vegas, Nevada
II	Isotopes, Inc. Westwood, New Jersey
ITEK	Itek Corporation Palo Alto, California
JAB	John A. Blume & Associates Research Division San Francisco, California
LRL	Lawrence Radiation Laboratory Livermore, California
NRDL	U. S. Naval Radiological Defense Laboratory San Francisco, California
REECo	Reynolds Electrical & Engineering Co., Inc. Las Vegas, Nevada
RFB, INC.	R. F. Beers, Inc. Alexandria, Virginia
SDC	Seismic Data Center Alexandria, Virginia
EG&G	Edgerton, Germeshausen & Grier, Inc. Las Vegas, Nevada
SL	Sandia Laboratory Albuquerque, New Mexico
SMU	Southern Methodist University Dallas, Texas
SRI	Stanford Research Institute Menlo Park, California
TI	Texas Instruments, Inc. Dallas, Texas
UA	United Aircraft El Segundo, California
UED	United Electro Dynamics, Inc. Pasadena, California
USBM	U. S. Bureau of Mines Washington, 25, D. C.
USC&GS	U. S. Coast and Geodetic Survey Las Vegas, Nevada
USGS	U. S. Geologic Survey Denver, Colorado
USPHS	U. S. Public Health Service Las Vegas, Nevada
USWB	U. S. Weather Bureau Las Vegas, Nevada